Aus dem Biomedizinischen Centrum

Lehrstuhl für Molekularbiologie

Institut der Ludwig-Maximilians-Universität München

Vorstand: Prof. Dr. rer. nat. Peter B. Becker

DDK Shapes Origin Chromatin Structure and Replication Efficiency by Finetuning INO80 Function

Dissertation

zum Erwerb des Doktorgrades der Naturwissenschaften

an der Medizinischen Fakultät der

Ludwig-Maximilians-Universität München

vorgelegt von

Priyanka Bansal

aus Delhi, Indien

2023

Mit Genehmigung der Medizinischen Fakultät

der Universität München

Betreuer:	Prof. Dr. rer. nat. Axel Imhof
Zweitgutachter(in):	Prof. Dr. Philipp Korber
Dekan:	Prof. Dr. med. Thomas Gudermann
Tag der mündlichen Prüfung:	01. Oktober 2024

LMU LUDWIG-MAXIMILIANS-UNIVERSITÄT MÜNCHEN

Dekanat Medizinische Fakultät
Promotionsbüro

Affidavit

Bansal, Priyanka

Surname, first name

I hereby declare, that the submitted thesis entitled

DDK Shapes Origin Chromatin Structure and Replication Efficiency by Finetuning INO80 Function

is my own work. I have only used the sources indicated and have not made unauthorised use of services of a third party. Where the work of others has been quoted or reproduced, the source is always given.

I further declare that the dissertation presented here has not been submitted in the same or similar form to any other institution for the purpose of obtaining an academic degree.

Maisach, 10.10.2024

Place, Date

Priyanka Bansal

Signature doctoral candidate

Table of Contents

List of Abbreviations

DNA	Deoxyribonucleic Acid
CHD	Chromodomain helicase DNA binding
bp	base pair(s)
ACS	ARS consensus sequence
ARS	Autonomously replicating sequence
ORC	Origin recognition complex
Dbf4	Dumb-bell factor 4
DDK	Dbf4 dependent kinase
nm	Nanometer
ds	double strand
H2A	Histone H2A
H2B	Histone H2B
H2A.Z	Histone H2A variant
H1	Histone H1
H5	Histone H5
H3	Histone H3
H4	Histone H4
NFR	Nucleosome free region
PTM	Post-translational modification
ATP	Adenosine triphosphate
INO80	Inositol requiring 80
ISW	Imitation switch
FACT	Facilitates chromatin transcription
Nhp6	Non–histone chromosomal protein 6
SAGA	Spt6-Ada-Gcn5 acetyltransferase
NuA4	Nucleosome acetyltransferase of H4
dA/dT/dC/dG	deoxy adenosine/thymidine/guanosine/cytidine
A	Adenine
T	Thymidine
G	Guanine
C	Cytosine

IOC	Iswi one complex
Arp	Actin related protein
N terminus	Amino terminus
SGD	Salt gradient dialyzed
RNA	Ribonucleic acid
DTT	Dithiothreitol
Fun30	Function unknown now
EDTA	Ethylenediaminetetraacetic acid
CDK	Cyclin-dependent kinase
S. cerevisiae	Saccharomyces cerevisiae
SDS	Sodium dodecyl sulfate
ss	Single-stranded
RSC	Remodel the structure of chromatin
Asf1	Anti-silencing factor 1
HIR	Histone regulatory
CAF1	Chromatin assembly factor 1
MCM	Mini chromosome maintenance
Vps75	Vacuolar protein sorting 75
Rtt	Regulator of ty1 transposon
PCNA	Proliferating cell nuclear antigen
RPA	Replication protein A
Spt6	Suppressor of ty 6
Chz1	Chaperone for Htz1/H2A-H2B dimer
Nap1	Nucleosome assembly protein 1
G1	Gap 1 phase of the cell cycle
S	Synthesis phase of the cell cycle
G2	Gap 2 phase of the cell cycle
M	Mitosis/Meiosis phase of the cell cycle
Cdc	Cell division cycle
Sic1	Substrate/subunit inhibitor of CDK
Fkh2	Forkhead transcription factor 2
Ndd1	Nuclear division defective 1
APC	Anaphase promoting complex
pre-RC	Pre-replicative complex

OD	Optical density
RS	Replication stress
Rad	Radiation sensitive
PP	Protein phosphatase
Rif1	Rap1 interacting factor 1
MRC	Mediator of the replication checkpoint
IP	Immunoprecipitation
DMSO	Dimethyl sulfoxide
HU	Hydroxyurea
Mat	Mating type
TiO_2	Titanium dioxide
Ies	Ino eighty subunit
MMS	Methyl methane sulphate
C terminal	Carboxy terminus
HSA	Helicase-SANT-associated
PCR	Polymerase chain reaction
5FOA	5-Fluoroorotic acid
URA	Uracil
MNase	Micrococcal nuclease
NADH	Nicotinamide adenine dinucleotide hydrogen
PEP	Phosphoenolpyruvate
LDH	Lactose dehydrogenase
LEU	Leucine
µl	Microliter
MS	Mass spectrum
IPTG	Isopropyl β- D-1-thiogalactopyranoside
Kb	Kilobase or 1000 bases in RNA or DNA
KDa	Kilodalton
L	litre
ml	millilitre
PMSF	Phenylmethylsulfonyl fluoride
SWI/SNF	Switch/sucrose non fermentable
GINS	Go-ichi-ni-san

Abstract

Eukaryotic genomic DNA is wrapped around histone proteins to form nucleosomes, the basic units of chromatin. Chromatin is a higher-order structure and key regulatory element for DNA-template processes. Nucleosomes can regulate the access to DNA during replication, transcription, recombination, and repair. Any deregulation of these processes can cause genomic instability and can result in diseases like cancer. Hence, it is crucial to gain insights into the fundamental mechanisms that regulate nucleosome dynamics.

Replication initiates at specific DNA sequences called origins of replication. In the budding yeast *Saccharomyces cerevisiae* (*S. cerevisiae*), origins are nucleosome-free regions (NFRs) flanked by arrays of well-positioned nucleosomes. This specific chromatin structure helps in origin selection and pre-replication complex assembly at origins. At the beginning of the S phase of the cell cycle, the pre-replication complex is converted into the active replication machinery by DDK (Dbf4-dependent kinase). The active replication machinery encounters nucleosomes as a barrier and therefore requires assistance of chromatin factors (ATP-dependent chromatin remodelers and histone chaperones).

Upon committing to cell division, in G1 phase, chromatin factors interact with origin recognition complex (ORC) to form arrays of well positioned nucleosomes. However, how these chromatin factors are regulated throughout the cell cycle is unknown. Because low levels of DDK have been observed at early origins during G1 phase of the cell cycle, we speculated that DDK might be involved in the regulation of chromatin factors at early origins of replication, possibly by direct phosphorylation.

In this study, we utilized *S. cerevisiae* to discover phosphorylation events by DDK with an emphasis on chromatin factors to understand the DDK phosphorylation network in the nucleus. Using a mass spectrometry omics approach, we found DDK phosphorylation events on many nuclear proteins. In particular, we identified the Arp8 subunit of INO80 to be phosphorylated by DDK. We found that Arp8 phosphorylation does not peak in S phase, but appears during G1, consistent with a role of DDK in phosphorylating and regulating INO80 function prior to S phase.

INO80 is a multi-subunit ATP-dependent chromatin remodeler and a known player of chromatin replication. We dissected the functional relevance of DDK-dependent phosphorylation on the INO80 complex. We showed that DDK phosphorylation of Arp8 is essential for the integrity of INO80, in particular for the interaction of Ino80 with the NHP10 and ARP8 modules. When Arp8 was not phosphorylated, it leads to defects in DNA

replication, structural changes within the INO80 complex which reduced ATP hydrolysis and generated incorrect nucleosomal spacing with larger linker length. In the model, we propose that during G1 phase, INO80 and DDK interact with ORC subunits at early origins of replication where DDK phosphorylates Arp8 subunit of INO80 for precise nucleosomes positioning.

Overall, our study provides a comprehensive resource of nuclear phosphorylation events that are regulated by DDK. Our study further establishes a model where INO80 activity to accurately position nucleosomes around origins of replication is regulated by direct phosphorylation of DDK prior to the onset of S phase replication. To our knowledge, this is the first example of any organism, where the nucleosome spacing activity of a chromatin remodeler is directly regulated by signals of the cell cycle machinery.

Zusammenfassung

Die genomische DNA von Eukaryoten ist um Histonproteine gewickelt und bildet Nukleosomen, die Grundeinheiten des Chromatins. Chromatin ist eine Struktur höherer Ordnung und ein Schlüsselelement für die Regulierung von Prozessen mit DNA-Matrizen. Nukleosomen können den Zugang zur DNA während der Replikation, Transkription, Rekombination und Reparatur regulieren. Jede Deregulierung dieser Prozesse kann zu genomischer Instabilität und damit zu Krankheiten wie Krebs führen. Daher ist es von entscheidender Bedeutung, Erkenntnisse über die grundlegenden Mechanismen zu gewinnen, die die Nukleosomendynamik regulieren.

Die Replikation beginnt an bestimmten DNA-Sequenzen, den so genannten Replikationsursprüngen. In der Bäckerhefe *Saccharomyces cerevisiae* (*S. cerevisiae*) sind die Ursprünge nukleosomenfreie Regionen (NFRs), die von Reihen gut positionierter Nukleosomen flankiert werden. Diese spezifische Chromatinstruktur hilft bei der Auswahl der Ursprünge und beim Aufbau des Prä-Replikationskomplexes an den Ursprüngen. Zu Beginn der S-Phase des Zellzyklus wird der Prä-Replikationskomplex durch die DDK (Dbf4-abhängige Kinase) in die aktive Replikationsmaschinerie umgewandelt. Die aktive Replikationsmaschinerie stößt auf Nukleosomen als Barriere und benötigt daher die Unterstützung von Chromatinfaktoren (ATP-abhängige Chromatin-Remodeller und Histon-Chaperone).

Beim Beginn der Zellteilung in der G1-Phase interagieren Chromatinfaktoren mit dem Origin Recognition Complex (ORC), um eine Reihe von gut positionierten Nukleosomen zu bilden. Wie diese Chromatinfaktoren jedoch während des gesamten Zellzyklus reguliert werden, ist unbekannt. Da an frühen Ursprüngen in der G1-Phase des Zellzyklus niedrige DDK-Konzentrationen beobachtet wurden, spekulierten wir, dass DDK an der Regulierung von Chromatinfaktoren an frühen Replikationsursprüngen beteiligt sein könnte, möglicherweise durch direkte Phosphorylierung.

In dieser Studie nutzten wir *S. cerevisiae*, um Phosphorylierungsereignisse durch DDK zu entdecken, wobei der Schwerpunkt auf Chromatinfaktoren lag, um das DDK-Phosphorylierungsnetzwerk im Zellkern zu verstehen. Mithilfe eines massenspektrometrischen Omics-Ansatzes fanden wir DDK-Phosphorylierungsereignisse an vielen Kernproteinen. Insbesondere identifizierten wir die Arp8-Untereinheit von INO80 als von DDK phosphoryliert. Wir fanden heraus, dass die Arp8-Phosphorylierung in der S-Phase nicht ihren Höhepunkt erreicht, sondern während G1 auftritt, was mit der Rolle von

DDK bei der Phosphorylierung und Regulierung der INO80-Funktion vor der S-Phase übereinstimmt.

INO80 ist ein ATP-abhängiger Chromatin-Remodeler mit mehreren Untereinheiten und ein bekannter Akteur der Chromatinreplikation. Wir untersuchten die funktionelle Bedeutung der DDK-abhängigen Phosphorylierung des INO80-Komplexes. Wir zeigten, dass die DDK-Phosphorylierung von Arp8 für die Integrität von INO80 wesentlich war, insbesondere für die Interaktion von Ino80 mit den Modulen NHP10 und ARP8. Wenn Arp8 nicht phosphoryliert wurde, führte dies zu Defekten bei der DNA-Replikation, zu strukturellen Veränderungen innerhalb des INO80-Komplexes, die die ATP-Hydrolyse reduzierten und falsche Nukleosomenabstände mit größerer Linkerlänge erzeugetn. In unserem Modell schlagen wir vor, dass INO80 und DDK während der G1-Phase mit ORC-Untereinheiten am frühen Replikationsursprung interagieren, wo DDK die Arp8-Untereinheit von INO80 phosphoryliert, um die Nukleosomen präzise zu positionieren.

Insgesamt bietet unsere Studie eine umfassende Quelle für Phosphorylierungen im Nukleus, die durch DDK reguliert werden. Unsere Studie stellt außerdem ein Modell auf, bei dem die Aktivität von INO80 zur genauen Positionierung von Nukleosomen um Replikationsursprünge durch direkte Phosphorylierung von DDK vor Beginn der S-Phasen-Replikation reguliert wird. Unseres Wissens nach ist dies das erste Beispiel, in irgendeinem Organismus, für die direkte Regulation eines Chromatin-Remodelers durch Signale der Zellzyklusmaschinerie.

List of figures

List of tables

Contributions to the Study

This thesis comprises my unpublished work. The research was conducted from October 2018 to November 2023 in the laboratory of Dr. Christoph F. Kurat at molecular biology division, Biomedical Center Munich. To ensure the success of this project, numerous individuals participated in collaborative efforts, each making valuable contributions to the study. I would like to mention each contributor's specific contributions within the context of the respective figures presented in the thesis.

My contributions in this study:

1) I designed, performed and optimized the method for finding phosphorylation sites on ATP-dependent chromatin remodelers.
2) I prepared cell cultures, synchronized cells for G1 arrest and cell cycle entry, purified yeast nuclei and prepared samples for mass spectrometric measurements.
3) I carried out literature searches, found appropriate controls for mass spectrometry data and analyzed the data in Appendix I and II.
4) From the resulting analysis, I identified and tested the role of phosphorylation by molecular cloning, site-directed mutagenesis, yeast transformation, tetrad dissection and yeast genetics to generate mutant strains of various histone chaperones and ATP-dependent chromatin remodelers. The mutant strains were tested for phenotypes using spot dilution assay.
5) After identifying the growth phenotype on Arp8, I added protein purification tags and confirmed the yeast strains with western blots.
6) I purified WT and mutant proteins, coordinated and optimized the workflow according to the requirements of different assays performed in collaboration.
7) I performed an in vitro kinase assay to show that Arp8 is directly phosphorylated by DDK.
8) I planned and designed the collaborative assay strategy. Together with literature review and interpretation of various collaborative results, I connected the dots with respect to the big picture to show the role of DDK phosphorylation in fine-tuning Ino80 function and thereby regulating origin chromatin structure and replication efficiency.

Collaborative efforts in this study:

1. In mass spectrometric experiments, the processed samples were run on mass spectrometer by Dr. Ignasi Forné at Zentrallabor für Proteinanalztik, in-house mass spectrometry facility. The mass spectrometry data in Figure 2.2, Figure 2.3, Figure 2.4, Figure 2.5, Figure 2.6 (C, D) and Figure 2.7 was analyzed and plotted by Dr. Shibojyoti Lahiri. During the analysis, Dr. Lahiri guided me through various components involved in the analysis.
2. The recombination frequency data in Figure 2.13 was produced by Dr. María Ángeles Ortíz-Bazán, Dr. Belen Gómez-González in Prof. Dr. Andrés Aguilera´s laboratory at University of Seville, Spain.
3. In the Flow cytometry data in Figure 2.6 (B) and Figure 2.14, was generated by Dr. Karl-Uwe Reusswig and Dr. Lorenzo Galanti respectively in Prof. Dr. Boris Pfander´s laboratory at Max Plank Institute of Biochemistry. I generated the mutant and wildtype strains, collected cells and performed cell cycle arrest and release, collected cell at mentioned time points, fixed cells and gave for flow cytometry analysis.
4. For the RNA sequencing data in Figure 2.15, I grew the WT and mutant yeast cells, Dr. Marisa Müller prepared the sequencing samples and Dr. Tobias Straub analyzed and plotted the data.
5. In Figure 2.16 and Figure 2.17, I purified the WT and mutant INO80 proteins and Dr. Chandni Kumar performed cross-linking mass spectrometry experiments, ran samples on mass spectrometer, analyzed and plotted the data.
6. In Figure 2.18, Dr. Petra Vizjak from Prof. Dr. Felix Müller-Planitz laboratory shared chromatin and the reagents to perform ATP hydrolysis assay. I conducted the assay, and Dr. Vizjak provided instruction and guidance on the procedure. Dr. Vizjak analyzed the data and I plotted the graph.
7. In Figure 2.19, I purified the WT and mutant INO80 proteins. Dr. Erika Chacin performed the nucleosome positioning assay and analyzed and plotted the resulting data

1. Introduction

1.1. Chromatin and genome organization

Genomes are DNA sequences that contain all the hereditary material of an organism. The DNA, when packed, occupies a significant portion of the nucleus. The genome of human cells is ~ 2 meters long and it is a major challenge to fit it into the limited space of a micrometer-sized cell nucleus. This is only possible because of chromatin, a higher order structure, where genomic DNA is tightly packaged. Chromatin is a DNA/protein complex whose basic repeating unit is the nucleosome [1]. The nucleosome consists of ~147 base pairs (bp) of double stranded DNA (dsDNA) wrapped ~1.65 times around the surface of an octamer of histone proteins (two copies of each H2A, H2B, H3 and H4). This histone octamer consists of a central tetramer of $(H3\text{-}H4)_{2,}$ that is flanked by H2A-H2B dimers on either side [2]. Short DNA segments, called linker DNA, connect nucleosomes to form nucleosomal arrays. The length of these linker DNA sequences varies between ~8 – 90 bp [3, 4] and this variation occurs within a single cell and between different species and tissues. The combined length of nucleosomal DNA and linker DNA is called as the nucleosomal repeat length (NRL), which varies between 150-250 bp depending on the organism and cell type [5]. The nucleosomal arrays, also known as “beads on a string”, are fibers with a diameter of 11 nm. Further folding of the chromatin fiber helps to accommodate the genome in the small nuclear space [5].

A hierarchical model of chromatin folding has long been proposed, in which the binding of linker histones and the interactions between neighbouring nucleosomes organize the nucleosomal arrays into the more condensed 30 nm fiber [6, 7]. The 30 nm fiber is thought to progressively assemble into helically folded 120 nm chromonema, 300 and 700 nm chromatids and finally mitotic chromosomes [8]. However, the evidence for the folding of the 30 nm fiber folding into a hierarchical higher order chromatin structure is lacking. Although higher order chromatin structure (~120 nm) has been observed by light and electron microscopy, it has not been inferred whether it actually forms via hierarchical folding of 30 nm fiber [9].

Models for higher order chromatin structure have been revised many times over the years. Currently, the most widely accepted hypothesis is the “loop extrusion model”. This model proposes that cohesin (a ring-shaped SMC complex), aided by ATP hydrolysis, captures and extrudes chromatin, forming loops. When two cohesin complexes meet, they are stopped by the CCCTC binding factor (CTCF), forming loop domains. These loops

contribute to the formation of topologically associating domains (TADs), regulating gene expression and other genomic processes [10]. TADs are the region of the genome that exhibit high levels of self-interactions and they play a crucial role in regulating enhancer-promoter interactions. They also act like barriers, keeping themselves separate from nearby TADs [5, 11, 12].

How is then the chromatin structure organized in a cell? At the smallest scale, the DNA double helix is packed together with histones to form ~11 nm nucleosomes arrays. At the intermediate scale, chromatin is organized into TADs [13]. At the same scale, regions with similar epigenomic characteristics compartmentalize chromatin into two regions, labelled as A and B [13, 14]. These compartments mainly consist of active and inactive chromatin, respectively. This organizational pattern is likely established through a mechanism distinct from TAD formation [13]. Active chromatin within compartment A tends to interact with other active chromatin segments and is found near specific nuclear structures such as nuclear speckles. In contrast, inactive chromatin in B tends to associate with inactive chromatin and associates with the nuclear lamina [13, 14]. On a larger scale, chromosomes are arranged into chromosome territories, with each chromosome occupying a distinct position within the nucleus [5, 15] (Figure 1.1). However, because chromatin is dynamic, these structures may not remain fixed for long periods of time.

Chromatin's dynamic nature means its structures can change over time. This dynamicity is essential for allowing regulatory DNA-binding proteins access to DNA during cellular processes like replication, transcription, or DNA repair. Over 80% of the Saccharomyces cerevisiae genome is organized into arrays of stable nucleosomes [16]. The positions of nucleosomes with respect to the regulatory elements can be critical, e.g. for gene regulation [17]. Other significant regions of the genome that are not in complex with nucleosomes are known as nucleosome-free regions (NFRs). NFRs are accessible parts of genome that can regulate DNA template associated processes [16]. For example, origins of replication or transcriptionally active gene promoters are characterized by the presence of an NFR in their core region [18].

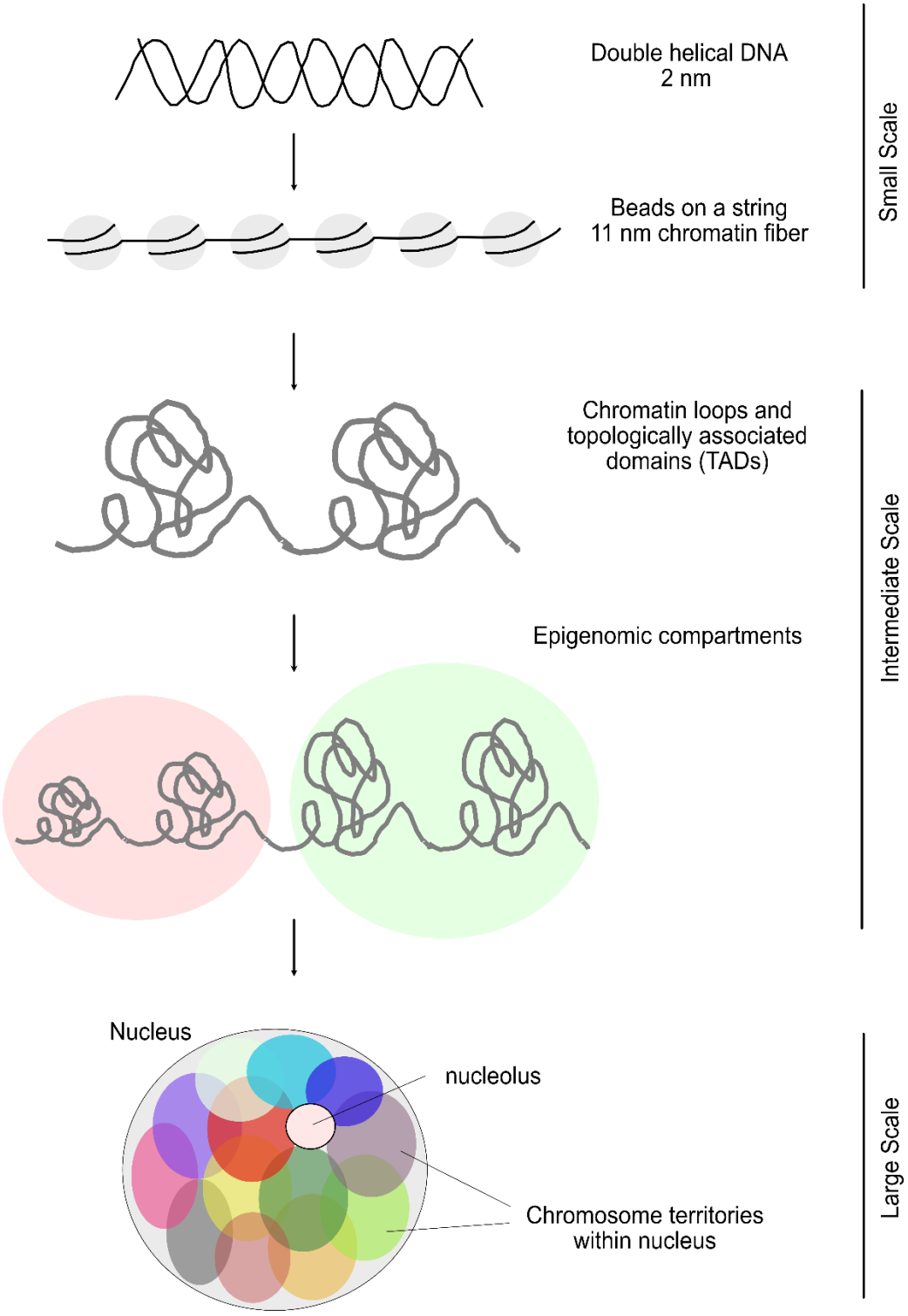

Figure 1.1.The evolving dynamic and fractal model for chromatin organisation

The figure summarizes chromosomal structural organisation at multiple scales. At the small scale, DNA is compacted into nucleosomes where 147 bp DNA wraps around histone octamer. At the intermediate scale, chromatin is organised into topologically associated domains and compartmentalized into epigenomic A/B compartments. At the largest scale, chromosomes are organised into chromosome territories. The figure is adapted from Hansen et. al., 2018 and Moraru and Schalch, 2019 [5, 13].

The organization of nucleosomes across the chromatin landscape is not uniform. Among numerous factors, the DNA sequence participates in determining the positions at which histone octamer bind DNA to form nucleosomes [17]. The binding of DNA to the histone octamer requires the energetically unfavorable bending of the DNA. This energy requirement is facilitated by the formation of multiple hydrogen and ionic bonds formed between the DNA and histones within the nucleosomes [19]. DNA sequences displaying a periodicity of ~10 bp especially in certain dinucleotides, promotes the bending and wrapping of DNA around the histone octamer, thereby supporting nucleosome formation [17, 20]. In this context, AT-rich dinucleotides are typically favored in the minor groove of the DNA, while GC-rich dinucleotides, are preferred in the major groove when facing the histone octamer [21]. Importantly, these dinucleotide periodicities are not limited to single species but are commonly found across various organisms including Archaea, Yeasts, Flies and Mammals. This suggests a conserved role of these sequences across different species [22-25].

In contrast to the dinucleotides that promote nucleosome formation, DNA sequences containing stretches of poly (dA:dT) or poly (dG:dC) stretches are notably inflexible. Wrapping and twisting these sequences around the histone octamer demands significant energy, making them less likely to integrate readily into nucleosomes [26, 27]. Poly(dA:dT) sequences are commonly found at promoters and replication origins, leading to nucleosome depletion in many species [28-30], although this is not observed universally. For example, in *S. pombe*, poly(dA:dT) tracts are not associated with nucleosome depletion; instead, they are favoured in the nucleosome core region [31]. While the ability of DNA to interact with the histone core is critical, it is not sufficient to establish spaced and phased nucleosome organizations. Nucleosome occupancy is influenced by additional extrinsic chromatin factors, such as ATP-dependent remodeling complexes, which specify nucleosome positioning patterns [32]. Additionally, there are other factors that can influence the binding of DNA to histone octamers, such as steric hindrance from other nucleosomes or the binding and action of other accessory proteins [17].

As mentioned, chromatin provides stability to eukaryotic genomes and has to be very dynamic. Chromatin organization is a key element in partitioning genomes into functionally distinct chromosomal domains and “chromatin factors” help in chromatin plasticity. For example, such factors can promote nucleosomes to (i) slide along DNA [33, 34], (ii) being fully or partly disassembled [35], (iii) be subjected to post-translational modification (PTM) [36, 37]. Finally, histones can be replaced by their sequence variants [38]. All these

mechanisms ensure DNA accessibility thus contributing to the regulation of DNA-template processes.

Chromatin factors contributing to the versatility and flexibility of chromatin are for example, ATP-dependent chromatin remodelers, histone chaperones or histone-modifiying enzymes. In replication, eukaryotic replisomes by themselves cannot replicate chromatin efficiently and therefore require the help from chromatin remodelers like INO80 (INOsitol requiring 80) or ISW1a (Imitation SWitch subfamily 1a), the histone chaperone FACT (FAcilitates Chromatin Transcription) / Nhp6 (Non-Histone chromosomal Protein 6) and histone-acetyl transferases SAGA (Spt-Ada-Gcn5 Acetyltransferase) and NuA4 (NUcleosome Acetyltransferase of H4) to replicate DNA [39]. Chromatin factors have also been shown to play an important role during transcription [40] and DNA repair [41]. In the following section I will discuss ATP-dependent chromatin remodelers and histone chaperones in more detail.

1.1.1. ATP-dependent chromatin remodelers

ATP-dependent chromatin remodeling complexes play vital roles in the nucleosomal organisation in chromatin. Chromatin remodelers harness the energy derived from ATP hydrolysis by a central ATPase motor [33, 42] to perform a wide range of actions on chromatin, for example, nucleosome sliding [42], destabilizing and restructuring of nucleosomes, eviction of nucleosomes [43] or switching canonical histones with histone variants [44, 45].

Remodelers can be classified in two main groups: firstly, the nucleosome translocation enzymes, which move or slide histone octamers on DNA. Secondly, histone exchange factors, which remove the entire histone octamer or exchange histones for histone variants [46].

Based on similarities or differences in their catalytic ATPase motor subunit, chromatin remodelers are grouped into four families: SWItch/Sucrose Non Fermentable (SWI/SNF), Imitation SWitch (ISWI), Chromodomain Helicase DNA binding (CHD) and INOsitol requiring 80 (INO80) [47] (Figure 1.2). In addition to the ATPase module, chromatin remodelers contain several other domains and accessory subunits that play a regulatory role over the ATPase motor and thereby influencing the specific outcomes within each remodeler family [48, 49]. The ATPase subunit in all remodelers families consist of two RecA-like lobes referred to as Lobe1 and Lobe 2 [47] (Figure 1.2). These two lobes are separated by a small

insertion in some families (such as in SWI/SNF, CHD and ISWI family) or large insertion in others (as seen in INO80 family) [50] (Figure 1.2).

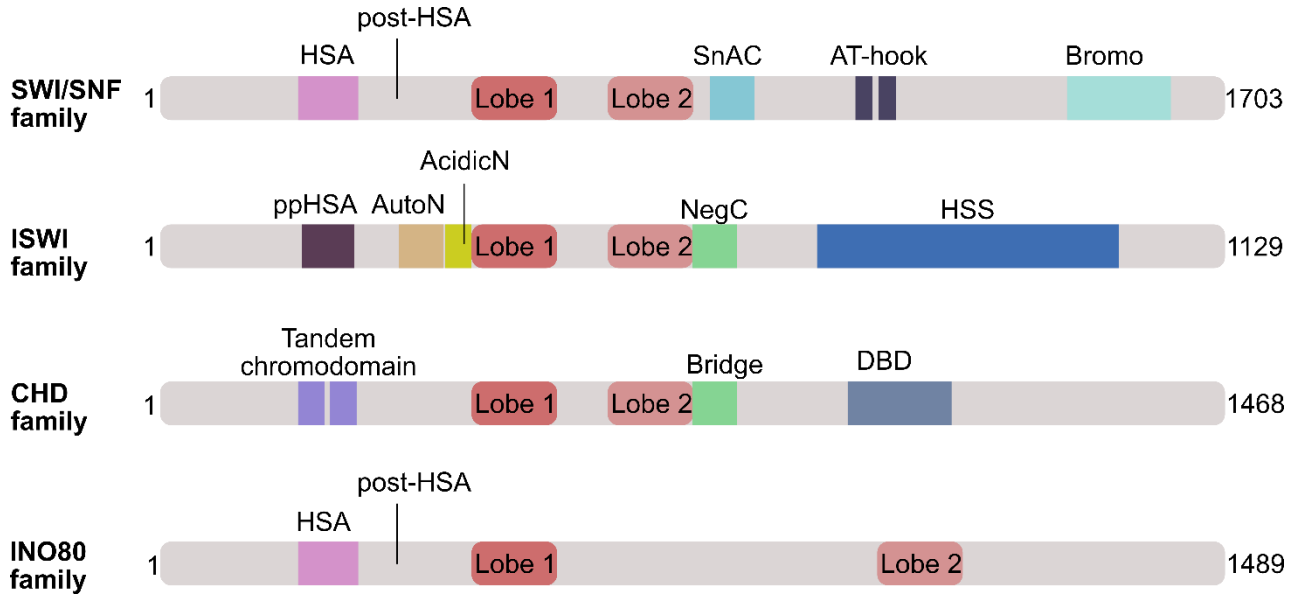

Figure 1.2. Domain organization of the ATPase subunits of nucleosome remodelers subfamilies

The ATPase subunit within all remodelers subfamiles possesses two RecA-like lobes, known as Lobe 1 and Lobe 2. These lobes are separated by a small insertion as observed in the SWI/SNF, ISWI, CHD families or a large insertion as seen in the INO80 family. Figure 1.2 is adapted from Clapier et. al., 2017 [51, 52] and the numbers display the total number of amino acids. Additionally, various motifs and domains are highlighted within each family, which are as follows: HSA: Helicase-SANT-Associated, SnAC: Snf2 ATP coupling, Bromo: bromodomain, ppHSA: post-post-HSA, AutoN: Auto-regulatory motif in N-terminal region, AcidicN: Acidic regions in N-terminal region, NegC: Negative regulator of coupling, HSS: HAND-SANT-SLIDE, DBD: DNA-binding domain,

The RecA like lobes can displace nucleosomes by an “wave propagation” mechanism**.** This involves a conformational change in the two lobes, driven by the cyclic binding and hydrolysis of ATP, which results in the translocation of DNA by 1 – 2 bp for each ATP molecule. However, the exact details remain obscure and might be different for each remodeler [48]. Depending on the type and number of associated subunits, specific role(s) for each complex may vary (Table 1).

Table 1: Overview of *S. cerevisiae* remodeler families, features, and functions

The ATPase is the catalytic subunit. Together with other additional subunits form a complex.

Family	Complex	ATPase	Additional subunit(s)	Function
ISWI	ISW1a	Isw1	Ioc3	Sliding and spacing
	ISW1b	Isw1	Ioc2, Ioc4	Sliding
	ISW2	Isw2	Itc1, Dpb4, Dls1	Sliding, spacing
CHD	CHD1	Chd1	-	Sliding, spacing
INO80	INO80	Ino80	Arp8, Arp5, Arp4, Ies1, Ies2, Ies3, Ies4, Ies5, Ies6, Nhp10, Taf14, Rvb1, Rvb2	Sliding, spacing and H2A.Z removal (under debate)
	SWR1	Swr1	Swc3, Swc5, Rvb1, Act1, Swc4, Arp4, Arp6, Swc7, Bdf1, Vps71, Rvb2, Yaf9 Vps72	H2A.Z incorporation
	FUN30	Fun30	-	Sliding, histone dimer exchange
SWI/SNF	SWI/SNF	Swi2/Snf2	Snf5, Snf11, Swp82, Rtt102, Snf6, Swi3, Arp9, Snf12, Swi1, Taf14, Arp7	Sliding, eviction
	RSC	Sth1	Rsc2, Rsc3, Rsc4, Rsc6, Rsc40, Rsc7/Npl6, Rsc8, Rsc9, Rsc58, Sth1, Arp7, Arp9, Taf14, Idb7, Rtt102	Sliding, eviction

The ISWI and CHD families: In *S. cerevisiae,* the ISWI family is defined by the existence of two paralogue proteins, Isw1 and Isw2. Together with other proteins, Isw1 and Isw2 form three distinct remodeling complexes with different biochemical activities: ISW1a, ISW1b and ISW2 [53] (Table 1). The CHD family in *S. cerevisiae* is represented by the monomeric Chd1 remodeler. The ATPase domain of CHD family is similar to that of ISW1 remodelers but also unique because of two tandemly arranged N terminus chromodomain [54].

In vitro, ISWI complexes can assemble and slide nucleosomes [55, 56]. All CHD and ISWI family remodelers, except ISW1b, can slide nucleosomes that are located at the end of a short DNA fragment to the centre of the fragment [57]. Because of this centring activity

CHD and ISWI remodelers are able to space the nucleosomes and results in the formation of regular nucleosome arrays. ISW1a, ISW2 and Chd1 remodelers have been shown to generate regular nucleosome arrays in irregularly spaced nucleosomes in chromatin generated by salt gradient dialysis (SGD) [55, 58-60]. *In vivo*, deletion of *ISW1*, *ISW2* and *CHD1* remodelers results in reduction of regular nucleosome arrays [61, 62]. In budding yeast, lacking of the ATPase subunits of these remodelers also show reduced levels of regular arrays on newly replicated DNA, suggesting defects in replication-dependent chromatin assembly [63, 64].

The INO80 family: In *S. cerevisiae* the INO80 and SWR1 remodelers belong to the INO80 family. Both, INO80 and SWR1 are multi subunit complexes (Table 1). INO80 family members perform editing functions in the genome and can regulate H2A.Z dynamics [44]. H2A.Z is a histone variant of the canonical histone H2A and shares 60% amino acid similarity with H2A [65]. H2A.Z provides specific structural and docking site properties to nucleosomes. For example, in mammals, during gene transcription, a H2A.Z binding protein can influence pausing and elongation of RNA polymerase II [66]. SWR1 cannot slide nucleosomes but catalyses the exchange of H2A with H2A.Z [45]. However, the role of another family member, INO80, in catalysing the reverse reaction is under debate. [44, 67]. Like Chd1, ISW1a and ISW2 remodelers, INO80 complex can also space nucleosomes *in vitro* [59, 68] and *in vivo* [69].

Fun30 is another remodeler of this family [70] and shares highest degree of homology with Swr1 and Ino80 subunit of INO80 remodelers [47]. *In vitro*, Fun30 can bind single stranded DNA (ssDNA), dsDNA and chromatin directly [71, 72] to stimulate its ATPase activity. A similar phenomenon has also been observed with other remodelers like ISW1a, SWI/SNF, RSC and SWR1. However, ATPase activity of SWR1 is stimulated only in the presence of canonical histones [34]. Fun30 was shown to reposition nucleosomes and to evict H2A-H2B dimers from chromatin templates [72, 73].

The SWI / SNF family: In S. cerevisiae, the SWI/SNF family represents SWI/SNF and RSC (Remodel the Structure of Chromatin) remodelers. RSC is highly abundant and is found in ~10-fold excess compared to the SWI/SNF complex [74]. RSC complex is essential for mitotic growth whereas SWI/SNF complex is not essential [75]. Despite these differences, RSC bears a striking resemblance to the SWI/SNF complex. RSC subunits Sth1, Rsc6 and Rsc8 are homologous to SWI/SNF subunits Swi2/Snf2, Swp73 and Swi3 respectively. Although, both RSC and SWI/SNF have unique subunits but some subunits for example, Arp7, Arp9 and Taf14 are shared between the two remodelers [75]. SWI/SNF family remodelers typically facilitate chromatin access as they slide and evict nucleosomes

and are important for gene activation or repression [76]. RSC primarily determines the width of NFRs by removing nucleosome at dA:dT rich regions. Depletion of RSC results in global nucleosome repositioning, i.e., both downstream and upstream nucleosomal arrays shift towards NFR resulting in narrower NFR [59, 77]. RSC can be activated by a GC rich motif or dA:dT tracts found in the yeast promoters [59, 76, 78]. However, the precise mechanism behind RSC activation by these sequences and how RSC links sequence recognition to nucleosome sliding or eviction remains unclear. In contrast to RSC, the SWI/SNF remodeler operates more favorably at highly expressed and stress-responsive genes, where it might coordinate with RSC to evict nucleosomes at these genes [79].

1.1.2. Histone chaperones

Histone chaperones can regulate and assist in the assembly as well as in the disassembly of histones into nucleosomes [80]. Histone chaperones are highly negatively charged proteins and have very little sequence similarities [81]. They influence chromatin dynamics in an ATP-independent manner [82]. They function in the nuclear transport, the storage or buffering, the degradation, the folding, the deposition and the recycling of histones [83, 84]. In general, histone chaperones can be classified as either H3-H4 or H2A-H2B chaperones, based on their preferential binding to H3-H4 or H2A-H2B respectively. Table 2 summaries histone chaperones in *S. cerevisiae* based on their classification, binding partners and functions [85].

Table 2: Histone chaperones from *S. cerevisiae*

Histone Chaperone	Chaperone Classification	Binding Partners	Functions
Asf1	H3-H4 family	H3-H4 dimer HIR complex CAF1 MCMs	Replication Repair Transcriptional regulation Promotes histone acetylation
Vps75	H3-H4 family	H3-H4 Rtt109	Repair Transcriptional regulation Promotes histone acetylation Telomere length maintenance
Rtt106	H3-H4 family	H3-H4	Replication

		CAF1	Transcriptional silencing Transcription repression
CAF1 Subunits: Msl1, Cac2 and Rif2	H3-H4 family	H3–H4 Rtt106 Asf1 PCNA	Replication Repair Transcriptional silencing
HIR Subunits: HIR1, HIR2, HIR3 and HPC2	H3-H4 family	H3–H4 ASf1 Swi/Snf	DNA synthesis independent nucleosome assembly Transcriptional repression Transcriptional silencing
Spt6	H3-H4 family	FACT	Transcription initiation and elongation
FACT Subunits: Spt16 and Pob3	H2A-H2B, H3-H4 family	H2A–H2B H3–H4 RPA MCMs Nhp6	Replication Repair Transcription Recombination
Chz1	Variant histone	H2A.Z-H2B	Transcription regulation H2A.Z deposition onto DNA
Nap1	Core / linker histone	H2A-H2B H3-H4 H1	Histone shuttling Transcription Linker histone deposition H2A.Z exchange
Nhp6	Required for activity of other chromatin factors	FACT Swi/Snf RSC	Nucleosome disassembly, binding and assembly Chromatin replication

Abbreviations: Asf1 (Anti Silencing factor 1), HIR (Histone Regulatory), CAF1 (Chromatin Assembly Factor 1), MCM (Mini Chromosome maintenance), Vps75 (Vacuolar Protein Sorting 75), Rtt106 (regulator of Ty1 transposon 106), Rtt109 (regulator of Ty1 transposon 109), PCNA (Proliferating Cell Nuclear Antigen), FACT (Facilitates Chromatin Transcription), RPA (Replication Protein A), Spt6 (Suppressor of Ty's), Chz1 (Chaperone for Htz1/H2A-H2B dimer), Nap1 (Nucleosome Assembly Protein 1) and Nhp6 (Non histone protein 6).

In order to relax the chromatin barrier, it must transiently disassemble to allow transcription, DNA replication and DNA repair machineries to access DNA and restore the

structure of chromatin after the process. Histone chaperones can also assist chromatin remodelers in doing their work. In this section, I will specifically talk about role of histone chaperone in chromatin replication.

Histone chaperones handle histones at the replication fork: DNA replication takes place during the S phase of the cell cycle. During replication, the chromatin landscape undergoes dramatic changes as progression of replication fork leads to disruption of parental nucleosomes ahead of the fork and restoration of nucleosomes behind the fork [86, 87]. Alongside DNA replication, the chromatin landscape on newly synthesized DNA is reestablished using newly synthesized histones as well as recycled parental histones, a process called replication-coupled nucleosome assembly [87]. Nucleosome assembly during histone exchange and processes like transcription occur throughout the cell cycle in a replication independent manner [88].

Ahead of the replication fork, a nucleosome is temporarily disassembled into $(H3\text{-}H4)_2$ tetramers and (H2A-H2B) dimers to allow the passage of the replication fork and nucleosomes are quickly reassembled onto newly synthesized daughter chromatids. The Asf1 chaperone could potentially act as a histone acceptor and disrupt $(H3\text{-}H4)_2$ tetramers [89, 90]. In yeast, Asf1 interacts with the PCNA loader RFC (replication factor C) and is required to maintain replisome integrity in the event of replication stress [91]. Another histone chaperone Nap1 might be involved in removing H2A-H2B dimers from DNA. Nap1 interacts with H2A-H2B in coimmunoprecipitation studies and can assemble chromatin *in vitro* [92].

FACT is another histone chaperone and is composed of the Spt16 and Pob3 subunits. Originally FACT was identified as a complex that destabilizes nucleosomes to promotes transcription elongation through nucleosomes *in vitro* [93]. Recent research has associated FACT not only with transcription but also with replication [94]. FACT plays important roles in both the disruption of parental nucleosomes and the recycling of parental histones [39, 95, 96]. FACT subunits interact with DNA Polymerase α [97], CMG (Cdc45-MCM-GINS) (Cell division cycle 45 - MiniChromosome Maintainence - Go-Ichi-Ni-San) complex [98] and Replication Protein A (RPA) [99]. FACT establishes multiple contact sites with DNA while maintaining components of partially disassembled nucleosome in its close proximity [94, 100]. Studies have shown that FACT-mediated transient dissociation of histone - DNA interactions promote MCM activity *in vitro* [39] and replication fork progression *in vivo* [101].

Chromatin assembly after replication is initiated by chaperone Asf1, where it delivers H3-H4 dimers to two other histone chaperones, CAF-1 and Rtt106 [102]. A CAF-1-H3-H4 complex binds to DNA and the cooperative DNA binding by CAF-1 promotes dimerization of

the CAF-1-H3-H4 complex and therefore forming $(H3\text{-}H4)_2$ tetramers [102, 103]. After $(H3\text{-}H4)_2$ tetramers have been assembled onto the DNA a dimer of H2A-H2B is incorporated by FACT or Nap1 [104]. FACT deposits newly synthesised histones as well as recycled parental histones [39, 95, 96]. In budding yeast, FACT interacts with CAF-1 and Rtt106, suggesting a collaboration among various histone chaperones [105].

1.2. The mitotic cell cycle and chromatin replication

During cell division, a parent cell undergoes division to yield two cells. Cell division usually occurs as part of a larger cell cycle. Prokaryotes divide by a means of binary fission whereas eukaryotic cell division occurs through either mitosis or meiosis. Moreover, prokaryotic DNA replication occurs inside the cytoplasm as they lack nucleus whereas eukaryotic DNA replication occurs inside the nucleus. In this Section I will discuss the regulatory cell cycle networks and, in particular the process of DNA replication.

1.2.1. The yeast cell cycle network

The cell cycle is a sequence of events in which growing cells replicate all its cellular and metabolic components and, in the end evenly distribute them between the parent and the daughter cell [106]. The genome is one of the most critical components to be replicated and distributed so that each daughter cell obtains the essential information needed to repeat the replication process [107]. The cell cycle is strictly regulated and highly conserved among eukaryotes [108]. The process is broadly divided into four phases: (i) the G1 (Gap 1) phase - where cells grow and under appropriate conditions (e.g. nutrient availability) commit to cell division; (ii) the S phase (Synthesis phase) – where DNA synthesis occurs and chromosomes are duplicated; (iii) the G2 (Gap 2) phase - a gap between S and M (Mitosis) phases and where possible defects from DNA synthesis can be repaired (Figure 1.3); and finally (iv) the M phase - where duplicated chromosomes are separated and equally distributed between the mother and daughter cell. After M phase the cells enter the G1 phase again and therefore complete a “cycle” [109].

These phases are characterized by coincident periodic gene regulation. The robust cell cycle control has many advantages: firstly, the cell cycle ensures an alternating cycle between S phase and M phase along with gaps to maintain cellular balance [110]. Secondly, a periodic expression halts cell cycle progression if any problems arise to repair the damage

and resume the cell cycle [107]. Therefore, the cell cycle ensures that genomes are duplicated faithfully to ensure integrity before proceeding towards cell division.

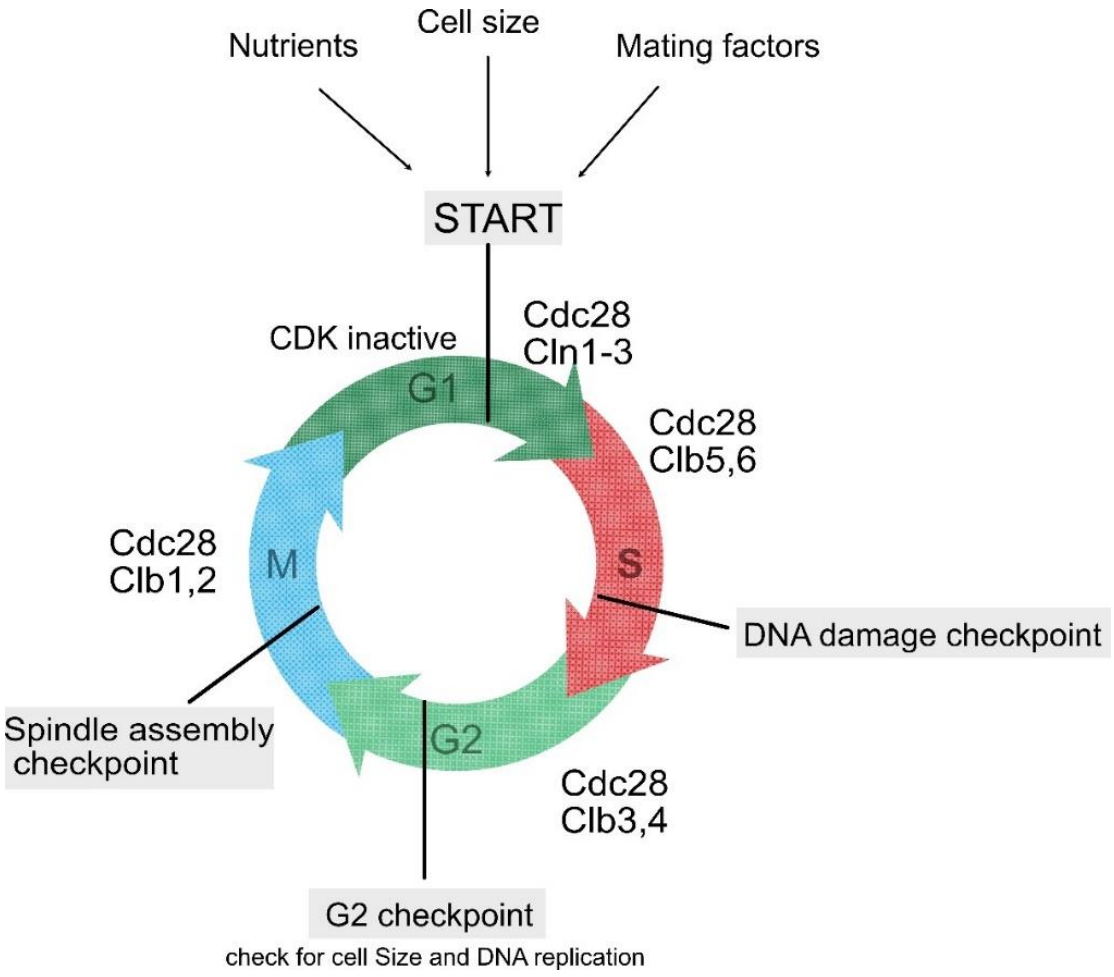

Figure 1.3. Yeast cell cycle regulation by CDKs

The cell cycle is divided into four phases (G1, S, G2 and M) and each phase is regulated by CDK activity. In yeast, Cdc28 associates with multiple cyclins (B-type cyclins, Cln1, 2 and 3 and Clb1, 2, 3, 4, 5 and 6) to phosphorylate different target proteins and thereby regulate the cell cycle. Entry into the cell cycle is based on various internal and external signals like cell size, nutrients, or mating factors. The cell cycle synchronizes the process of replication with subsequent cell division and the various check points ensure proper availability of nutrients, error free DNA replication and equal division of genetic material between the two cells.

The central regulators for the cell cycle progression are Cyclin-Dependent Kinases (CDKs) [111]. CDKs are serine and threonine kinases and their action depends on small regulatory proteins, the cyclins. As the name would suggest cyclin abundance fluctuates over the cell cycle as a result of protein synthesis and degradation and importantly the

activity of CDKs is regulated by the presence of cyclins [111]. In *S. cerevisiae,* only one CDK, namely Cdc28 (Cell division cycle 28) associates with multiple cyclins (B-type cyclins, Cln (CycLiN)1, 2 and 3 and Clb (CycLin B) 1, 2, 3, 4, 5 and 6) during different phases of the cell cycle (Figure 1.3). This allows phosphorylation of different target proteins and thus the flexible regulation of critical cell cycle events [107, 111].

In *S. cerevisiae*, based on environmental and internal signals like nutrient availability, presence of pheromones, attainment of a critical size, or the metabolic status a cell decides whether to enter cell cycle or undertake an alternative developmental program like entry into stationary phase. This decision point is called START [110, 112] (Figure 1.3). After committing to the cell cycle in the G1 phase, Cdc28 partners with Cln3 and activates the transcription factors, SBF (Swi4/6 cell cycle box (SCB) Binding Factor) and MBF (Mbp1 and Swi6 cell cycle box (MCB) Binding Factor) [113, 114]. Active SBF and MBF activate transcription of Cln1 / Cln2 and Clb5 / Clb6 respectively [115]. During the early G1, SBF is inactive because it is bound to Whi5 (WHIskey 5) [116]. As Cdc28/Cln3 accumulates beyond a certain threshold, it phosphorylates Whi5 multiple times [117], to cause its translocation from nucleus to cytoplasm, which results in the loss of SFB inhibition [116, 118]. The Sic1 (Substrate/Subunit Inhibitor of Cyclin-dependent protein kinase) inhibitor represses the activity of Cdc28/Clb5 and Cdc28/Clb6 by forming a complex with Cdc28/Clb5 and Cdc28/Clb6 [119, 120]. Sic1 is hyper-phosphorylated by Cdc28/Cln1 and Cdc28/Cln2 and which is a signal for Sic1 degradation through the SCF (Skp-Cullin-F-box) ubiquitin-mediated pathway [121]. Sic1 degradation increases Clb5 and Clb6 levels and the active Cdc28/Clb5 and Cdc28/Clb6 will start DNA replication and trigger the cell to enter S phase. DNA in S phase is carefully replicated and proofread. In case of DNA damage, replication is partially halted and the damage checkpoint is activated to repair DNA and ensures faithful DNA duplication and entry into M phase [109, 122].

After successful DNA replication, the transcription factor Mcm1 (Minichromosome maintenance 1), together with Fkh2 (ForKHead transcription factor 2) and co activator Ndd1 (Nuclear Division Defective 1) regulates Clb2 expression. The positive feedback loop for Clb1 and Clb2 activity enhances Clb1 and Clb2 expression and promotes cell-cycle events involved in mitotic entry during M phase [123]. Cdc28/Clb2 phosphorylates and inhibits SBF to downregulate transcription of G1 phase cyclins [124]. Also, Cdc28/Clb1 and Cdc28/Clb2 phosphorylates the APC (Anaphase promoting complex) [125]. The APC drives the cell cycle by ubiquitinating key proteins for proteolysis [126]. APC is activated by binding to the WD (Tryptophan-Aspartic acid repeat) repeat-containing protein Cdc20 (Cell division cycle 20) and Cdh1 (Cdc20 homologue 1). APC regulates the exit from mitosis and other events in late mitosis/G1 by binding to Cdc20 and Cdh1 respectively [127]. Cdc20 protein levels peak

up during mitosis to form Cdc20-activated APC (mitotic form of APC) that targets destruction box (D-box) containing proteins for proteolysis [128]. The entry into anaphase is determined by the spindle assembly checkpoint. An unattached kinetochore activates spindle assembly checkpoint where Bub1-Bub3 (Budding Uninhibited by Benzimidazole) and Mad2 (Mitotic Arrest Deficient) binds to Cdc20 directly and inhibit its ability to activate APC [129]. When all the chromosomes are connected to spindle pole and properly aligned in the metaphase plate, Cdc20-APC becomes active and ubiquitinates securin for proteolytic degradation. In M phase securin is phosphorylated by Cdc28/Clb1 and Cdc28/Clb2 near D-box therefore reducing its destruction by Cdc20-APC. Upon high Cdc20-APC activity, some securin is degraded releasing small amount of separase, which cleaves Scc1, a subunit of cohesin protein complex and enables the dissociation of cohesin [130]. Additionally, Cdc20-APC can also degrade B-type cyclins, including Clb1, 2 and Clb5, 6 [131]. Consequently, anaphase starts along with sister chromatid separation. As one pole of the spindle enters the bud and correctly locates there, the Cdc14 (Cell division cycle 14) phosphatase will be released from the nucleolus [132], dephosphorylates securin at Cdc28/ Clb1 and Cdc28/Clb2 sites and via a positive feedback loop increases the rate of ubiquitin mediated securin degradation by APC [133]. Late in mitosis, Cdc20 is degraded in an Cdh1-APC dependent manner. Cdh1 is a stable protein and present throughout the cell cycle. Cdh1 protein interaction to APC is regulated in a phosphorylation dependent manner. Cdh1 targets are recognised by the presence of D-Box and KEN motifs [128]. Cdc14 dephosphorylates Cdh1 to form Cdh1-APC, and targets Clb2 and Cdc20 for proteolysis. After successful spindle assembly and cytokinesis, the cell comes back to stationary G1 phase, waiting for signal for another round of cell division.

1.2.2. Replication occurs only once per cell cycle

As mentioned in the previous section, during S phase of the cell cycle, the genome is duplicated to ensure equal distribution of the genetic material between mother and the daughter cells following cell division [106, 134]. Also, replicated DNA is repaired with high fidelity to maintain genetic and genomic stability. Furthermore, following replication, the pre-replicative chromatin environment is re-established in order to preserve the cell identity [87]. The coordination of replication during the cell cycle with concurrent cellular processes such as gene transcription, protein translation and energy metabolism is achieved by action of CDK and Dbf4 (dumb-bell factor 4)-dependent kinase (DDK) [134, 135]. During S-phase CDK partners with the cyclin Clb5 and Clb6 to form S phase-CDK. Similarly, DDK is formed by the catalytic subunit Cdc7 and the regulatory subunit Dbf4. Dbf4 regulates DDK activity in an analogous manner to the cyclins. Both kinases, S phase-CDK and DDK are essential to initiate the process of DNA replication [135] (see below).

Replication initiates at specific DNA sequences called as origins of replication. In *S. cerevisiae*, origins are ~150bp autonomously replication sequences (ARS's) which contain a short 11bp AT-rich conserved sequence called as ARS consensus sequence (ACS) [136]. Budding yeast has ~400 confirmed origins evenly spread across 16 chromosomes [16, 137-139]. Interestingly, yeast origins are also characterized by array of well positioned nucleosomes as the ACS element lies within AT-rich NFRs [140, 141]. Origins are bound by the ORC (Origin Recognition Complex) to facilitate loading of replicative helicase (Mcm2-7/Cdt1; MCM) and initiate the process of chromosome replication [134]. In addition to the canonical role of ORC as the MCM loader, ORC interacts with chromatin remodelers (INO80, ISW1, ISW2 and Chd1) via Orc1 and regulates origin-adjacent nucleosome organization which is essential for replication [142].

Yeast cells initiate replication in two distinct steps. The first step is called origin licensing, where, during late mitosis and G1 phases of the cell cycle, all origins are bound by ORC [143]. The presence of other licensing factors, Cdc6 and Cdt1, leads to the recruitment and loading of two MCM complexes onto double stranded DNA [144]. However, the loaded MCM double hexamer is inactive for DNA unwinding and the resulting complex is called pre-replicative complex (pre-RC) [145] (Figure 1.4 A). Pre-RC´s are formed on chromatin to mark the potential sites for origin activation [134].

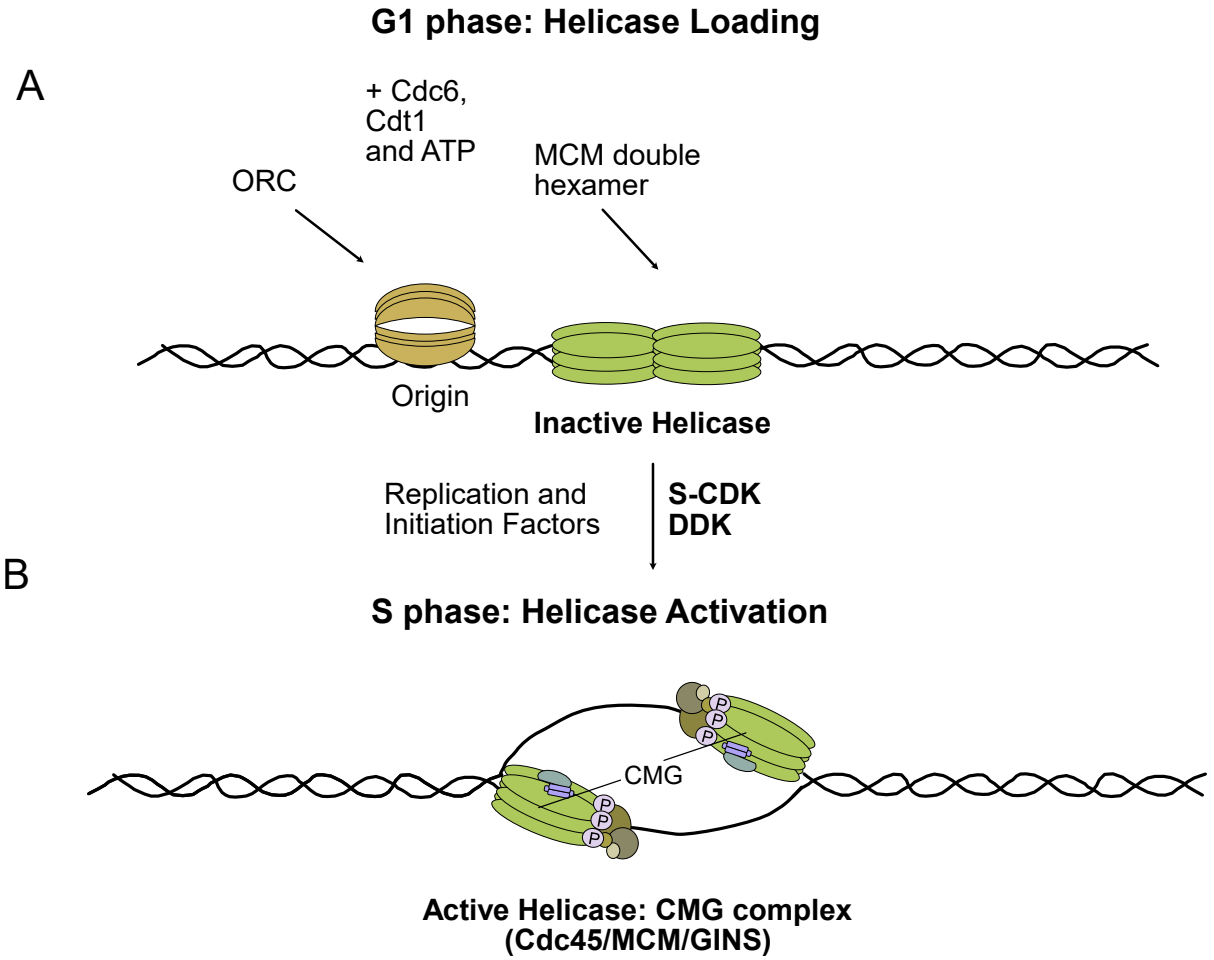

Figure 1.4. Two-step mechanism of DNA replication initiation

(A) Loading mechanism of the eukaryotic replicative helicase. In G1 phase of the cell cycle, origins are bound by ORC (origin recognition complex) and other initiation factors like Cdc6, ATP and Cdt1 to lead to recruitment of MCM2-7 hexamer.

(B) During S phase, S phase CDK and DDK with other replication and initiation factors promote activation of loaded MCM2-7 hexamers to form active CMG helicases during origin firing.

The figure 1.4 is adapted from Coster et al 2014 [146] and Douglas et al 2018 [147].

Amazingly, whether yeast or humans, the entire genome is replicated in exactly one complete round of replication. As said above, helicase loading is restricted to G1 phase of the cell cycle and this is because S-CDK inhibits pre-RC formation in other phases than S phase [148, 149]. During G1 phase, S-phase CDK is inactivated by Cdh1-APC and the CDK inhibitor Sic1 [150]. From late G1 phase until mitosis, S-phase CDK levels increase and thus inhibit origin licensing by multiple mechanisms [151]. Firstly, late G1 and S-CDKs regulate Cdc6 stability by direct phosphorylation and targeting it for ubiquitin mediated proteolysis

[152, 153]. Secondly, phosphorylation of Cdc6 by G2 and M-phase CDKs blocks the licensing activity of Cdc6 [154, 155]. Thirdly, S-phase CDK phosphorylation controls the nuclear export of the MCM [156, 157]. As Cdt1 interacts with MCM, this also translocates Cdt1 to the cytoplasm to prevent it from being involved in another loading step [158]. Finally, ORC is inhibited by S-CDK phosphorylation of Orc2 and Orc6 [159]. In this elegant way, the cell cycle machinery controls re-licensing such that genome is replicated exactly once per cell cycle.

To ensure the relatively large eukaryotic genomes (e.g. 14 mega base pairs in yeast to 3 giga base pairs in human) are replicated in a timely manner during the relatively short S phase (e.g. ~15 minutes in yeast and ~8 hours in humans), replication has to initiate from multiple replication origins [135]. Interestingly, from all origins licensed, firing is happening only to a subset of origins during an unperturbed cell cycle. At the beginning of S phase, DDK directly phosphorylates the MCM complex [160] and generates the binding site for the firing factors Sld3, Sld7 and Cdc45 [160, 161]. Alongside with DDK, S-CDK phosphorylates Sld3 and another initiation factor Sld2, which facilitates association of the GINS complex and DNA polymerases δ and ε to inactive pre-RC [162, 163]. This then converts the pre-RC into the active helicase or the CMG complex [164, 165]. Now, two active CMG complexes move in opposite direction to support bi-directional DNA unwinding and replication elongation [134] (Figure 1.4 B).

Replication initiation from one origin more than once leads to re-replication, an event that generates multiple copies of single genomic regions [166]. This leads to genetic imbalance and promotes genome instability [167, 168]. The phenomenon of genomic instability is observed in many cancers and therefore genome duplication is under stringent cell cycle control [168], thus, as described above, it is of utmost importance for cells to control replication initiation very stringently during the cell cycle.

1.2.3. Chromatin is inhibitory to the replisome

The natural substrate of replication is not naked DNA but chromatin and it is therefore not surprising that replication is strongly influenced by the nucleosome organisation and the chromatin landscape [169].

On the one hand, Chromatin helps to specify the sites of replication initiation and therefore is important for origin selection [39]. *In vitro*, pre-RC formation and initiation on naked DNA templates does not strictly depend on the sequence of the ACS. However,

chromatinization of the template dramatically influences the ability of ORC to bind stably at ACS and to form the pre-RC [39, 170].

On the other hand, chromatin is inhibitory to replication machinery. After origin selection, MCMs are loaded onto origins and MCMs are converted to active CMG helicase complex. However, after origin firing at the onset of S phase, the replication machinery encounters nucleosomes as a barrier [39, 170, 171] and cells have to take a significant effort to relieve this chromatin barrier. For example, additional chromatin factors like FACT/Nhp6, INO80 or ISW1A and histone acetylation are required for efficient chromatin replication [39].

Intriguingly, although a natural barrier for replication, chromatin is beneficial for origin function. ACS motifs in ARS are free of nucleosomes which is occupied by ORC to initiate replication. Binding of ORC at origins influences the positions of origin-proximal nucleosomes [16, 141]. Repositioning of origin-proximal nucleosomes reduces helicase loading and origin function [172, 173] and the loaded helicases seem to interact with these nucleosomes [174]. It has been shown that in addition to MCM loader, ORC also functions as a barrier factor for nucleosome positioning. Barrier factors act as a reference point for remodelers with spacing activity (INO80, ISW1a, ISW2 and Chd1) to generate arrays of spaced nucleosomes at the origins. The nucleosome architecture at origin might help in escape of activated helicase from origin and therefore is crucial for replication and cell viability. This suggests that chromatin per se is a barrier to replication but is also essential for origin selection and activation [142].

Chromatin replication is a dual process in which chromatin is simultaneously transiently disassembled to allow the passage of replication fork and the synthesis of new DNA. To counteract this necessary disassembly of chromatin, ATP dependent chromatin remodelers, histone chaperones and epigenetic modifiers are needed re-establish chromatin post replication [39, 175]. Histones on chromatin are subjected to histone acetylation to modulate the structure of chromatin and directly correlates to gene activity [176, 177]. It has been shown that the histone acetylation in the vicinity of replication origins promotes their functionality [178]. Also, histone acetylation by yeast histone acetyltransferases NuA4 / SAGA promotes chromatin replication *in vitro* [39]. Moreover, acetylated histones lead to the recruitment of a S-phase CDK regulated chromatin segregase, Yta7 (Yeast Tat-binding Analog 7) to promote chromatin replication [179]. Overall chromatin structure and landscape regulates the process of chromatin replication.

1.2.4. DDK regulates replication and plays a role beyond S phase

Compared to CDK, where many targets have been identified and described, only a few have been identified for DDK. The reason for this is, at least in part, the presence of a consensus site in CDK target proteins [180], in contrast to DDK, where no consensus site has been described so far. It was suggested that a serine or a threonine followed by an acidic residue at the +1 position might be a putative DDK phosphorylation motif [181]. Furthermore, sequential phosphorylation events, where a negative charge at the +1 position is introduced by a prior phosphorylation event by a second kinase, were proposed to be important for DDK phosphorylation [182].

During the process of replication elongation, the ongoing replication fork can come to a halt when it encounters obstacles e.g. a protein barrier or a DNA damage site. To resume stalled replication, it is necessary to preserve stability of the fork because the loss of essential proteins from replisomes or disengaging them from DNA could cause fork instability and ultimately, the collapse of the replication fork [167, 183]. The DDK-dependent phosphorylation of Mcm4 during replication initiation and its maintenance within the CMG complex during replication elongation correlates with replication fork stability [184, 185] (Figure 1.5 A). In budding yeast, the checkpoint adapter protein Mrc1 together with Tof1 and Csm3 is essential for maintaining the connection between CMG helicase and replisome [186, 187]. Also, Mrc1 is required to regulate the speed of the replication fork [188, 189]. The initial association of Mrc1 with chromatin during replication initiation is DDK dependent [190].

In line with this, the checkpoint kinase Rad53 (RADiation sensitive 53) physically interacts with DDK such that DDK cannot phosphorylate the MCM complex anymore, leading to inhibition of origin firing [191-194]. Most interesting, Rad53 does not phosphorylate DDK during this interaction (Figure 1.5 B). DDK further assists in the checkpoint response by phosphorylating Rad9, a component of the repair pathway, which promotes Rad9 release from damaged chromatin to facilitate Rad53 associated repair [195, 196]. If not repaired, DNA damage accumulation can cause genomic instability, which is a prime feature of pre-cancerous and cancerous cells [167]. DDK is highly-expressed in several primary tumors and tumor cell lines [197-203]. DDK over expression has also been associated with poor prognosis in thyroid cancers [204], advanced clinical stage in ovarian cancers [205] and breast cancers [206]. Currently, regulation of DDK levels in tumor cells is being explored as an appealing strategy for tumor therapy [207].

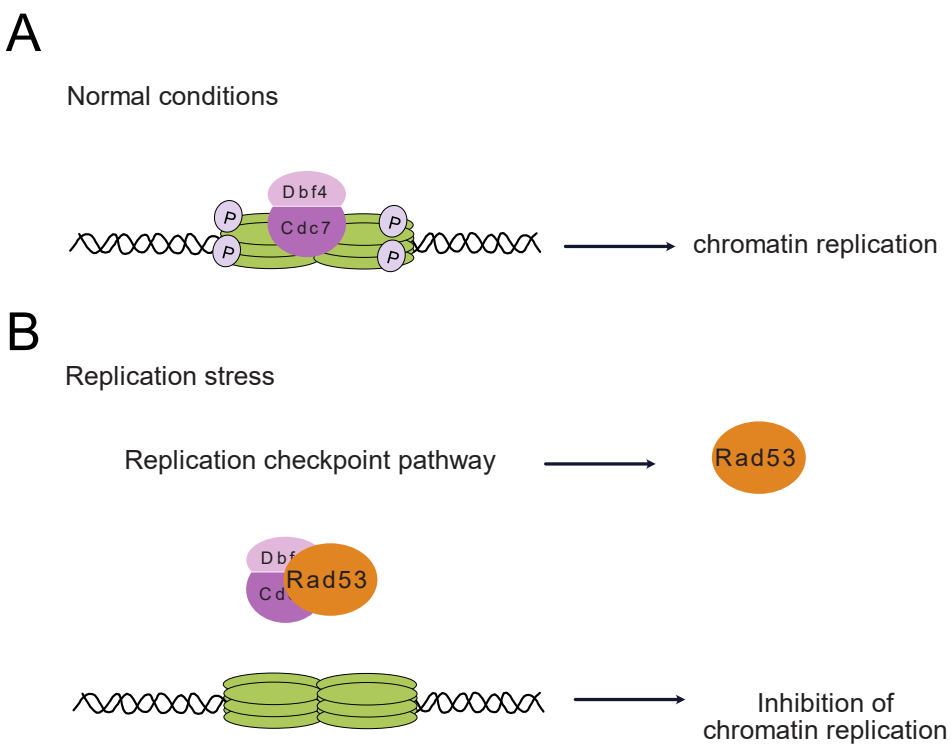

Figure 1.5. DDK inhibition by Rad53 in kinase independent manner

(A) DDK phosphorylates Mcm2 and Mcm4 subunits of MCM complex during replication initiation and maintains phosphorylation to support chromatin replication

(B) Under replication stress like conditions, replication checkpoint pathway activates checkpoint effector kinase Rad53. Rad53 phosphorylates various proteins involved in DNA damage pathway in a kinase dependent manner. However, in a kinase independent manner Rad53 physically binds to DDK and inhibits chromatin replication.

DDK has also been shown to play a role in post-replicative chromatin formation. For example, in budding yeast, DDK phosphorylates the histone chaperone CAF1 [208, 209], CAF1 binds PCNA (Proliferating Cell Nuclear Antigen) and deposits H3-H4 tetramers behind the replication fork on newly synthesized DNA [210, 211]. Also, it has been shown that Mcm2 can function as histone chaperone distributing parental histones H3-H4 tetramers onto newly synthesized DNA on the lagging strand [212, 213]. Since Mcm2 is a target of DDK mediated phosphorylation, it might be possible that DDK phosphorylation regulates Mcm2 chaperone activity [183].

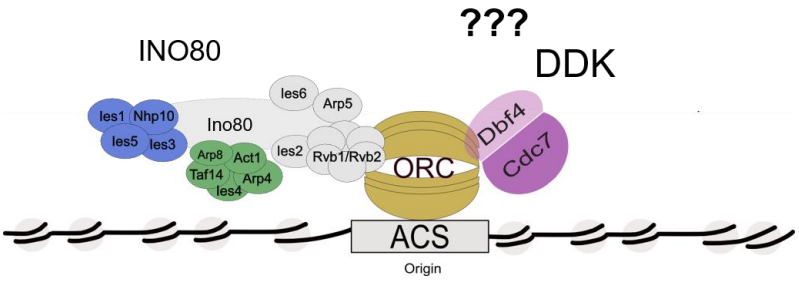

Figure 1.6. Proposed model of DDK function at replication origins during G1 phase

Beyond S phase, low levels of DDK activity are present during G1 phase, where Dbf4 is recruited to early origins [214, 215] through its interaction with forkhead transcription factors Fkh1 and Fkh2 [216] and the Orc2 subunit of ORC [217, 218]. However, the role of DDK at early origins during G1 phase remains unclear. It could be that DDK starts to phosphorylate the MCM complex in G1 phase, which might be important for efficient peak-phosphorylation during S phase. Or it could be that DDK has another, yet unknown target at early origins in G1 phase. Most interestingly, it has recently been revealed that ORC serves a second significant function beyond its conventional role in acting as the MCM loader. ORC interacts with INO80, the major chromatin remodeler involved in replication, via its Orc1 subunit. This is important to generate well-spaced nucleosomal arrays at origins. This chromatin architecture is established in G1 phase prior to MCM loading and is important for productive replication initiation [142]. We speculated that DDK might phosphorylate chromatin remodelers like INO80, which might be important for this process (Figure 1.6).

1.3. Aim of the thesis

As mentioned above, DDK is somewhat of a mysterious kinase and it has proven difficult to map DDK targets because of complete lack of a DDK-consensus phosphorylation sequence. In line with this, very little is known if and if yes, how chromatin factors that function in replication are regulated. We hypothesize that chromatin factors, analogously to replication factors might be regulated by signals of the cell cycle machinery too, in part via phosphorylation by DDK.

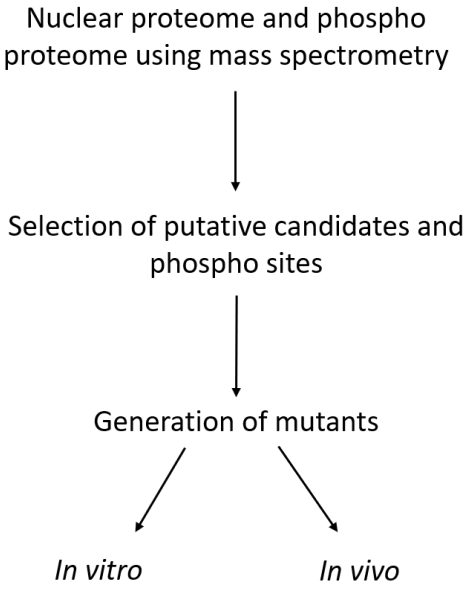

Figure 1.7. Workflow of the study

To answer these questions, I employed mass spectrometry approaches to find DDK targets. Specifically, I established methods to inhibit DDK directly and indirectly and performed nuclear phospho-proteomes and proteomes to define the DDK nuclear phospho-proteome with a special emphasis on chromatin factors. Data analysis of my proteomics data revealed DDK-specific phospho sites on many chromatin factors including the ATP-dependent chromatin remodeler INO80 or the histone chaperone Spt6. Further, we will mutate phospho-sites on interesting candidates from our mass spectrometry data and test their effect on chromatin replication using various *in vitro* and *in vivo* approaches (Figure 1.7).

In section 2.2 I investigated the role of phospho sites on the Arp8 subunit of INO80 to pinpoint, biochemically as well as cell biologically, that INO80 is a bona-fide target of DDK and that phosphorylation is critical for INO80 function. In discussion, I will also discuss about DDK phospho sites on Spt6 and show that Spt6 might be the novel candidate for chromatin replication.

2. Results

2.1. Mass spectrometry

In order to obtain an overview of a DDK-dependent phosphorylation network in the nucleus, we employed unbiased label-free mass spectrometry.

We were most interested in identifying proteins and protein complexes that modulate chromatin structures (chromatin factors) that are involved in DNA template processes like DNA replication. Yeast cells undergo a closed mitosis and detecting phosphorylation sites on chromatin factors is challenging as they are low in abundance compare to other proteins of the cell [219]. Highly abundant cytoplasmic peptides can mask low abundant chromatin associated peptides [220] such that they are either lost in sample processing or cannot be identified during database search. Further, detected phosphorylation sites on nuclear targets might be difficult to associate with a kinase after whole-cell fractionation. For example, after cell fractionation, a kinase, which is normally excluded from the nucleus and has cytoplasmatic targets could, get access and phosphorylate nuclear proteins, thus increase the false positive rate.

These reasons make it difficult to identify DDK-associated phosphorylation events on chromatin factors in whole cell proteomes. Therefore, we decided to enrich for nuclear fractions to increase analytical sensitivity of phosphorylation events. We designed our experiments to generate nuclear proteomes and nuclear phospho proteomes under conditions where DDK is active or not.

We performed nuclear fractionation to enrich chromatin associated proteins and phosphorylation sites. Using this approach, we could find DDK-dependent phospho sites on all chromatin factors instead of targeting only one chromatin factor.

2.1.1. DDK inhibition

2.1.1.1. DDK inhibition using temperature

DDK is an essential kinase [134] and therefore cannot be deleted. As an alternative strategy, we used the *cdc7-4* allele [221]. This is a temperature-sensitive version of *CDC7*, which shuts down DDK activity at non-permissive temperature (37 ^{o}C). Normally, yeast cells

are grown at 30 ° C but *cdc7-4* cells have an optimal growth rate at 25 ° C (permissive temperature). This eliminates DDK function very effectively compared to other strategies like making use of chemical DDK inhibitors, which tend to be quite unspecific with a broad range of action and thus inhibit other kinases as well. However, one disadvantage of this strategy is temperature-associated changes in protein abundance or protein phosphorylation.

Using *cdc7-4* allele containing yeast strain, we grew cells at 25 ° C (DDK is active) and 37 ° C (DDK is inactive) for 3 hours and isolated the nuclear fractions (Figure 2.1 i)). Four biological replicates were collected and processed for mass spectrometry using a EasyPhos TiO_2 based phospho peptide enrichment protocol for nuclear phospho proteome [222] (Figure 2.2 i). We also performed nuclear proteomes [222] to normalize changes in levels of phosphorylation to corresponding changes in protein amounts.

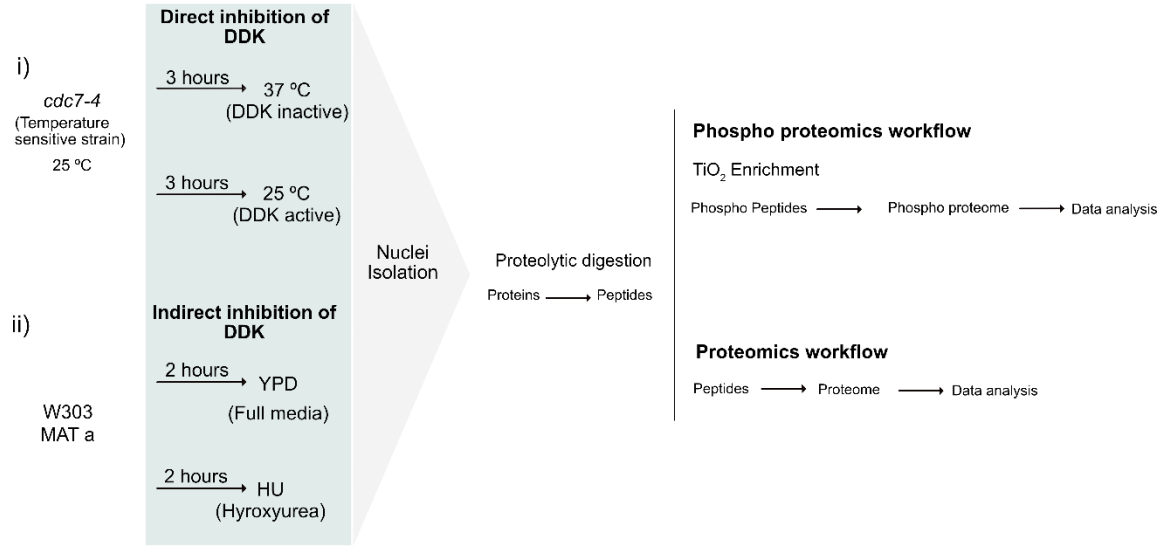

Figure 2.1. Work flow for mass spectrometry sample processing

We found ~2500 proteins in the nuclear proteome dataset of four biological replicates. We first analysed for the enrichment of nuclear proteins and observed 32% enrichment of nuclear proteins. The secretory pathway for membrane bound protein production includes the Endoplasmic Reticulum (ER) attached to the nucleus and the Golgi apparatus which transport nuclear proteins to other membrane bound organelles. Additionally, many mitochondrial proteins are also found in nucleus to regulate gene expression and metabolic function of the cell [223]. This suggests that our nuclear protein enrichment works and we found overall 60% enrichment of nuclear proteins (Figure 2.2).

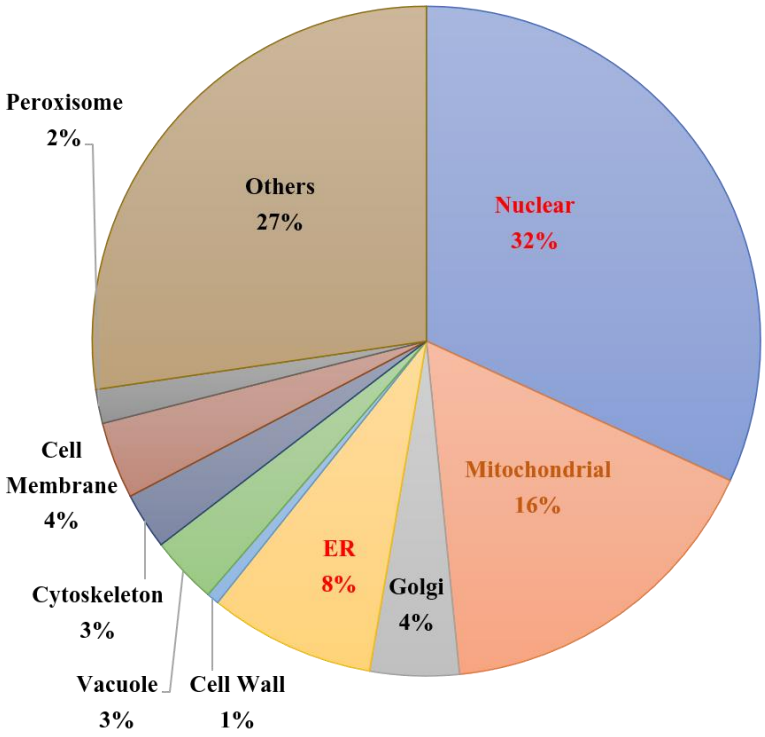

Figure 2.2. Pie chart representing the enrichment of proteins of the nucleus and nuclear associated organelles in isolated nuclear fractions.

We observed ~4000 phospho sites in our complete dataset of four biological replicates. The four biological replicates in this experiment increases the probability of detection and better filtering of low abundant phospho peptides compared to unmodified peptides. In phospho proteomes due to changes in protein abundance, all phospho sites were normalised to nuclear whole proteomes. The 25% of phospho sites which account for variability within the dataset are plotted in a heat map (Figure 2.3). These 25% phospho sites between DDK active or DDK inactive sample cluster and contributes to the maximum variance that categorises either phenotype with unique phospho sites.

As mentioned previously, DDK phosphorylates the unstructured N-terminal tails of Mcm2, Mcm4, and Mcm6 at multiple sites to initiate replication [224]. In our raw phospho proteome dataset, we find 30 phosphorylation sites on MCM complex subunits. Upon analysis, we found 17 phosphorylation events on different MCM subunits to be present in DDK active (Appendix I, Table 14), showing that our approach works.

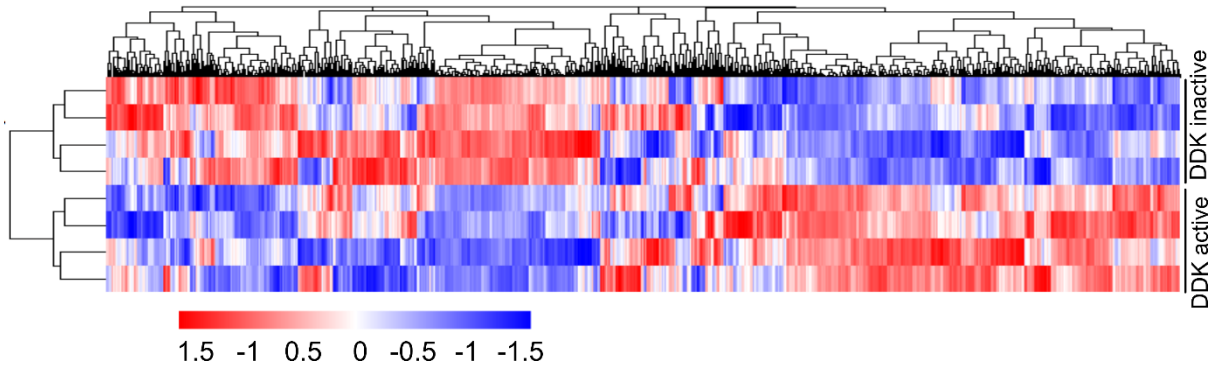

Figure 2.3. Phosphorylation events upon direct DDK inhibition using the temperaure sensitive *cdc7-4* allele

Heat map representing log_2 foldchange of ~1150 phosphorylation sites over four biological replicates upon DDK inhibition using the temperature sensitive *cdc7-4* strain. The changes in total phospho proteome were normalized to changes in nuclear proteome. The columns marked with DDK active represent four biological replicates of the control sample where cells were grown at 25 ° C and the columns marked with DDK inactive represent four biological replicates of the treatment group where cells were grown at 37 ° C. The black lines represent the hierarchical cluster analysis pattern of phospho sites across four replicates. Blue indicates downregulated phospho sites and red indicates upregulated phospho sites, intensity of the either colour indicates the magnitude of phosphorylation.

DDK inhibition using temperature is accompanied with certain constrains and limitations. *cdc7-4* cells normally grow at 25 ° C and DDK is inhibited by growing cells at 37 ° C. However, both 25 ° C and 37 ° C are not optimal for yeast because the ideal temperature for growing yeast cells is 30 ° C. Both 25 ° C and 37 ° C could activate heat-shock associated processes and thus influence temperature associated phospho sites. Because of this, we decided to perform a second screen where DDK was inhibited in a different way. Our rationale of this two- pronged strategy was to define a “high confidence list” of proteins that were found in both screens where DDK inhibition resulted in a reduction of phosphorylation events.

2.1.1.2. DDK inhibition by checkpoint activation

As described above (Figure 1.5), the checkpoint kinase Rad53 can physically inhibit DDK, independent of its kinase activity. We hypothesized that we could use this ability of Rad53 to inhibit DDK and would avoid temperature-associated problems of the *cdc7-4* strategy. However, apart from physically inhibiting DDK, this would also trigger the damage

response and activate Rad53's kinase activity to phosphorylate proteins involved in DNA damage pathway [225-227].

Taking advantage of damage dependent DDK inhibition during replication stress, we designed another experiment where we inhibited DDK using hydroxyurea (HU), a replication stress drug. HU depletes the cells of dNTPs [228] and results in stalled replication forks. Upon prolonged treatment with HU, stalled replication forks collapse into DSBs and activates the checkpoint [229]. We grew WT cells for 2 hours in presence and absence of HU at the optimal temperature 30 ^{o} C and isolated the nuclear fractions (Figure 2.1 ii). As with the other screen, four biological replicates were collected and processed for mass spectrometry using a EasyPhos TiO_2 based phospho peptide enrichment protocol for nuclear phospho proteomes [222] (Figure 2.1). We also performed nuclear proteome [222] to normalize changes in levels of phosphorylation with corresponding change in protein.

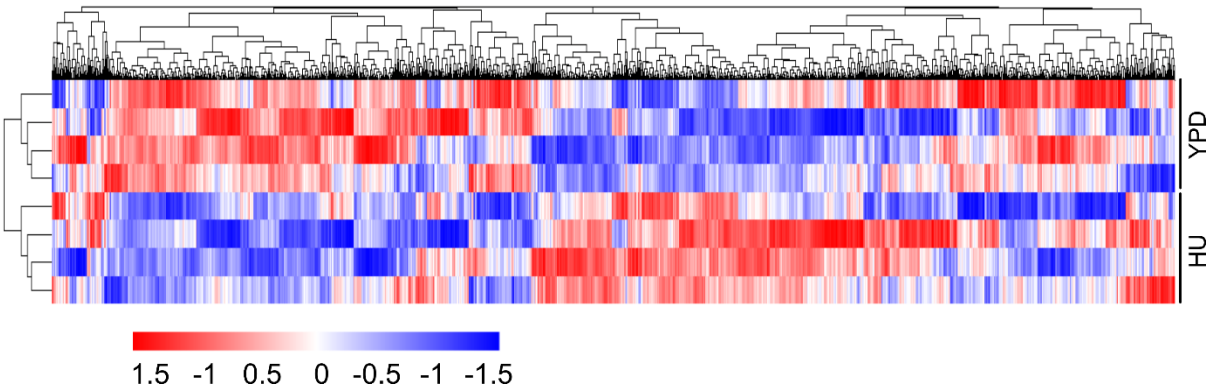

Figure 2.4. Complementary screen to find DDK phospho sites by DDK inhibition using checkpoint activation

Heat map representing log_2 foldchange of ~2450 phosphorylation sites over four biological replicates upon DDK inhibition using replication stress. The changes in total phospho proteome were normalized to changes in nuclear proteome. The columns marked with YPD represent four biological replicates of the control sample where cells were grown in full media and the columns marked with HU represent four biological replicates of the treatment group where cells were grown in presence of hydroxyurea. The black lines represent the hierarchical cluster analysis pattern of phospho sites across four replicates. Blue indicates downregulated phospho sites and red indicates upregulated phospho sites, intensity of the either colour indicates the magnitude of phosphorylation.

We observed ~6000 phospho sites in our dataset over four biological replicates. As stated in section 2.1.1.1, the four biological replicates in this experiment increases the probability of detection and better filtering of low abundant phospho peptides compared to

unmodified peptides. In phospho proteomes due to changes in protein abundance, all phospho sites were normalised to nuclear whole proteomes. The top 25% of phospho sites which account for variability within the dataset is plotted in a heat map (Figure 2.4). These phospho sites cluster between YPD or HU sample and contributes to the maximum variance that categorises either phenotype with unique phospho sites

As expected, replication stress activates Rad53 kinase activity and we found phosphorylation of proteins involved in DNA Damage pathway like Mrc1, Rad9, and Dun1 [230]. As expected, we found 14 phosphorylation events on Rad9, 25 on Mrc1 and 12 on Dun1 appearing when cells were treated with HU (Appendix II, Table 15), showing that HU induced the checkpoint. However, as with the *cdc7-4* screen, we focused on phospho-sites which were downregulated upon HU treatment.

2.1.2. Overlap of DDK inhibition datasets to find potential DDK sites

We then compared our nuclear phospho proteome datasets from the two different approaches. As mentioned in the previous section, our rationale was that sites which were downregulated upon inhibition in both screens would be our “high confidence” sites. Thus, we were specifically looking for phospho sites which were down-regulated upon temperature and HU dependent DDK inhibition. When we analyzed our two datasets, we found 479 and 1092 phosphorylation events which were downregulated upon temperature and HU treatment respectively. Upon overlap of the two datasets, we found 301 common phospho sites which were downregulated upon both temperature and HU treatment and defined those as our “high confidence” hits (Figure 2.5 A).

Next, we performed gene ontology (GO) analysis on the overlapping phospho sites between two data sets using Saccharomyces Genome Database (SGD). The unbiased functional annotation analysis of the 301 overlapping phospho sites revealed GO term associated with molecular functions like, protein S/T kinase activity, chromatin binding, mRNA binding, protein binding and ATP binding (Figure 2.5 B). Within these 301 overlapping phospho sites between the two datasets we specifically focused on the INO80 complex, as INO80 is known to regulate chromatin replication *in vitro* [39]. We found phospho sites on Ino80, Arp8, Ies2 and Ies4 subunits of INO80 complex which were down-regulated upon temperature and HU dependent DDK inhibition. Because we only found Arp8 to be phosphorylated by DDK in an *in vitro* kinase assay (Figure 2.11), we focused on Arp8.

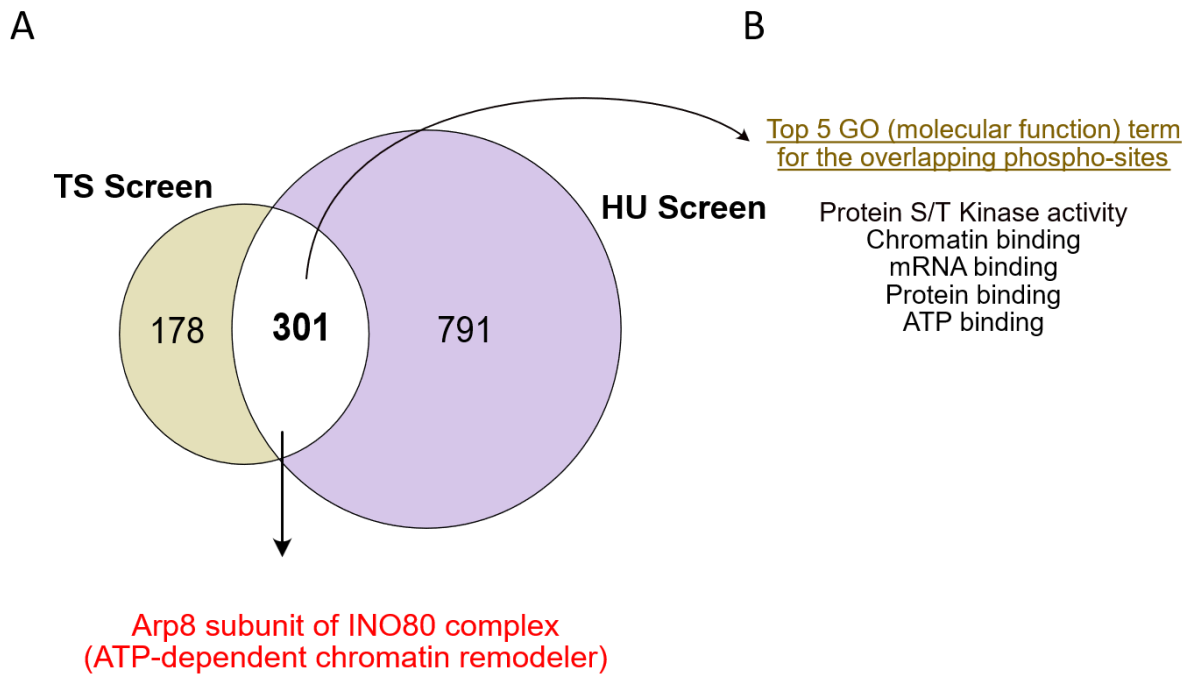

Figure 2.5. Overlap of mass spectrometry datasets to find DDK phospho sites

(A) Venn diagram shows the overlap of our two mass spectrometry datasets, where DDK was inhibited using temperature and HU. We found 301 common phospho sites between the two datasets. (B) Gene ontology analysis of 301 common phospho sites between two datasets associates with molecular functions like protein S/T kinase activity, chromatin binding, mRNA binding, protein binding and ATP binding.

2.1.3. Cell cycle mass spectrometry

During S phase, DDK plays a specific role by phosphorylating MCM complex to initiate the process of chromatin replication. We next questioned if most of DDK-dependent phosphorylation happens in S phase and if yes, if the same is true for Arp8.

We performed mass spectrometry experiments to determine temporal changes of phospho proteomes throughout an unperturbed cell cycle. To do so, we grew MAT a wildtype cells in YPD at 30 ° C until cells reached OD 600nm = 0.2 and arrested cells in G1 phase with alpha factor pheromone. A second dose of alpha factor was added after 60 mins. Cells were washed with equal amount of prewarmed YP media and cells were resuspended in 1.2 L of YPD. 200 ml sample of cells were collected as 0 min time point (T0) and remaining cells were grown at 30 ° C. During growth, 200 ml sample of cells were collected

at 10, 20, 30, 45, 60 mins time (T10, T20, T30, T45, T60) point to capture different phases of the cell cycle. All the collected samples were treated with 10% sodium azide (NaN_3) for 5 mins on ice so that most metabolic activity was shut down to get a snapshot of the phosphorylation status of the nuclear factions at each time point. From each time point sample, 1ml sample was prepared for flow cytometry and rest of the sample was used to prepare nuclei. Nuclear fraction was isolated from four biological replicates (Figure 2.6 A). Later, nuclear fractions were processed for mass spectrometry using a EasyPhos TiO_2 based phospho peptide enrichment protocol for nuclear phospho proteome [222] (Figure 2.2). We also performed nuclear proteome [222] to normalize changes in levels of phosphorylation with corresponding change in protein.

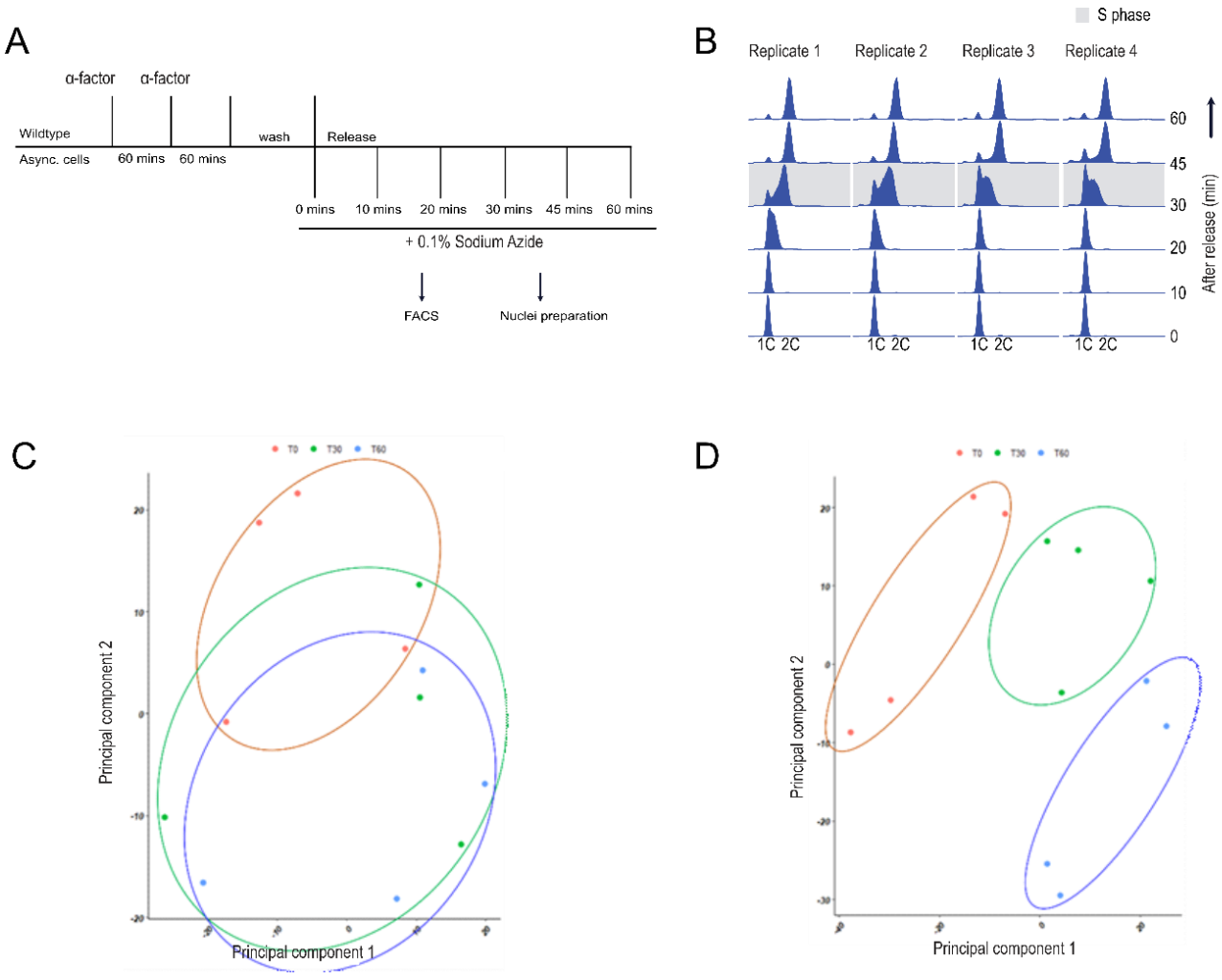

Figure 2.6. Nuclear proteome and nuclear phospho proteome over an unperturbed cell cycle

(A) Workflow of cell cycle arrest and release experiments and sample collection for cell cycle time points.

(B) Following release, the progression through S phase was monitored using flow cytometry. 30 min samples appear to be S phase. 1C and 2C indicate non-replicated or replicated DNA, respectively.

(C) PCA (principal component analysis) plot showing protein distribution in T0, T30 and T60 timepoints over four biological replicates.

(D) PCA (principal component analysis) plot showing phosphorylation mark distribution in T0, T30 and T60 timepoints over four biological replicates.

In (C) and (D), the T0 time point is represented by orange circle, T30 time point is represented by green circle and T60 time point is represented by blue circle.

Using flow cytometry, we first determined which time point would correspond to the S phase. We observed that T30 sample correspond to the S phase as it contains a significant population of dividing cells (Figure 2.6 B). In our nuclear proteome and phospho proteome dataset over an unperturbed cell cycle, we observed ~4,000 proteins that are regulated by ~12,000 phospho sites across all time points together. Taking extreme time points (T0 and T60) and a middle time point (T30), we analysed nuclear proteome and phospho proteome data to see how proteins are regulated by phosphorylation marks. Upon clustering we observed a large overlap of proteins between T0, T30 and T60 suggesting same proteins might be regulating at different phases of cell cycle (Figure 2.6 C). However, when we looked at phosphorylation marks in the same time points, we observed a completely different pattern of phosphorylation marks that were present in each cell cycle phase (Figure 2.6 D). This suggests that based on different phosphorylation signature on proteins, the phospho sites not only defines but also regulates different cell cycle phases (Figure 2.6 C and D). Therefore, phosphorylation plays an important role in cell cycle control and progression towards cell division.

Firstly, we wanted to validate our cell cycle Mass spectrometry data and analysed the major target of DDK, the MCM complex and wanted to know if phosphorylation peaks in S phase, as described [224]. In the raw data, intensity values with zero in whole dataset were imputed, averaged from four replicates and $\log_2$ (intensity) of averaged intensity were calculated. We found 15 phosphorylation sites on the N-terminal of Mcm4 subunit which were phosphorylated in S phase (T30). We plotted $\log_2$ (intensity) of three sites (S120, S52 and S56) out of these 15 sites across different timepoints of the cell cycle and observed highest phosphorylation of these sites in T30 time point or S phase of the cell cycle (Figure 2.7 A). As expected, the phosphorylation levels peak in S phase, which nicely demonstrates that our cell cycle datasets are meaningful.

Similar to Mcm4 phospho sites we analysed and plotted $\log_2$ (intensity) of Arp8 phospho sites across different timepoints of the cell cycle. We observed a different phosphorylation pattern for Arp8 phospho sites compared to the Mcm4 phospho sites. Arp8 phosphorylation

events were highest during the G1 phase and decreases slowly as the cell cycle progresses (Figure 2.7 B). These results indicate that DDK phosphorylation of Arp8 occurs during the G1 phase and is mainly maintained throughout the cell cycle. This is in line with our hypothesis that DDK might phosphorylate Arp8 prior to S phase in G1, possibly to influence INO80's function in setting up nucleosomal arrays at origins of replication.

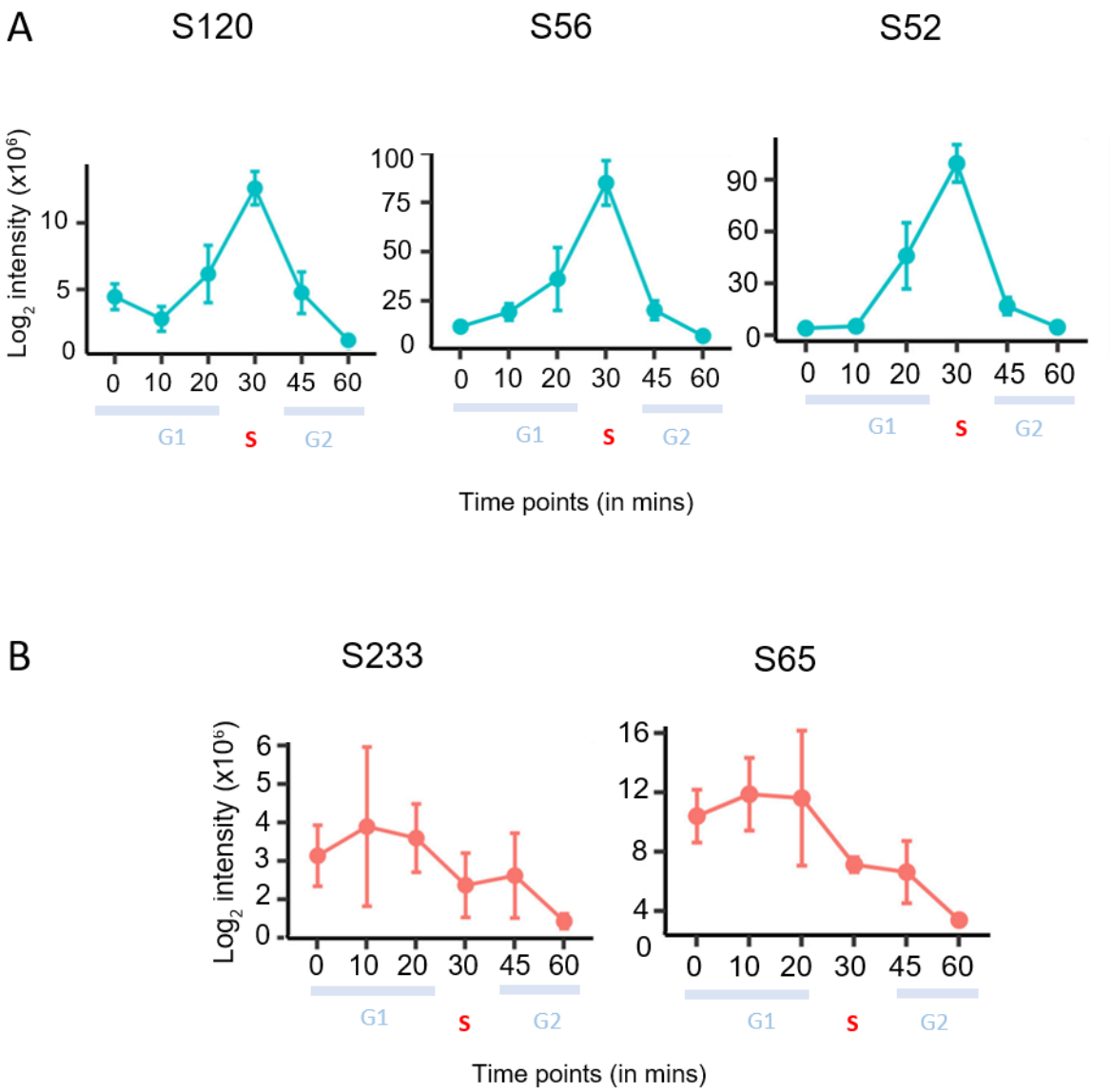

Figure 2.7. Mcm4 and Arp8 phosphorylation over an unperturbed cell cycle

(A) Graphs representing phosphorylation of three N-terminal Mcm4 sites (S120, S56 and S52) at different time points over an unperturbed cell cycle.

(B) Graphs representing phosphorylation of S233 and S65 phosphorylation site on Arp8 at different time points of unperturbed cell cycle.

2.2. INO80 is a known player of chromatin replication

INO80 is an evolutionarily conserved, multi-subunit chromatin remodeling complex and plays a central role in chromatin remodeling and genomic stability. INO80 comprises the main ATPase Ino80, the actin and actin-related proteins Arp4, Arp5 and Arp8, Ino-eightly subunits Ies2, Ies4 and Ies6, Taf14 and the AAA^+- ATPases Rvb1 and Rvb2 [231]. INO80 is shown to be associated with many cellular processes for example, transcription, replication, and DNA damage [232]. INO80 promotes replication fork progression during DNA synthesis [233] and yeast cells without a functional INO80 complex progress slowly during a normal S phase [234]. Additionally, INO80 plays an important role in rescue and restart of stalled replication forks under replication stress like conditions. INO80 complex has been mapped at replication origins when yeast cells were challenged with HU [234-236]. *ino80* mutants fail to resume replication upon acute treatment with genotoxic drugs like HU and MMS (methyl methane sulphate) [234, 235, 237, 238] suggesting INO80's role not only in DNA replication but also in the recovery from replication stress.

Further evidence for INO80's role during replication came from *in vitro* studies. Replication of naked DNA template using purified proteins was successfully reconstituted [170, 239]. However, upon challenging the system with chromatin template, replication required additional factors. Rates of replication on chromatin template were restored upon addition of histone chaperone FACT/Nhp6, histone acetylation and the ATP-dependent chromatin remodeler INO80 [39]. This shows that INO80 plays an important role in chromatin replication. However, the exact role of INO80 during replication remained enigmatic until recently, where it was shown that INO80 is important for establishing the chromatin architecture at origins, for efficient replication initiation [142].

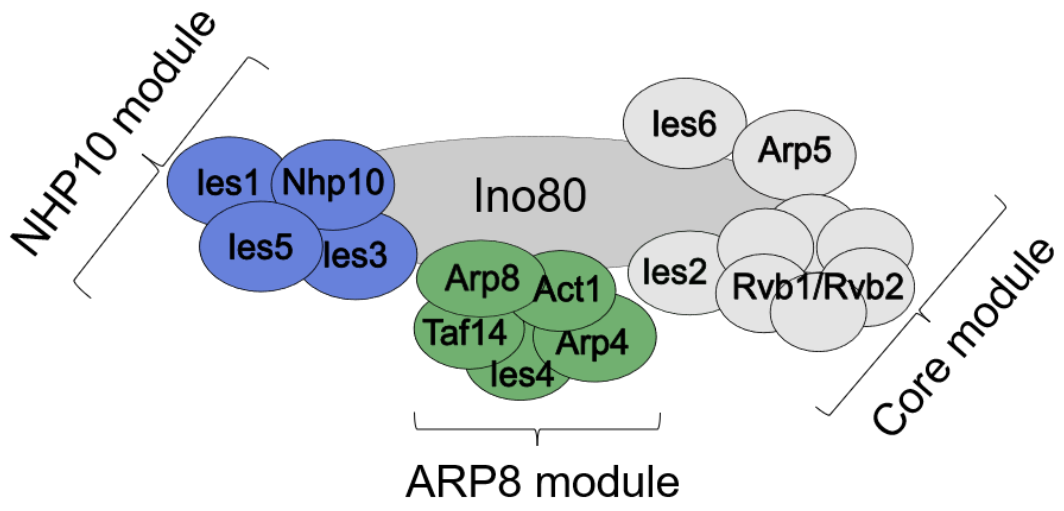

Figure 2.8. INO80 architecture

Cartoon representation of INO80 complex. Ino80 here represents the ATPase subunit which serves as the platform for the assembly of other subunits within the complex. Each module, which comprises one or more proteins is indicated. Protein subunits marked in blue, green and grey represents the NHP10 module, Arp8 module and core module respectively.

The Ino80 subunit in INO80 is an assembly platform for other subunits: The N terminal part of Ino80 interacts with Nhp10 module (a subcomplex of INO80 subunits Ies1, Ies3, Ies5 and Nhp10) and this interaction is important for INO80's nucleosome sliding efficiency [240]. The middle region of Ino80 contains the HAS domain which binds to the Arp8 module (a subcomplex of Arp8, Arp4, Taf14, Ies4 and actin in INO80 complex) [231, 241]. The C terminal region of Ino80 forms the core module containing Snf2-type ATPase, Ies2, the Arp5-Ies6 complex, and the Rvb1-Rvb2 AAA^{+}- ATPases [242] (Figure 2.8). Deletion of either Arp8 or HAS domain on Ino80 leads to loss of whole Arp8 module and results in remodeling-defective INO80 complex, suggesting that Arp8 module is critical for INO80 function [231, 243, 244].

The Arp8 module subunits Arp4, actin, Taf14 and Arp4 are also part of other chromatin remodeling complexes, however, INO80 has a unique Arp8 subunit [245]. Deletion of Arp8 leads to loss of actin and Arp4 from the complex and INO80 loses its ability to bind DNA [243]. Structural studies of actin-Arp4-HAS(Ino80)-Arp8 tetramer have identified the Arp8 module as a sensor of DNA [246]. However, in structural analysis, the N-terminal part of Arp8 is missing from amino acids 1 to 254 and this missing region associates with extranucleosomal / linker DNA and is therefore required for Arp8 module to bind to DNA [245]. The binding of Arp8 module to DNA couples ATP hydrolysis to nucleosome

repositioning and is essential for proper docking of Ino80 and Arp5 subunit to nucleosomes [245].

2.2.1. INO80 is a bona-fide target of DDK

In our mass spectrometry datasets, we found phospho sites on Ino80, Ies4, Arp8 and Ies2 subunits of the INO80 complex. We focused on Arp8 because serine 65 (S65) and serine 233 (S233) of Arp8 were down-regulated upon DDK inhibition in both datasets. In the datasets, where DDK was inhibited by temperature, we found S233 phosphorylated in the samples where cells were grown at 25 °C (DDK active) but not in the 37 °C samples (DDK inactive). When DDK was inhibited by Rad53, we found S65 in addition to S233 in YPD samples (DDK active). Similar to the temperature screen, both sites were not detectable in the presence of HU (DDK inactive). Together, both screens suggest that S65 and S233 in the Arp8 subunit of INO80 are bona-fide phosphorylation sites of DDK (Figure 2.9).

By applying our two-pronged screening strategy, we propose that we identify DDK targets with high confidence. However, as with every screen, it is difficult to rule out that phosphorylation might be caused by indirect events. To overcome this problem, we employed an *in vitro* kinase assay to directly test if Arp8 is phosphorylated by DDK. In such an assay, purified substrate (INO80) and kinase (DDK) are incubated in the presence of radioactively labelled γ-ATP to monitor the kinase-mediated transfer of the γ-phosphate group onto the substrate.

We firstly mutated both S64 and S233 in Arp8 to alanines in a strain with a FLAG tag on the C-terminus of the Ino80 subunit of INO80 and we termed this strain *arp8-P*. Because of the FLAG tag, we then purified wild type and Arp8-P mutant INO80 complexes. Figure 2.10 A, shows that both complexes could be purified to homogeneity and all subunits of both complexes could be identified by PAGE followed Coomassie staining.

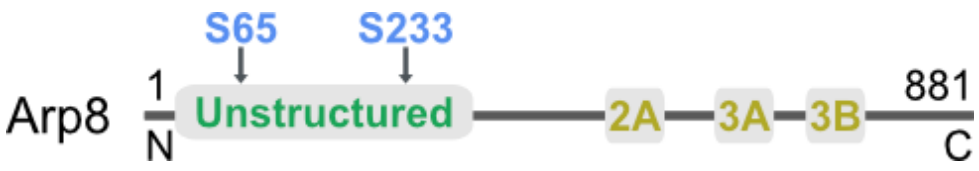

Figure 2.9. DDK dependent phospho sites on Arp8 subunit of INO80 complex

The figure represents Arp8 with 881 amino acids. Serine 65 and serine 233 in N terminus unstructured region of Arp8 were mutated to alanine by site directed mutagenesis.

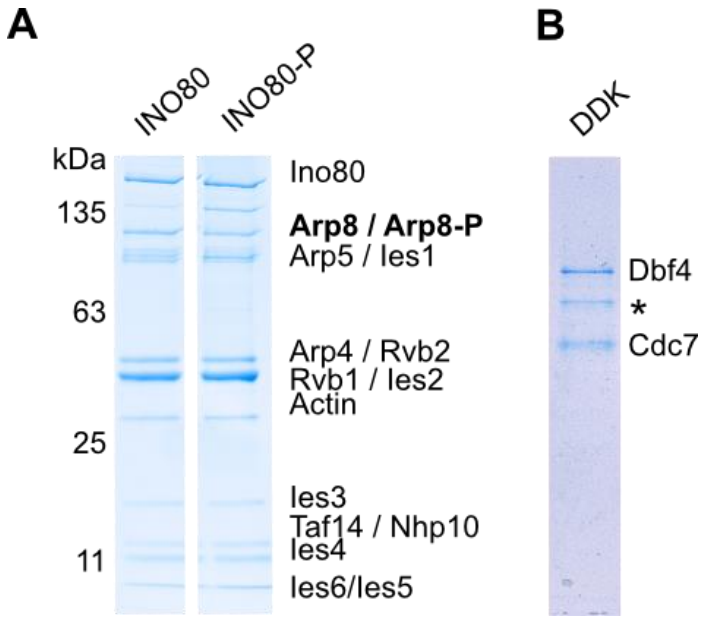

Figure 2.10. Protein purification of WT INO80, INO80-P mutant and DDK

(A) SDS-PAGE analysis of purified WT INO80 and mutant INO80-P complex.

(B) SDS-PAGE analysis of purified DDK.

kDa refers to size of protein in kilodaltons.

We next purified DDK (Figure 2.10 B) and used physiological concentrations of the kinase and the substrates (e.g. 5 nM DDK and 15 nM INO80 WT and mutant complexes) in the *in vitro* kinase assays. As described previously [247], we also observed autophosphorylation of DDK in our assay as represented by the asterisk (Figure 2.11; lanes 1 and 3). Remarkably, for the 15 subunit INO80 WT complex, we detected that specifically one subunit was phosphorylated by DDK (Figure 2.11, lane 1). This highlights that our *in vitro* kinase assay is highly specific and that DDK does not phosphorylate other serines or threonines in the complex. The phosphorylated subunit runs at about ~100 KDa and would in principle correspond to the Arp8 subunit. We did not observe any phosphorylation in the *arp8-P* mutant INO80 complex, confirming that the phospho-protein is indeed Arp8 (Figure 2.11; lanes 2 and 4). Together, the results from our *in vitro* kinase assays as well as from *in vivo* mass spectrometry experiments now show that S65 and S233 in Arp8 are bona-fide targets of DDK.

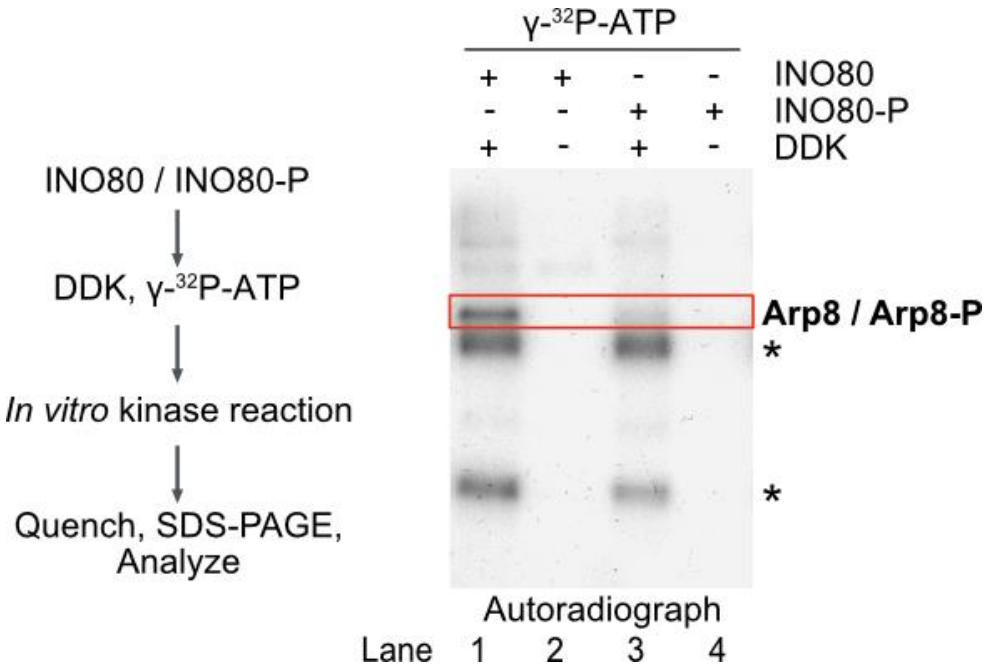

Figure 2.11. DDK phosphorylates Arp8 subunit of INO80 complex

In vitro kinase assay using purified DDK with INO80 and INO80-P. The asterisk represents autophosphorylation of DDK. The red rectangle represents ~100 KDa Arp8 subunit of INO80 which is phosphorylated by DDK. N=2.

2.2.2. *In vivo* analysis of *arp8-P* mutant

2.2.2.1. *arp8-P* mutants are highly sensitive to HU

Firstly, we tested possible effects of *arp8-P* mutant on cell viability using growth assays on optimal conditions and in the presence of various drugs. We performed 10-fold serial dilution on full media (YPD), in presence of HU or MMS (Methyl Methane Sulphonate). MMS generates DNA damage by methylating adenines and guanines in the DNA whereas HU generates replication stress by depleting dNTP pools within cells. After 2 days of incubation at 30 º C, we observed that *arp8*-P shows a mild growth phenotype on YPD relative to the *ARP8* WT. Whereas MMS addition did not result in a detectable growth defect using this assay, HU supplementation was highly toxic for the *arp8-P* mutant (Figure 2.12). These results suggest that Arp8 phosphorylation by DDK might be important for faithful replication rather that MMS-induced DNA damage response.

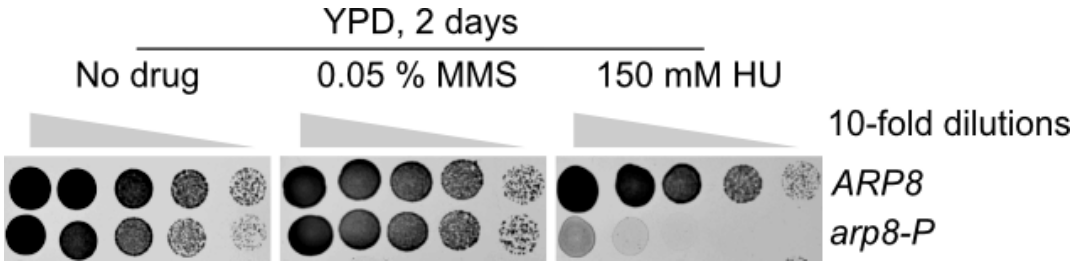

Figure 2.12. Spot dilution assay to measure cell viability

Spot dilution growth assays with tenfold serial dilution with *ARP8* and *arp8-P*. YPD, yeast extract, peptone, dextrose full medium; MMS, Methyl Methane Sulphate; and HU, Hydroxyurea. N=2.

2.2.2.2. *arp8-P* mutants show defects in DNA replication *in vivo*

Because, *arp8-P* mutants were highly toxic in the presence of HU, we next asked if replication was impaired by following S phase progression. Difficulties in S phase progression often lead to the generation of recombinogenic DNA damage, and homologous recombination is the major pathway for repairing DNA double stranded breaks [248]. To test recombination levels of the *arp8-P* mutant, we used a plasmid-based assay where we transformed *ARP8* WT and *arp8-P* strains with pRS316-L plasmid containing two *LEU2* truncated-repeats recombination system [249]. Recombinants were selected on SC (synthetic complete) media lacking leucine and uracil.

In support of a role in S phase progression and consistent with our HU phenotype, we observed an increase in spontaneous levels of homologues recombination in the *arp8-P* mutant compared to *ARP8* WT (Figure 2.13). This result suggests that Arp8 phosphorylation by DDK prevents DNA damage during S phase and support the role of INO80 in replication.

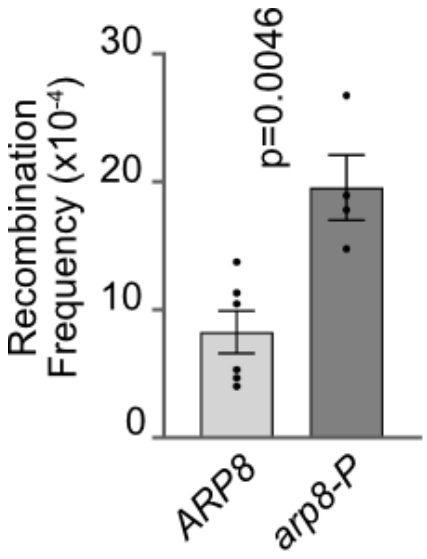

Figure 2.13. Recombination frequency of *ARP8* and *arp8-P* cells

Increase of recombination frequency in the *arp8-P* mutant compare to *ARP8* WT. The Graph is plotted with standard mean and error and p-values was obtained by using two tailed unpaired t-test calculation. N=4, X axis: recombination frequency ($x10^{-4}$).

Next, we asked if the *arp8-P* mutant might also influence DNA synthesis *in vivo*? We followed S phase progression by arresting cells in the G1 phase using alpha factor pheromone. After washing and removing the alpha factor, cells were released into fresh YPD to resume the cell cycle and S phase progression was monitored using flow cytometry. Consistent with HU toxicity and the increased recombination rate of the *arp8-P* mutant (Figure 2.12 and 2.13), we observed a significant replication phenotype compared to *ARP8* WT cells (Figure 2.14). *arp8-P* mutants displayed a 10 mins delay to enter S phase compared to *ARP8* WT (Figure 2.14). Further, we observed that a significant fraction of *arp8-P* mutant cells were stuck in the G1 phase and did not even enter S phase (Figure 2.14). Interestingly and in line with a replication phenotype of the *arp8-P* mutant, a similar phenomenon was observed in *orc1*-mutants, where the nucleosomal architecture at origins of replication was disrupted [142]. Together, our *in vivo* analyses point to a role of DDK-dependent Arp8 phosphorylation for efficient replication. Our FACS profiles further suggest that this might be connected to the INO80´s function to organize chromatin at origins or replication.

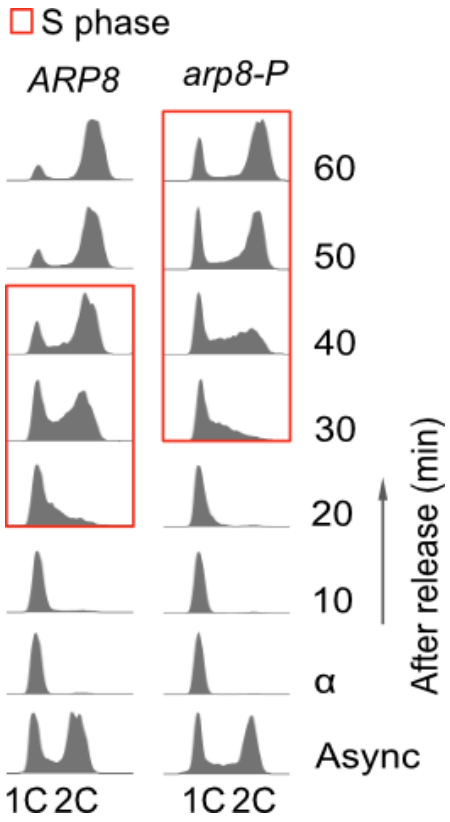

Figure 2.14. Progression of *ARP8* and *arp8-P* cells throughout the cell cycle

ARP8 Wild type and *arp8-P* mutant cells were synchronized in G1 phase using alpha-factor. After release, the progression through S phase was monitored using flow cytometry. The designations 1C and 2C indicate non-replicated or replicated DNA, respectively. N=2.

2.2.2.3. Transcriptome Analysis

As described in the previous section, our *in vivo* analyses point to a role of DDK-dependent phosphorylation of the Arp8 subunit of the INO80 complex in chromosome replication, possible by stimulating INO80´s activity to positioning nucleosomes at origins of replication. However, INO80 binds to NFR of transcription start sites (TSS) of over ~90% of yeast gene promoters [250] and deletion of catalytic Ino80 subunit leads to transcriptional mis-regulation of over 15% of the yeast genome [251], showing that the INO80 complex plays a crucial and global role in gene transcription. Because of this, the replication defects we observed in the *arp8-P* mutant could be in principle, the result of miss-regulated transcription To test this, we performed an RNA sequencing experiment to determine changes in the transcriptome of *arp8-P* mutant compared to *ARP8* WT cells. To allow efficient detection of functionally relevant transcripts we depleted rRNA species, generated

libraries and performed high-throughput illumina whole transcriptome sequencing. The changes in transcripts levels of the *arp8-P* mutant relative to the *ARP8* WT were plotted as log_2(fold change) on the X-axis and -log_{10}(P-value) on the Y-axis in a volcano plot (Figure 2.15). Relative to WT, overall transcription levels did not change significantly in the cell cycle and replication- related genes, however, we observed a miss-regulation of a few metabolic genes. This strongly suggests that the observed phenotypes are specific for replication rather than being the consequence of miss-regulated transcription. However, we cannot rule these metabolic genes might also influence replication to some extent.

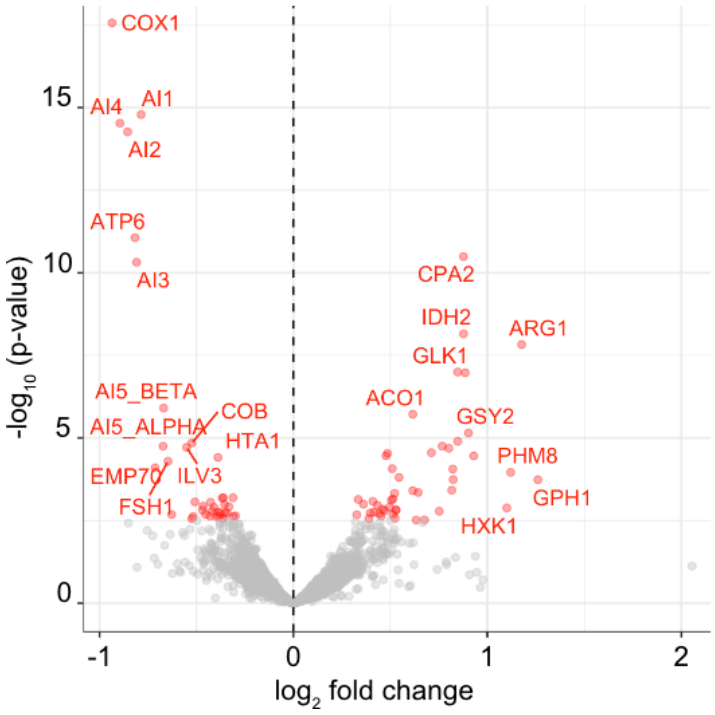

Figure 2.15. Transcriptome analysis of *arp8-P* vs *ARP8*

Volcano plot representation of differential expression of genes in the *arp8-P* versus the *ARP8* WT. Each dot on the plot represents an individual gene. Log_2(fold change) represents changes in gene expression with respect to phosphorylation. Log_2(fold change) above or below zero on X-Axis represents genes that are upregulated or downregulated in *arp8-P*. Red dots represent the gene which are significantly up or down regulated. N=3, X-axis: Log_2 (fold change). Y-axis: -log_{10} (P-value).

2.2.3. Sub-module interaction changes within INO80 complex

We next asked how phosphorylation in an unstructured region of Arp8 could have such a significant impact on INO80 function. As discussed in the previous section, INO80 is ~ 1MDa (MegaDalton) ATP-dependent chromatin remodeler complex which comprises 15 subunits. However, due to complexity and size of the INO80 complex the interaction and changing conformation between each subcomplex (ARP8 module, NHP10 module and core module) becomes difficult to study and therefore the information regarding structural and quantitative details of INO80 is limited. Also, the unstructured region of Arp8 where the phosphosites are located could not be resolved by cryo-electron microscopy [242]. To overcome our limitations, we employed a method where chemical cross-linking is coupled to mass spectrometry (XL-MS). XL-MS is a versatile tool to investigate the topology and architecture of enriched or purified protein complexes [252]. Cross-linking of proteins can be achieved in solution in near physiological conditions with homobifunctional reagents such as DSBU (Disuccinimidyl dibutyric urea) [253]. This symmetrical urea derivative with ~12.5Å spacer arm length functionally reacts rapidly and irreversibly to form colvalent bond with amino acids (mainly lysine (K) side chains) in near spatial proximity. These covalent bonds provide information on proximity and are restrained by the length of spacer arm. For most cross-linkers this ranges from 7 – 30 Å [254]. A cross-linker which reacts with lysine is prefered [255] over others that react with carboxlic acids (asparate, glutamate) or thiols (cysteine) [256], because lysines are more frequently exposed on protein surfaces at physiological conditions and therefore are more easily accessible.

A cross-link reaction could generate various cross-linked species. There are four types of cross-linked peptides known: i) mono link or dead end cross-link where one reactive group of cross-linker forms a covalent bond with amino acid but the other group does not due to hydrolysis of reactive group; ii) loop-links where two amino acid residues within a peptide react with the cross-linker; iii) inter cross-links where two residues of different proteins are in spatial proximity; iv) intra cross-links where two residues of same peptide are in spatial proximity [257]. The two latter types, intra and inter cross-links provide information on the conformational status of a protein and its interaction with other proteins respectively [254, 257].

A small scale cross-link reaction (1 µg) with INO80 WT or INO80-P mutant was first titrated with incresing concentrations of DSBU ranging from 25 – 208 µM at 30 ^{o} C for 20 minutes. The reaction was then quenched by adding ammonium bicarbonate. We observed

that INO80 WT starts to cross-link at a lower (58 µM) DSBU concentration whereas INO80-P cross-links at a higher (100 µM) DSBU concentration (Figure 2.16). The reactions were carefully monitored to prevent over cross-linking. This already shows that the mutant INO80-P complex behaves differently to the WT complex.

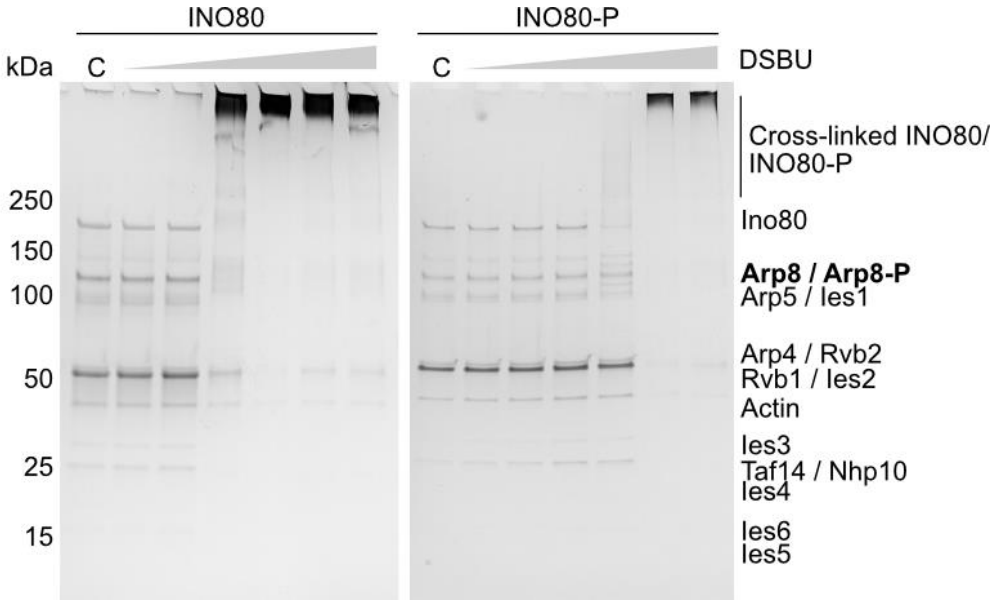

Figure 2.16. Cross-linking reaction with INO80, INO80-P and DSBU cross-linker

SDS-PAGE and silver stain analysis of the DSBU cross-linker titration of INO80 or INO80-P with DSBU cross-linker. C refers to control reaction without any cross-linker and kDa refers to size of protein in kilodaltons. INO80 or INO80-P was tested with 25 – 208 µM DSBU as represented by grey triangle on the top.

Next, we analyzed our cross-link reactions by mass spectrometry. The cross-links were measured on a TimsTOF Pro Instrument and files were searched in MaxQuant (V2.02.0). The cross-link network map for WT INO80 and INO80-P mutant complex are depicted in Figure 2.17. Consistent with previous results [242, 258, 259], we observed in INO80 that the Ino80 subunit is the main connector and interacts specifically with other submodules such as NHP10, ARP8 and RUVB. The N-terminus of Ino80 cross-links to the NHP10 module, where we observed various inter cross-links between the Ino80 and the Ies3, and Nhp10 subunits. In the middle part, Ino80 cross-links with the ARP8 module where we observed cross-links between Ino80 and the Arp8 and Arp4 subunits. At the C-terminus, Ino80 cross-links with the core module, where we observed inter cross-links between Ino80 and the Ruvb1 and Ruvb2

subunits. Also, we observed various intra cross-links on different subunits within the complex (Figure 2.17 A).

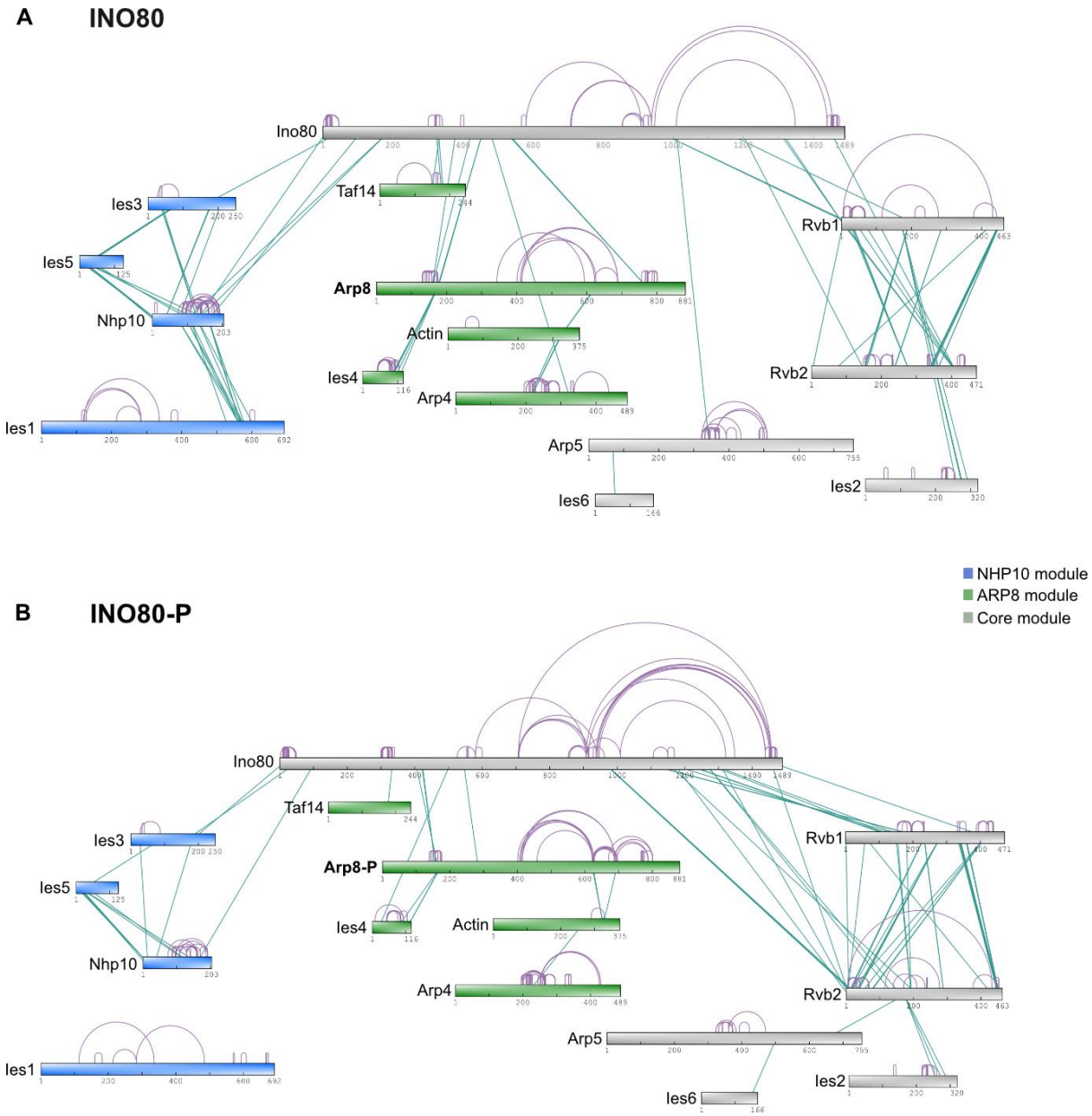

Figure 2.17. Cross-linking reaction with INO80, INO80-P and DSBU cross-linker followed by mass spectrometry

(A) Cross-link network map of various subunits of the WT INO80 complex.

(B) Cross-link network map of various subunits of the mutant INO80-P complex.

The submodules ARP8, NHP10 and core are colour coded in blue, green and grey respectively. Inter cross-links are represented in green and intra cross-links are represented in purple within the complex.

Strikingly, compared to the wildtype complex, we observed that cross-links at N-terminus of Ino80 are less in the mutant complex and has changed significantly within the interactions with the NHP10 module. In the middle part of Ino80, cross-links with the ARP8 module subunits also changed, suggesting an overall structural change within the complex when phosphorylation is missing. In contrast, at the C-terminus Ino80 cross-links with core module complex have significantly incresed e.g. inter cross-links between Ino80 and Ruvb1 and Ruvb2 are different between wild type and mutant complex (Figure 2.17 B). This all shows that loss of DDK-dependent phosphorylation of Arp8 of the INO80 complex goes hand in hand with significant structural changes within the complex.

2.2.4. INO80 phosphorylation is important for ATP hydrolysis and nucleosome spacing

2.2.4.1. ATP hydrolysis assay

The N-terminus of Arp8 (residues 1-254) associates with DNA and is required for the ARP8 module to bind to extranucleosomal/linker DNA. This binding of ARP8 module to linker DNA couples ATP hydrolysis to nucleosome repositioning and for the proper docking of catalytic subunit and ATPase domain of Ino80 subunit [245]. Because S65 and S233 are present in this region we next asked if ATP hydrolysis is affected in the INO80-P mutant complex. We performed an ATP hydrolysis assay where hydrolysis of ATP is linked to the oxidation of NADH by enzymatic reactions (Figure 2.18 A). First, the ADP produced by the ATPase is regenerated by pyruvate kinase (PK). In parallel, PK catalyses the conversion of phosphoenolpyruvate (PEP) into pyruvate. Subsequently, pyruvate undergoes reduction to form lactate through the action of lactate dehydrogenase (LDH), which involves the oxidation of NADH. The reaction is measured by consumption of NADH at 340 nm in a plate reader. We used DNA and chromatin as substrates because chromatin binding can stimulate ATPase activity of remodeler as has been already shown for ISW1, SWR1, RSC and SWI/SNF. We tested saturating concentration of DNA or chromatin to achieve maximum ATP hydrolysis by INO80 complex and calculated ATP molecules hydrolysed per enzyme per second. Interestingly and in line with structural studies, we observed that the rate of ATP hydrolysis by INO80-P is reduced by ~50% compared to INO80 WT in presence of both

DNA or chromatin as substrates (Figure 2.18 B). Thus, our data shows that DDK dependent phosphorylation of Arp8 at S65 and S233 is crucial for the ATP hydrolysis function of INO80.

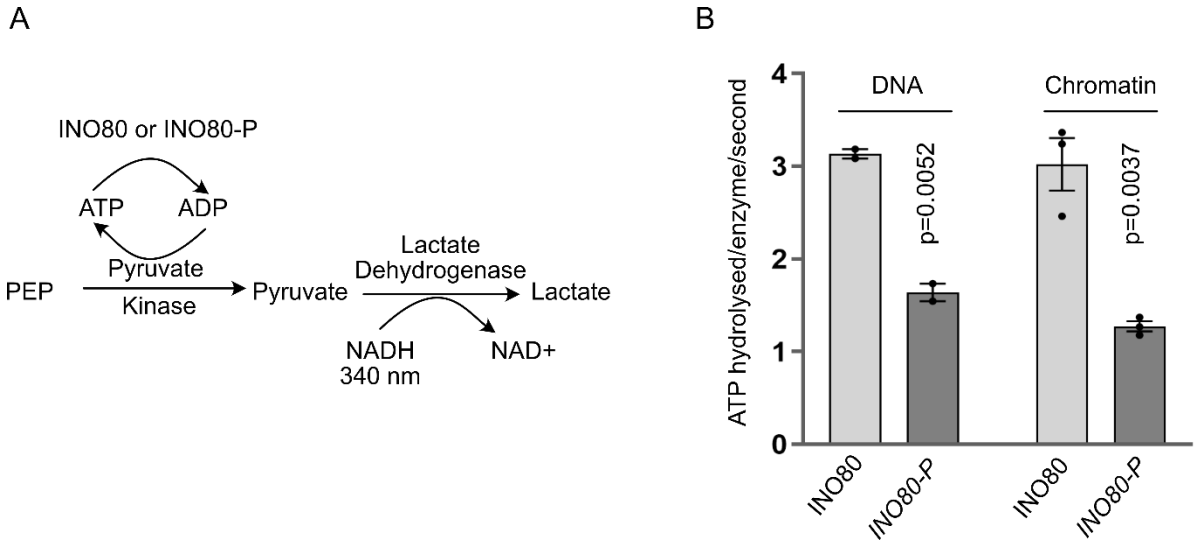

Figure 2.18. Phosphorylation of Arp8 by DDK is important for ATP hydrolysis of the INO80 complex

(A) Schematic of the assay to measure ATP hydrolysis rates. (B) ATP hydrolysis rates of INO80 WT and INO80-P in the presence of DNA (N=2) and Chromatin (N=3). The graphs are plotted with standard mean and error and p-values were obtained by using two tailed unpaired t-test calculations. Y-axis: ATP hydrolysed/enzyme/second.

2.2.4.2. Nucleosome positioning assay

Significant regions of the genome that are not in complex with nucleosomes are known as nucleosome-free regions (NFR). In replication, origins are characterized by presence of NFR in their core region and both sides of origins are well positioned array of nucleosomes [18]. ORC is a master regulator of chromatin structure at replication origins and collaborates with chromatin remodeler like INO80 to attain the origin adjacent chromatin landscape [142].

We thus asked if Arp8 phosphorylation by DDK might be important for the generation of these well-positioned arrays of nucleosomes at origins [142]. Salt gradient dialysis (SGD) was utilized to assemble chromatin, incorporating a plasmid library of ~300 origins and purified histones, thereby obtaining SGD chromatin (Figure 2.19 A). SGD chromatin was further incubated with ORC and INO80 or INO80-P. Nucleosome positions were determined through limited digestion with micrococcal nuclease (MNase) coupled to high-throughput illumina sequencing (MNase-seq) [59, 142]. A composite plot of SGD chromatin at all origins

aligned to their ACS element showed INO80 could generate *in viv*o like nucleosome arrays in the presence of ORC as previously shown [142]. Relative to WT, INO80-P with ORC could generate the NFR and position +/- 1 nucleosomes. Interestingly and in line with our cross-linking MS experiments, the arrays beyond +/- 1 nucleosomes were shifted from the +/- 2 nucleosomes onwards (Figure 2.19 B). Interestingly, we observed that arrays at early origins (Figure 2.19 C) were more affected compare to the late origins (Figure 2.19 D). In addition, INO80-P with ORC generated larger linker lengths and therefore incorrect spacing and shifted arrays of nucleosomes compared to WT.

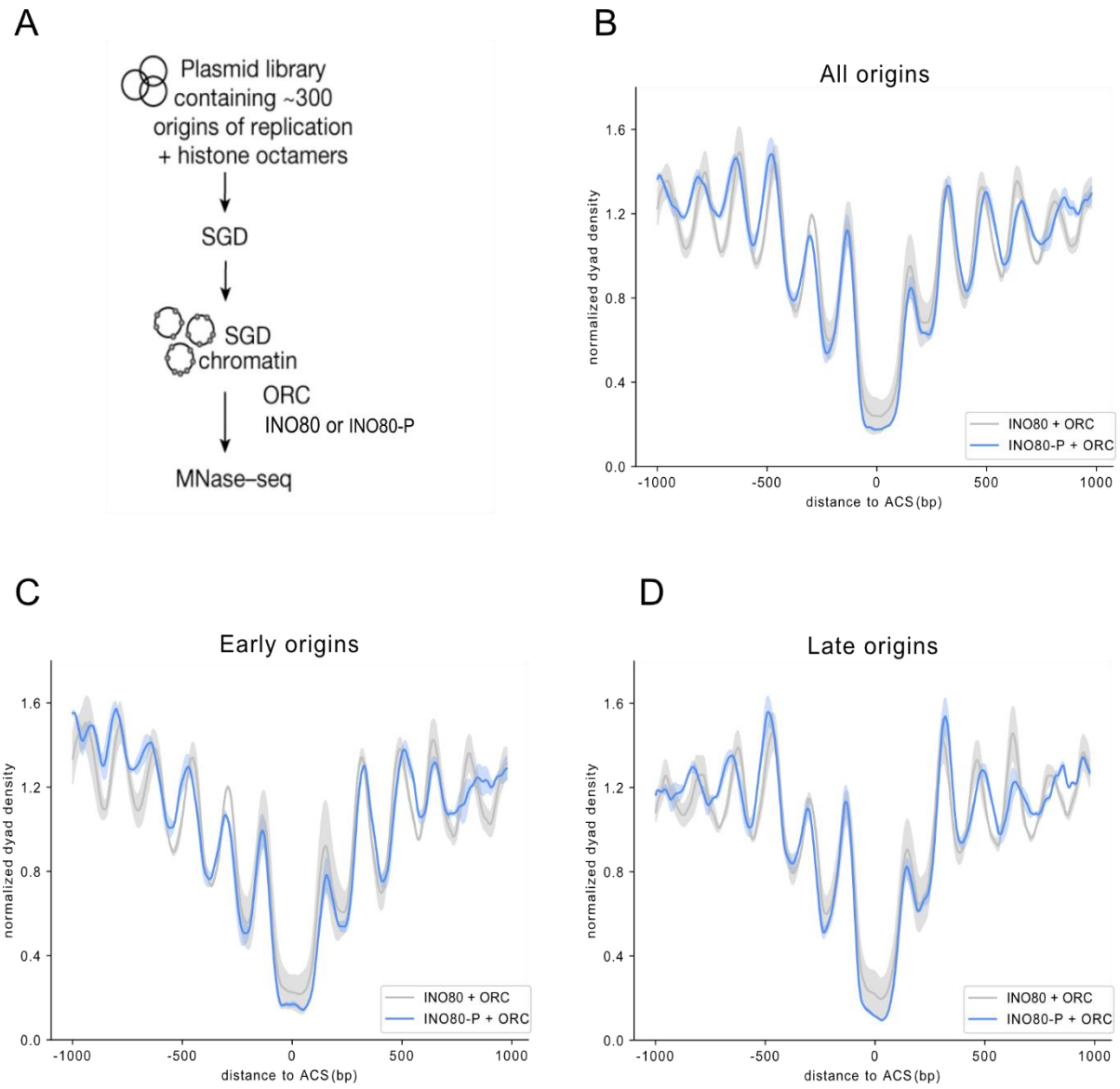

Figure 2.19. Phosphorylation of Arp8 by DDK is important for finetuning INO80 function in establishing nucleosome spacing at origins of replication

(A) Schematic of the assay to measure nucleosome spacing at origins of replication. (B) Composite plot of MNase-seq data of ~300 replication origins (most origins) (C) early replicating origins and (D) late replicating origins *in vitro* aligned to the ORC (origin recognition complex) binding sites ACS (ARS-consensus sequence). SGD (salt gradient dialysis) chromatin was assembled with high assembly degree [142]. NFR corresponds to nucleosome free region and bp corresponds to basepair. Average of N=2 independent replicates are plotted and the shading in the plot represents the standard mean and error.

3. Discussion

Many cellular functions can be controlled by post-translational modifications (PTMs) of proteins, such as phosphorylation, ubiquitination, or acetylation. This regulation enables cells to respond swiftly to changes in external or internal cues. For example, in an event of temporary metabolic change, changes in protein production would be much slower in comparison to PTMs, which can rapidly adjust the activity of metabolic proteins [260]. The mapping of PTMs on amino acids is a challenging task because they are low in abundance, highly complex and dynamic in nature [261]. Protein phosphorylation is a very prominent PTM that regulates essentially all cellular processes and has been studied quite extensively over the decades [222, 262]. Kinases phosphorylate their substrate proteins by adding a γ-phosphate group from ATP to mostly serine or threonine, and in some cases onto tyrosine residues. About two-third of cellular proteins harbour one or more phosphorylation sites [263]. Over the years, many high-throughput studies and computational approaches have increased the depth of knowledge of protein phosphorylation networks in different organisms. Several large scale quantitative phospho proteomics studies have been conducted on yeast cells to determine the changes in protein phosphorylation in response to different stimuli [264-267]. However, the identification of functional phosphorylation events still relies on low throughput methods. As a result, the biological relevance of most phosphorylation events has not yet been determined [260, 268].

The process of replication is also governed by the oscillating activity of kinases. The kinase actions of CDK and DDK control replication by phosphorylation of various substrates. For CDK, many non-replication targets were identified over the last decades. In contrast, apart from the MCM complex, very few DDK targets have been identified. Finding kinase targets is always a challenging task. In classical approaches, phosphorylation sites are biochemically identified on a substrate of interest and then mutated to either mimic or prevent the phosphorylation event [269]. Often phosphorylation events are endpoint measurements to uncover signalling networks in yeast using deletion strains [265, 270]. In the case of kinase deletions, cells would silence kinase activity in response, would often compensate via other, unspecific kinase activities [270]. The identification of DDK targets is challenging for the following reasons: Firstly, DDK is an essential kinase [134] and cannot be deleted and secondly, DDK in comparison to CDK, does not have a consensus sequence. Therefore, a comprehensive view of DDK-dependent global changes in phosphorylation events remains under-investigated.

3.1. Mass spectrometry to find DDK targets

We employed mass spectrometry for an unbiased label-free identification of DDK-dependent phosphorylation events. In our strategy, we specifically targeted DDK using two different approaches: firstly, we targeted DDK directly by using the *cdc7-4* allele. This is a temperature sensitive version of DDK where cells are viable at 25 ^{o} C and DDK activity is abolished at restricted temperature (37 ^{o} C). Secondly, we targeted DDK indirectly using activation of the checkpoint kinase Rad53. In both cases, we conducted nuclear proteomes. In most proteomic studies, nuclear proteins are often less prevalent due to their low abundance [220] and highly abundant cytoplasmic proteins often mask the changes in nuclear proteins. Therefore, performing nuclear fraction enrichment helps to filter nonspecific cytoplasmic protein activity. As yeast does not dissolve its nuclear envelope during cell division, it is a very powerful system to perform nuclear fractionation experiments. Also, the study of nuclear proteomes can give a much broader view on phospho-events happening on chromatin.

In our datasets we found mostly nuclear proteins were enriched in the nuclei fraction (Figure 2.2), showing that our nuclear enrichment worked. We found DDK-dependent phosphorylation events on the MCM complex that were absent when DDK was inhibited (Appendix I, Table 15) [160, 271]. This suggests that we can successfully find DDK-dependent phosphorylation on nuclear proteins. Temperature dependent inactivation of DDK in *cdc7-4* dataset, could activate heat shock proteins and associated phosphorylation events and result into indirect temperature effect. In the second dataset, we use hydroxyurea to activate Rad53. This inhibits DDK activity, but also triggers the DNA damage response pathways. Indeed, we observed an increase in phosphorylation of known DNA damage associated proteins like Mrc1, Rad9, and Dun1 (Appendix II, Table 16) [230]. However, for both our datasets, we collectively took a closer look on DDK phosphorylation events which were downregulated upon DDK inhibition. We defined this overlap in downregulated 301 phospho sites in 187 proteins as our “high-confidence” DDK dataset. We specifically focused on INO80 complex, as INO80 is known to regulate chromatin replication *in vitro* [39]. Also, INO80 together with ORC establishes well positioned nucleosome arrays at origins of replication which is a crucial prerequisite for efficient chromosome replication [142].

3.2. INO80 is a target of DDK

Previous studies have shown that the chromatin remodeler INO80 promotes replication fork progression at the origins of replication. Under replication stress-like conditions, INO80 rescues the stalled replication fork and restarts replication at these forks. [39, 142, 233-236]. INO80 is a multi-subunit chromatin remodeler and the ATPase subunit Ino80 is the platform for assembly of other subunits within the complex. The middle region of Ino80 contains the HAS domain which binds to Arp8 module (a subcomplex of Arp8, Arp4, Taf14, Ies4 and actin in INO80 complex) [231, 241]. Deletion of either Arp8 or HAS domain on Ino80 leads to loss of whole Arp8 module and results in remodeling defective INO80 complex suggesting that Arp8 module is critical for INO80 function [231, 243, 244]. Further studies showed that Arp8 is a unique subunit of INO80 complex. The N terminus of Arp8 (1-254 residues) associates with DNA and is required for Arp8 module to bind to linker/extranucleosomal DNA [245]. From our mass spectrometry results, we found two important DDK-dependent phospho sites (S65 and S233) within the N terminus region of Arp8 subunit of INO80 complex. Our results show S65 and S233 on Arp8 are phosphorylated by DDK and regulate chromatin modulating activity of INO80 complex. When Arp8 is not phosphorylated, it leads to significant changes in cross-linking between Ino80 subunit with NHP10, ARP8 and RUV modules, suggesting overall structural changes within the INO80 complex (Figure 2.17). These structural changes might affect association of ARP8 module with DNA / chromatin, which further reduces ATP hydrolysis and generates incorrect spacing with larger linker length (Figure 2.18 and 2.19). Therefore, DDK dependent phosphorylation is crucial for the function and integrity of the INO80 complex. How the two phosphorylation events of Arp8 accomplish that is unknown. Structural studies with the higher resolution like cryo-electron microscopy might give further insights into this process.

3.3. Model of the study

The temporal separation of helicase loading and activation in eukaryotes provides a control to prevent re-replication of chromosomal DNA. Helicase activation is achieved by the action of kinases where DDK primarily phosphorylates the MCM complex to initiate replication. DDK fulfills its replicative function at the levels of individual origins and is required throughout S phase for sequential replication initiation [272, 273]. DDK activity is regulated by the abundance of Dbf4 protein levels which oscillate during the cell cycle.

Interestingly, Dbf4 is recruited to early origins in G1 phase [214, 215] however why DDK is present in G1 phase is not clear.

The catalytic subunit Cdc7 of DDK has been shown to bind chromatin throughout the genome during G1 phase of the cell cycle [274, 275]. Binding of Cdc7 onto chromatin is stabilized by Dbf4 preferably on ACS sites [274]. Dbf4 has been shown bound to ORC containing chromatin fraction in G1 phase in the absence of MCM loading [217]. Dbf4 physically associates with Orc2 subunit of ORC complex through its N-terminal domain [218]. This suggests that Dbf4 targets Cdc7 to origins during G1 phase in an ORC and cell cycle-dependent manner. Association of DDK and ORC at early origins during G1 phase is a limiting factor and necessary for the creation of initiation-competent origins to promote replication initiation [217]. Dbf4 binding at individual origins acts as “local control” for timely origin firing.

Also, ORC’s role is central to the replication as it is required for the assembly and initiation step of the replication. Eukaryotic genome replication occurs in the context of nucleosomes and ORC interacts with chromatin remodelers (INO80, ISW1a, ISW2 and Chd1) via Orc1 in G1 phase of the cell cycle and regulates origin-adjacent nucleosome organization which is essential for replication [142].

Our results are in line with previous reports and we propose a model where in the G1 phase of the cell cycle, INO80 and DDK interact with ORC subunits at early origins of replication, where DDK phosphorylates Arp8 subunit of INO80 (Figure 3.1). From our cell cycle mass spectrometry data, we observed Arp8 phosphorylation in the G1 phase of the cell cycle (Figure 2.7 B). Since the Arp8 module is a DNA sensor of INO80 complex [245, 246], phosphorylated INO80 might sense chromatin to modulate chromatin structure to generate phased nucleosome arrays at origins of replication. When Arp8 subunit is not phosphorylated, we observed replication defects and structural changes within the ARP8 and NHP10 module of INO80 complex [276]. The structural changes resulted in reduced ATP hydrolysis rates by the INO80 complex (Figure 2.18 B) and generated incorrect nucleosome spacing with larger linker length. Further, we observed that early origins are more affected than late origins in nucleosome positioning assay (Figure 2.19 C and D). This outcome aligns with previously shown ChIP data where DDK is recruited to early origins [214, 215]. These data suggest a model where changes within one submodule leads to overall conformational change of the INO80 complex, finetunes its function and determines the nucleosome spacing activity, especially at early origins of replication. These findings may help shed light on the rationale behind the timing of early origins firing early and late origins firing late during replication.

We believe that a basal nucleosome positioning might exist at all origins throughout the genome which could be accomplished by the unphosphorylated INO80. Prior to S phase, DDK dependent phosphorylation of INO80 at early origins might i) finetune INO80 function; ii) stabilize INO80 and Orc1 interactions at the early origins; iii) recruit INO80 at early origins and iv) ensures correct conformation of the complex which might be important for INO80's association with DNA and/or with ORC. This association would determine the chromatin architecture adjacent to the early origins and would lead to early origin firing. The nucleosome landscape at initiation-competent early origins would push early origins to be fired early and help activated helicases to escape efficiently during S phase. These generated differences in nucleosome landscape through DDK phosphorylation during G1 phase would allow DDK to act as "local control" and would contribute to determines which origins are fired in a timely manner during the S phase.

In contrast, under replication stress conditions, the N-terminal of Dbf4 binds to Rad53, the checkpoint kinase, rather than Orc2 [218]. In this scenario, Rad53 physically captures DDK, rendering it inaccessible [191-194]. Now, DDK is unavailable to phosphorylate the MCM complex and origin firing is inhibited. Under these circumstances, it would not make sense to activate INO80's DDK-dependent function to prepare for early origin firing. Indeed, we observed a loss of Arp8 phosphorylation when the checkpoint was activated by the addition of HU. This indicates the presence of a phosphorylation-based mechanism for regulating origin firing and responding to replication stress.

To our knowledge, this is the first example of any organism, where the nucleosome spacing activity of chromatin remodelers is directly regulated by signals of the cell cycle machinery. It remains to be elucidated how exactly such changes in one module withing the multi subunit organization like INO80 transmit information to the core ATPase of the complex resulting in different spacing.

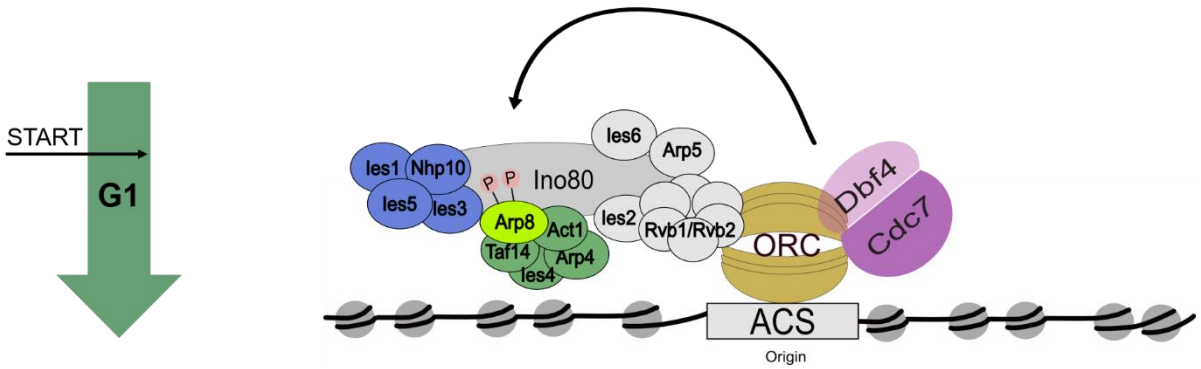

Figure 3.1. DDK finetunes INO80 function via phosphorylation at origins of replication

DDK is associated to chromatin via its interaction with Orc2 and INO80 associates to chromatin via its interaction with Orc1. At origins of replication prior to the S phase of the cell cycle, DDK phosphorylates Arp8 subunit of INO80 complex and phosphorylated INO80 phase nucleosome arrays (peculiar chromatin architecture) to promote chromatin replication.

3.4. Future studies

Altogether, we have established a mass spectrometry-based pipeline to find DDK targets by inhibiting DDK chemically/indirectly and physically/directly. The mass spectrometry datasets give us a comprehensive view of nuclear phosphorylation events throughout various conditions. Our experiments will provide information about DDK targets which support DNA replication and upon replication stress response inhibit DNA replication. Additionally, these experiments will yield a list of DDK targets that are not directly related to replication but are involved in other cellular processes. Importantly, we expect that these datasets will be the basis for many detailed follow up studies.

For example, it has been shown that INO80, ISW1a, ISW2 and Chd1 collaborate with ORC to generate phase nucleosome array at replication of origins [142]. It could be that, chromatin remodeling activity of other chromatin remodelers like ISW1a, ISW2 and Chd1 is also regulated by DDK via phosphorylation to maintain chromatin architecture at origins of replication, similarly to INO80. Indeed, we observed DDK dependent phospho sites on ISW1a, ISW2 and Chd1 in our mass spectrometry dataset. Chromatin factors are involved in many other cellular processes like transcription, repair, and recombination. It could be that regulation by replication kinases like DDK specifically “label” chromatin factors to work for the process of replication.

For example, Spt6 is one of the interesting candidates as a recent study showed it's role in chromatin replication. *spt6* mutants showed replication and S phase progression defects and are sensitive to replication stress causing drugs. Additionally, *spt6* mutants have decreased loading of the MCM complex at replication origins suggesting that Spt6 promotes origins licensing [277]. These results are similar to INO80's role in origin licensing by generating initiation-competent origins. Could it be that Spt6 at origins might also be regulated by DDK dependent phosphorylation?

3.5. Spt6 might be a novel candidate for chromatin replication and a putative target of DDK

In our 301 phospho sites on 187 proteins, we found DDK-dependent phospho sites on many chromatin factors, one interesting candidate is Spt6. Spt6 is a conserved H3/H4 histone chaperone and has important well-defined roles during several steps in transcription like initiation, elongation and termination [278-280]. Studies in yeast and mammalian cells showed that Spt6 directly interacts with histone H3 and could assemble nucleosomes *in vitro* [281], suggesting that direct Spt6-histone interactions could contribute to maintain the chromatin structure. Indeed, *spt6* mutants induce changes in chromatin structure *in vivo* and suppress the depletion of the Swi/Snf ATP dependent chromatin-remodeling complex [281-283].

During transcription Spt6 collaborates with other histone chaperones like FACT and Nhp6 [284]. Both, Spt6 and FACT need assistance of Nhp6 in order to bind to nucleosomes *in vitro* [281, 285, 286]. FACT regulates transcription by facilitating the histone removal in front of elongating RNA polymerase II as well as nucleosome reassembly in the back of passing RNA polymerase II [93, 287]. FACT is also essential for chromatin replication *in vitro* [39]. Since Spt6 and FACT work together to maintain chromatin structure during transcription, we speculated that Spt6 and FACT could together regulate chromatin structure during replication, possibly in a redundant manner.

Figure 3.2. DDK-dependent phospho sites on Spt6

The figure represents Spt6 with 1451 amino acids. Serine 134, serine 155 and serine 206 in N-terminal region of Spt6 were mutated to alanine by site directed mutagenesis.

In our mass spectrometry datasets, we found several phospho sites on Spt6. In the DDK dataset, where DDK was inhibited by temperature, we found phospho sites on serine 134 (S134), serine 155 (S155) and serine 206 (S206). In HU dataset, where DDK was inhibited by checkpoint activation, we found the same phospho sites S134, S155 and S206 on Spt6 (Figure 3.2). As with Arp8 the sites were downregulated upon DDK inhibition at 37 º C as well as in HU condition.

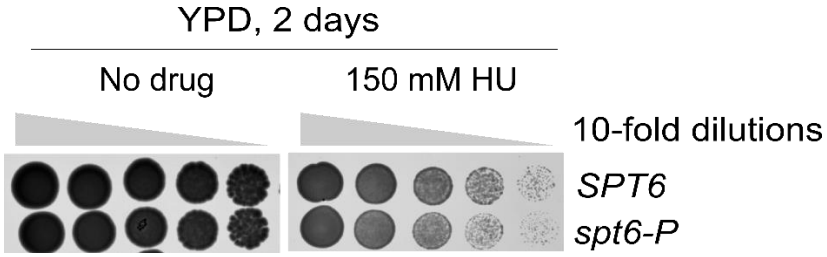

Figure 3.3. SPT6 is a novel factor of replication

Spot dilution growth assays with tenfold serial dilutions of *SPT6* WT and *spt6-P* mutant cells. YPD, yeast extract, peptone, dextrose full medium; and HU, Hydroxyurea. N=2.

For initial testing of putative involvement in replication, we mutated S134, S155 and S206 into alanine. We tested our *spt6-P* mutant using the same growth assay that we used to test the *arp8-P* mutation (Figure 2.12). We determined the growth of *spt6-P* mutant and wildtype *SPT6* cells on full media (YPD) and in presence of HU+YPD. Relative to WT, we observed that *spt6-P* grows normally on YPD. Interestingly and in line with a possible involvement in replication *spt6-P* mutant show a mild but reproducible sensitivity to HU (Figure 3.3) after 2 days of incubation at 30 º C.

It will be interesting to see if purified Spt6 can stimulate replication on chromatin, possibly in collaboration with FACT. FACT is essential for chromatin replication *in vitro* [39], it will be interesting to study, if Spt6 and FACT together regulate chromatin dynamics during replication.

4. Materials and Methods

4.1. Materials

4.1.1. Yeast strains

Here is a compilation of yeast strains used in this study. The sources are provided to indicate whether the strain was generated during this thesis or acquired from previously published studies.

Table 3: List of yeast strains used in this study

Strain	Genotype	Source
yPB 1	MAT a, *leu2-3,112 trp1-1 can1-100 ura3-1 ade2-1 his3-11,15*	[288]
yPB 2	MAT α, *leu2-3,112 trp1-1 can1-100 ura3-1 ade2-1 his3-11,15*	[288]
yCFK 51	MAT a, *his3Δ1 leu2Δ0 met15Δ0 ura3Δ0*	[289, 290]
yCFK 43	MAT α, *his3Δ1 leu2Δ0 lys2Δ0 ura3Δ0*	[289, 290]
yCFK 92	MAT a, *leu2-3,112 trp1-1 can1-100 ura3-1 ade2-1 his3-11,15 cdc28-as1*	[291]
yCFK 95	MAT a, *leu2-3,112 trp1-1 can1-100 ura3-1 ade2-1 his3-11,15 cdc28-as1, Ino80-3x FLAG::NAT*	This study
yCFK 96	MAT a, *leu2-3,112 trp1-1 can1-100 ura3-1 ade2-1 his3-11,15 cdc28-as1, Rsc2-3x FLAG::NAT*	This study
yCFK 23	MAT a, *ade2-1 ura3-1 his3-11,15 trp1-1 leu2-3,112 can1-100, cdc7-4, pep4:: Hyg, his3::HIS3pRS303/SLD3-13MYC, trp1::TRP1pRS304/SLD2, leu2::LEU2pRS305/ SLD7, CDC45, ura3::URA3pRS306/ DPB11*	[221]
yPB 3	MAT α, *his3Δ1 leu2Δ0 lys2Δ0 ura3Δ0 ARP8::ARP8-S65A, S233A*	This study
yPB 4	MAT a, *his3Δ1 leu2Δ0 ura3Δ0 ARP8::ARP8-S65A, S233A*	This study
yPB 5	MAT α, *his3Δ1 leu2Δ0 lys2Δ0 ura3Δ0 ARP8::ARP8-S65A, S233A, Ino80-3x FLAG::NAT*	This study
yPB 6	MAT a, his3Δ1 leu2Δ0 ura3Δ0 ARP8::ARP8-S65A, S233A, Ino80-3x FLAG::NAT	This study
yPB 7	MAT a, *his3Δ1 leu2Δ0 met15Δ0 ura3Δ0, Ino80-3x FLAG::NAT*	This study

yPB 8	MAT a, *leu2-3,112 trp1-1 can1-100 ura3-1 ade2-1 his3-11,15 SPT6::URA3, leu2-3,112::LEUpRS305-SPT6*	This study
yPB 9	MAT a, *leu2-3,112 trp1-1 can1-100 ura3-1 ade2-1 his3-11,15 SPT6::URA3, leu2-3,112::LEUpRS305-SPT6-S134A, S155A, S206A*	This study
yPB 10	MAT a, *leu2-3,112 trp1-1 can1-100 ura3-1 ade2-1 his3-11,15 SPT6::URA3, leu2-3,112::LEUpRS305-SPT6-S94, S134A, S155A, S206A*	This study
yCFK 81	MAT a, *ade2-1 ura3-1 his3-11,15 trp1-1 leu2-3,112 can1-100, bar1::Hyg, pep4::KanMX, SPT6- 3xFLAG::NAT*	[142]
yPB 11	MAT a, *leu2-3,112 trp1-1 can1-100 ura3-1 ade2-1 his3-11,15 SPT6::URA3, leu2-3,112::LEUpRS305-SPT6-S94, S134A, S155A, S206A, Ino80-3x FLAG::NAT*	This study

4.1.2. Plasmids

Here is a compilation of plasmids used in this study. The sources are provided to indicate whether the plasmid was generated during this study or obtained from previously published studies.

Table 4: Plasmids used in the study

Plasmid Name	**Source**
pRS416-ARP8 +/- 1Kb	[69]
pRS305-SPT6 including promotor	This study
pRS416-ARP8, S65, S233	This study
pRS305-SPT6 including promotor + S134, S155 and S206	This study
BP83	[39]

4.1.3. Antibodies

In this study, we used Anti-FLAG (mouse IgG M2) monoclonal antibody at 1:5000 dilution for western blots. The antibody was obtained from Sigma with product number F3165.

4.1.4. Oligonucleotides

Here is the catalogue of oligonucleotides used in this study. All oligonucleotides were synthetized and ordered from Sigma. “F” and “R” are used to distinguish between forward and reverse primers respectively.

Table 5: Oligonucleotides used in this study

Name	5'-3' Sequence	Purpose	Purification
oPB1	TAAATTACTAGTCAATAGTACATAAAT ACAGGGATACAATCGCACCTAACCGG ATCCCCGGGTTAATTAA	*URA* integration at *ARP8* locus F	Desalt
oPB2	TGCAAAGACCTTTCAGAAAAAAAGAT AACAAAAACTTCCATATGCATATCGAA TTCGAGCTCGTTTAAAC	*URA* integration at *ARP8* locus R	Desalt
oPB3	CGTAGTTGGATCTGAGACACCCAGAG CTGTAACAGGTCTTTCTGTTGACCCA	*ARP8* Serine 65 SDM F	Desalt
oPB4	TGGGTCAACAGAAAGACCTGTTACAG CTCTGGGTGTCTCAGATCCAACTACG	*ARP8* Serine 65 SDM R	Desalt
oPB5	GAGAAATAACAACACTAGCCAAATAG CTAGTACCAACACACCAGATGTTAT	*ARP8* Serine 233 SDM F	Desalt
oPB6	ATAACATCTGGTGTGTTGGTACTAGC TATTTGGCTAGTGTTGTTATTTCTC	*ARP8* Serine 233 SDM R	Desalt
oPB7	TAAATTACTAGTCAATAGTACATAAAT ACAGGGATACAATCGCACCTAACATG TCGCAAGAAGAAGCAG	*arp8* integration at *ARP8* locus F	Desalt
oPB8	TGCAAAGACCTTTCAGAAAAAAAGAT AACAAAAACTTCCATATGCATATCCTA GTACGTGAAAATACATTTATATTGTAA	*arp8* integration at *ARP8* locus R	Desalt

	G		
oPB9	CCGTGCAAGATGACTTATTT	*ARP8* locus integration check F	Desalt
oPB10	AGCCGTCTAAGCGGGACTAT	*ARP8* locus integration check F	Desalt
oPB11	TGAGGAACCCATTGATATTCCG	*ARP8* S65 sequencing F	Desalt
oPB12	GTCTGCACAGCAGGTGGTGCCCT	*ARP8* S65 sequencing R	Desalt
oPB13	AGACTAGGACGTATTAAAGCT	*ARP8* S233 sequencing F	Desalt
oPB14	GATCCAGGATGTATCACGATA	*ARP8* S233 sequencing R	Desalt
oPB15	GACCATCCTGTCGTAGTTCCAA	*ARP8* sequencing F	Desalt
oPB16	GCAAAAGCATAAGTCAAGATGGAATT AAGGAAGCGGCAAGTGCATTGGCAC GTACGCTGCAGGTCGAC	*INO80* C-terminus 3xFLAG F	Desalt
oPB17	GATAGACATTAACTCCGCTTAATGTAA ATAACACAATATGAATACCTTTTATCG ATGAATTCGAGCTCG	*INO80* C terminus 3xFLAG R	Desalt
oPB18	ATCAACTTGAAAATTTGTGGGA	*ARP8* sequencing R	Desalt
oPB19	CGGCCGCTCTAGAACTAGTGCTACGC CCAACCCAACCAAAG	*SPT6* promoter cloning F	Desalt
oPB20	TCTCTTCCATAAAAGGCAAATTCTATG TAAAGATTCTAGGC	*SPT6* promoter cloning R	Desalt
oPB21	TTTGCCTTTTATGGAAGAGACGGGAG ATTC	*SPT6* 1-750 bp cloning F	Desalt
oPB22	CATGACCATCACCAAAAATGTCATAC ATCTCG	*SPT6* 1-750 bp cloning R	Desalt
oPB23	CATTTTTGGTGATGGTCATGACTACG ATTG	*SPT6* 750-3606 bp cloning F	Desalt
oPB24	CGAGGTCGACGGTATCGATACTAACG GTAGTTGTTCATTC	*SPT6* 750-3606 bp cloning R	Desalt
oPB25	AAGACGAAGATGAGGCAAGA	*SPT6* sequencing primer 1	Desalt

oPB26	GATATCAAGAATTAAGAGCAG	*SPT6* sequencing primer 2	Desalt
oPB27	TGAACCTGCTCAGTGTTAAG	*SPT6* sequencing primer 3	Desalt
oPB28	TGATATTGTCAACCTGGTAA	*SPT6* sequencing primer 4	Desalt
oPB29	GTGATATATATTGACTATGCT	*SPT6* sequencing primer 5	Desalt
oPB30	AGCGAACAGGTCATTAATTGCCTAGA ATCTTTACATAGAATTTGCCTTTTCGG ATCCCCGGGTTAATTAA	*URA* integration at *SPT6* locus F	Desalt
oPB31	GTCAAAGTAATAATAAAATTAATAATA ACAATGGACACTACATACGCATGAAT TCGAGCTCGTTTAAAC	*URA* integration at *SPT6* locus R	Desalt
oPB32	AAGAAACTGGACAACGGTTA	*SPT6* locus integration check F	Desalt
oPB33	GTTGAAGCGTTCTAGTTTAC	*SPT6* locus integration check R	Desalt
oPB34	AGACGCTTCTAAAATCTAACAGTAGTA AGAATAGAATGAACAACTACCGTCGT ACGCTGCAGGTCGAC	*spt6* C-terminus 3xFLAG F	Desalt
oPB35	GGAACAAAAGCTGGGTACCGGGCCC CCCCTCGAGGTCGACGGTATCGATAA TCGATGAATTCGAGCTCG	*spt6* C-terminus 3xFLAG F	Desalt
oPB36	TGACAACGATGAAACTAAAGCGCCTA GTGAGGAAGAAGAAGGAGAAGATGT C	*SPT6* Alanine 28 SDM F	Desalt
oPB37	GACATCTTCTCCTTCTTCTTCCTCACT AGGCGCTTTAGTTTCATCGTTGTCA	*SPT6* Alanine 28 SDM R	Desalt
oPB38	AGAAAGAGAAGAAGATGATCGACTAT CCGAAGATGATTTGGATTTGTTAAT	*SPT6* Alanine 94 SDM F	Desalt
oPB39	ATTAACAAATCCAAATCATCTTCGGAT AGTCGATCATCTTCTTCTCTTTCT	*SPT6* Alanine 94 SDM R	Desalt
oPB40	GCGAGATTGATGAAGAAAG	LEU locus downstream integration check of	Desalt

		pRS305 Primer 1	
oPB41	ACGTTTACAATTTCCTGATGCG	LEU locus downstream integration check of pRS305 Primer 2	Desalt
oPB42	GCTGAAACGCAAGGATTG	LEU locus upstream integration check of pRS305 Primer 1	Desalt
oPB43	ATTTCCCCGAAAAGTGCCAC	LEU locus upstream integration check of pRS305 Primer 2	Desalt

4.1.5. Solutions and Buffers

Here is the catalogue of solutions and buffers used in this study.

Table 6: Description of Buffer and solutions

Buffer/solution name	**Composition**
1.33X Gibson reagent buffer	5X Gibson assembly buffer, (0.005 U/µl) T5 exonuclease, 0.033 U/µl Phusion polymerase, 5.33 U/µl Taq Ligase
5X Gibson assembly buffer	450 mM Tris-HCl pH 7.5, 25% PEG 8000, 50 mM $MgCl_2$, 50 mM DTT, 1 mM dNTPs, 5 mM NAD
5X TBE buffer	VWR (J885-4L)
1X TE	10 mM Tris-HCl, 1 mM EDTA, pH 7.5 or 8.0
Pre incubation solution	0.7 M β-mercaptoethanol and 2.8 mM EDTA pH 8.0
Ficoll buffer	18% Ficoll, 20 mM KH_2PO_4 pH 6.8, 1 mM $MgCl_2$, 0.25 mM EGTA, 0.25 mM EDTA
Genomic DNA resuspension buffer	0.9 M sorbitol, 50 mM Na-Pi pH 7.5, 140 mM β-mercaptoethanol
Zymolyase solution (for tetrad dissection)	0.1 M NaPO4 pH 7.4,1.2 M sorbitol, 2.5mg/ml zymolyase 100T
Single stranded carrier DNA	10 mg/ml salmon sperm DNA, 10 mM Tris-HCl pH 8.0, 1mM EDTA

1X LioAc buffer	0.1 M LiOAc, 10 mM Tris-HCl pH 8.0, 1 mM EDTA
Protein lysis buffer	0.288 M β-mercaptoethanol and 0.2 M sodium hydroxide
1X SDS running buffer	2.5 mM Tris, 19.2 mM glycine, 0.01% SDS, pH 8.3
Staining solution	7.5% (v/v) acetic acid, 5% (v/v) EtOH
Coomassie Brilliant Blue	0.25% (w/v) Coomassie Brilliant Blue G-250, 100% EtOH (Ethanol)
Western Blot transfer buffer	48 mM Tris-HCl, 39 mM glycine, 10% SDS, 20% MeOH (Methanol)
1X PBS	137 mM NaCl, 2.7 mM KCl, 10 mM Na_2HPO_4, 1.8 mM KH_2PO_4, in dH_2O, pH 7.4
1X PBST	1X PBS, 0.1% Tween20

4.1.6. Chemicals and consumables

Table 7: Sources of Chemicals and consumables

Description	**Manufacturer (Catalogue number)**
BamHI	NEB (R0136L)
HindIII	NEB (R0104S)
AgeI	NEB (R3552)
DpnI	NEB (R0176S)
EcoRI	NEB (R0101L)
NucleoBond Xtra Midi	Macherey-Nagel (740410.50)
NucleoSpin Gel and PCR Cleanup	Macherey-Nagel (740609.250)
NucleoSpin Plasmid EasyPure	Macherey-Nagel (740727.250)
Phusion High-Fidelity DNA Polymerase	NEB (M0530S)
Proteinase K	Bioline (BIO-37039)
T4 DNA Ligase	NEB (M0202L)
T4 DNA Polymerase	NEB (M0203L)
T4 Polynucleotide Kinase	NEB (M0201L)
T5 exonuclease	NEB (M0363S)
Taq DNA Polymerase	NEB (M0273S)
Taq Ligase	NEB (M0208S)
XbaI	NEB (R0145S)
Zymolyase-100T	Gerbu Biotechnik (07665)

1 kb DNA Ladder	NEB (N3232S)
10 bp DNA Ladder	Life technologies (10821015)
100 bp DNA Ladder	NEB (N3231S)
3-Indoleacetic acid	Sigma (45533)
3XFLAG peptide	Sigma (F4799)
5-Fluoroorotic Acid Monohydrate (5-FOA)	Biozol (F59500)
50 bp DNA Ladder	NEB (N3236S)
Agarose Universal	Bio&SELL (BS20.46.500)
Alpha factor	Hölzel Diagnostika, GenScript (RP01002)
Ampicillin	Roth (K029.2)
Anti-Flag M2 Affinity Gel	Sigma (A2220)
Aprotinin	Genaxxon (M6361.0100)
Bacto Agar	BD Biosciences (211820)
Bacto Peptone	Life technologies (211820)
Bromophenol Blue	Sigma (B0126-25G)
Chloroform	VWR Chemicals (22711.324)
ClonNAT (Nourseothricin)	Werner BioAgents GmbH (5.000.200)
Complete Protease Inhibitor Cocktail tablet	Sigma (11836145001)
Coverslips	Roth (0657.2)
Cryobox	Kisker Biotech (R034-7)
Difco Yeast Nitrogen Base	BD Biosciences (291920)
DMSO	Sigma (D2438)
dNTPs	NEB (N0447S)
Drop out powder components (Ade, Ala, Asn, Asp, PABA, Cys, Glu, Gln, Gly, Ile, Myo-Inositol, Leu, Lys, Met, Phe, Pro, Ser, Thr, Trp, Tyr, Ura, Val)	Sigma (A8626, A7627, A9256, A5040, C1276, G1251, G3126, G8790, I2752, I5125, L8000, L5626, M9625, P2126, P0380, S4500, T8625, T0254, T3754, U0750, V0500)
DTT (Dithiothreitol)	Life technologies (R0861)
ECL Western Blotting detection reagents	Sigma (GERPN2235)
EDTA (Ethylenediaminetetraacetic acid)	Pan Reac Appli Chem (131669.1210)
EGTA (Ethylene glycol-bis(β-aminoethyl ether)-N,N,N′,N′-tetraacetic acid)	Roth (3054.3)

EtOH 100% - high quality	Sigma (32205-2.5L-M)
EtOH 96% - low quality	CLN GmbH (N-1196.9025)
Ficoll PM400	Sigma (F4375)
G418	Sigma (G8168)
Galactose	Sigma (G0625)
Glass beads	Roth (N030.1)
Glass slides	Roth (H879.1)
Glucose	VWR (1.08342.1000)
Glycerol	VWR (1.04092.2500)
Glycogen	Sigma (10901393001)
Haemocytometer	Fischer Scientific (11314052)
HEPES	VWR Chemicals (1.10110.1000)
Histidine	VWR (1.04351.0100)
Hydroxyurea	Sigma (H8627)
Hygromycin B	Thermo Fisher Scientific (10687010)
IGEPAL	Sigma (I8896)
Isoamyl alcohol	Roth (T870.1)
Isopropanol (2-Propanol)	Sigma (34863-2.5L-M)
$K_2HPO_4.3H_2O$	VWR (1.05099.1000)
KCl	Sigma (P9541)
KH_2PO4	VWR (1.04873.1000)
Leupeptin	Genaxxon (M6100.0100)
LiCl (Lithium Chloride)	VWR (25009.236)
Magnesium Chloride	VWR (25108.295)
Methyl methanesulfonate	Sigma (129925)
Methylene Blue	Roth (A514.1)
Milk Powder (Bio Magermilchpulver)	ReformKontor (3030)
NAD (Nicotinamide adenine dinucleotide)	NEB (B9007S)
Nitrocellulose membrane	Kisker (D10600018)
Nonstick RNase-free Microfuge Tubes 0.5ml	Life technologies (AM12350)
Nonstick RNase-free Microfuge Tubes, 1.5ml	Life technologies (AM12450)

PEG (Polyethylene glycol) 3350	Sigma (P-3640)
PEG 8000	Promega (V3011)
Pepstatin	Genaxxon (M6359.0100)
Phenol:Chloroform:Isoamyl alcohol (25:24:1)	Roth (A156.1)
PMSF (Phenylmethylsulfonylfluoride)	Sigma (P7626)
Potassium acetate	VWR (1.04820.1000)
Protease Inhibitor Cocktail	Sigma (P8215)
SDS-PAGE gel, NuPAGE Bis-Tris Protein Gel, 10%, 12%, and 8-16%	Serva (0043266.01, 0043280.01, 0043263.01)
Sodium chloride	Serva (30183.01)
Sodium deoxycholate	Sigma (D6750)
SDS (Sodium dodecyl sulfate)	Serva Electrophoresis (20765.03)
Sodium hydroxide	Neolab (LC-4994.2)
Sodium perchlorate	Sigma (381225)
Sorbitol	Serva Electrophoresis (35230.02)
Trichloroacetic acid (TCA)	Sigma (T0699)
Triple Color Protein Standard II	Serva (39257.01)
Triple Color Protein Standard III	Serva (39258.01)
Tris ultrapure	Diagonal (A1086.1000)
Triton X-100	Sigma (T8787)
Tween-20	Sigma (P9416)
Ultra Pure Salmon Sperm DNA Solution	Life technologies (15632011)
Whatman blotting paper	VWR (588-3148)
Yeast Extract	BD Biosciences (212750)
Zirconia/Silica Beads 0.5mm diameter	Biospec (11079105z)
β-Mercaptoethanol	Sigma (M6250)
IGEPAL CA630	Sigma (18896)
Bicinchoninic acid (BCA) protein assay kit	Pierce (23225)
TCEP(Tris(2-carboxyethyl) phosphine hydrochloride)	Sigma (C4706)
CAM (2-chloroacetamide)	Sigma (C4706)
Lys-C	Wako Japan (125-05061)

Trypsin	Sigma (T7575, proteomics grade)
Titansphere TiO_2	GL Sciences Inc (501021315)
C8 material	Empore - 3M (2214)
SDB-RPS (Styroldivinylbenzol Reversed Phase Sulfonat) material	Empore - 3M (2241)
TFA (Trifluoroactetic acid)	Merck (108262)
ACN (Acetonitrile)	Roth (8825.1)
Iodoacteamide	Sigma (I1149)
RNAse A	Sigma (R 4875)
proteinase K	Sigma (P 2308)
ATP (Adenosine triphosphate)	Sigma (A3377)
NADH	Sigma (N4505)
PEP (phosphoenolpyruvate)	Molecula (16921512)
Lactic dehydrogenase/pyruvate kinase	Sigma (P0294)
384 well plates	Greiner (781101)
4X NuPAGE™ LDS Sample Buffer	Invitrogen (NP0007)
PhosSTOP	Sigma (4906845001)

4.1.7. Yeast and Bacteria media composition

Table 8: Yeast, Bacteria media and plates composition

Description	**Components**
YPD (full media / plates)	20 g/l peptone, 10 g/l yeast extract, 20 g/l glucose, 1 g/l KH_2PO_4, 100 mg/l adenine. (Add 25g/l Bacto agar for plates)
YNB (synthetic media / plates)	6.7 g/l Yeast Nitrogen Base, 1.6 g/l amino acid dropout-mix (-His, -Leu, -Ura, -Trp), 20 g/l glucose, pH 5.4. Optional supplement with 84 mg/l His / Trp / Ura, 168 mg/l Leu. (Add 25g/l Bacto agar for plates)
5 FOA plates	6.7 g/l Yeast Nitrogen Base, 1.6 g/l amino acid dropout-mix (-His, -Leu, -Ura, -Trp), 20 g/l glucose, pH 5.4. Supplement with 84 mg/l His / Trp, 168 mg/l Leu, 50 mg/l Ura, 25g/l Bacto agar and 0.1% 5-FOA.
YPD media	20 g/l peptone, 10 g/l yeast extract, 20 g/l glucose.
Sporulation plates	2.5 g/l Yeast Extract, 1 g/l glucose, 15 g/l potassium acetate, 20 g/l Bacto agar. Mix all components and autoclave. Add 20ml of Amino acid stock.

Amino acid stock	adenine 4 g/l, uracil 4 g/l, leucine 2 g/l, tryptophan 2 g/l, tyrosine 0.8 g/l, phenylalanine 10 g/l, methionine 2 g/l, arginine 2 g/l, histidine 2 g/l, lysine 2 g/l. Kept in dark area at room temperature.
LB media / plates	25g/l premixed LB broth (Roth)

4.2. Methods

4.2.1. Yeast Strain generation

Yeast strains in this thesis were generated via standard genetic techniques and were originated from the W303 or S288c genetic background. The appropriate background and genotype for each strain are provided next to the strain. To delete a gene and replace with a selection marker, desalted oligonucleotides were designed with 50 bp of homology before the start codon and after the stop codon of the target gene. The selection marker was then amplified through PCR using plasmids based on pRS- or pFA6a, with the Phusion DNA Polymerase. The melting temperature (Tm) for each primer pair was calculated using the NEB Tm Calculator online tool (https://tmcalculator.neb.com). Amplified DNA was purified from agarose gels using the Gel and PCR Clean-up kit. All constructs were transformed according to the transformation protocol (see general methods). To verify the deletions and mutations in genes, the modified loci were validated by PCR either using genomic DNA or by colony PCR.

Certain strains were generated through a process mating, sporulation, and tetrad dissection. Firstly, haploid strains of mating type (MAT) a and α background that possessed the desired mutations or deletions were mated on a non-selective YPD plate for 4 hours. Multiple diploids were either selected based on auxotrophic or drug marker or, when appropriate, picked and cultured in a non-selective YPD media. The diploid cells were then patched on a sporulation plate and incubated at 30 ^{o} C for 3-4 days for sporulation. Afterwards, spores were dissected using Singer MSM 400 dissection microscope onto YPD plates. These spores were grown at 30 ^{o} C for 2 - 3 days and subsequently, they were replica plated onto plates containing appropriate selection markers and haploids with appropriate mating type were stored as glycerol stocks in YPD at -80 ^{o} C.

***arp8-P* strain:** *ARP8* along with its native promotor and terminator, was amplified PCR using genomic DNA and subsequently cloned into pRS416 plasmid. Using site directed mutagenesis, serines S65 and S233 was mutated to alanines A65 and A233 respectively. In parallel, *URA3* marker were amplified from pFA6-URA plasmid using *ARP8* 50 bp homology primers before the start codon and after the stop codon to delete *ARP8* with *URA3* marker and transformed in BY4742 strain. Positive colonies were selected on -URA plates because of integration of *URA3* marker at *ARP8* locus and confirmed with colony PCR. *ARP8* gene containing A65 and A233 was PCR amplified from the plasmid pRS416 and transformed into strain where *URA3* is integrated at *ARP8* locus. Positive colonies were selected on 5FOA (5-

Fluoroorotic acid) plates. 5FOA converts *URA3* gene product to 5-fluororuracil, which is toxic to the cells. Therefore, *URA3* positive cells would not survive on the 5FOA plates and the resultant strain would be *URA3* negative where *ARP8* locus is replaced with *ARP8* gene containing A65 and A233 (strain yPB3). MAT a type strain was generated by mating yPB3 with BY4741, followed by sporulation, tetrad dissection, mating type check and sanger sequencing. The resultant strain pYPB4 is MAT a with *ARP8* gene containing A65 and A233.

To purify the INO80 complex, we tagged Ino80 subunit with 3xFLAG-tag at the C terminus. 3xFLAG together with clonNAT marker was amplified from pBP83 plasmid and chromosomally inserted at the C-terminus of the gene before the stop codon. Positive clones were selected on YPD+clonNAT plate and FLAG tag integration at *INO80* was confirmed by western blot (yPB5 and yPB6).

***spt6-P* strain:** *SPT6* including its native promotor was PCR amplified from genomic DNA and cloned into pRS305. Using site directed mutagenesis, S134, S155 and S206 was mutated to alanine A134, A155 and A206. In parallel, *URA3* marker was amplified from pFA6-URA plasmid by using *SPT6* 50 bp homology primers before the start codon and after the stop codon. The amplified *URA3* marker was then employed to delete *ARP8* and the transformation was carried out in W303 diploid strain. In a diploid strain only one copy of *SPT6* was deleted with *URA3* marker. Positive colonies were selected on -URA plates because of integration of *URA3* marker at *SPT6* locus and confirmed with colony PCR. Plasmid pRS305 is an integrative plasmid and restriction digestion of *LEU2* marker was used to integrate the plasmid at *LEU2* locus within the genome. pRS305 with cloned *SPT6* gene and *SPT6* gene containing mutated S134, S155 and S206 was linearised with *Age I* digestion and transformed in W303 *SPT6/SPT6Δ::URA3* (*leu2-3,112 trp1-1 can1-100 ura3-1 ade2-1 his3-11,15)*. The positive colonies were selected on -LEU plates and plasmid integration upstream and downstream of *LEU2* locus was confirmed by colony PCR. Positive colonies were sporulated and tetrad dissected to obtain haploid spores containing single copy of SPT6 genes. *URA3* and *LEU2* negative haploids were selected where WT *SPT6* is deleted with *URA3* and cloned *SPT6* plasmid with and without mutations is integrated at LEU2 locus.

4.2.2. Mass Spectrometry

4.2.2.1. Nuclei Preparation

Yeast nuclei were isolated following a previously established protocol [292]. Cells were cultivated overnight until they reached the OD 600nm = 0.8 - 1.0, measured using aThermo Scientific GENESYS 20 spectrophotometer, in 200 or 500 ml YPD complete media. Yeast cells were harvested by centrifugation at 4 ^{o}C, 4500 x g for 10 minutes (mins) (Beckman Coulter JLA 8.1 rotor) and the pellets were washed once with cold distilled water. The washed pellet was weighed (wet weight) and resuspended in 2 times wet weight of preincubation solution containing 0.7 M β -mercaptoethanol and 2.8 mM EDTA pH = 8.0. The cells were shaken for a duration of 25 - 30 mins at 30 ^{o}C, then they were washed with 40 ml of cold 1 M sorbitol, and finally the pellet was resuspended 5 ml buffer (5 mM β -mercaptoethanol in 1 M sorbitol) per gm wet weight of the pellet. OD 600 of resuspended pellet was determined using 1:100 dilution in water. To digest the cell wall (spheroplasting), Zymolyase was freshly dissolved in water and added to the cell pellet. A quantity of 2 mg of zymolyase was added for every g of wet weight and the mixture was incubated at 30 ^{o}C for a duration of 20 - 30 mins. The cell wall digestion was considered complete when the absorbance at 600 nm had decreased to 80 - 90% of the starting OD. The spheroplasts were harvested by centrifugation (4 ^{o}C, 2500 x g, 5 mins, TX-1000 rotor ThermoFisher Scientific). They were then washed with 40 ml cold 1 M sorbitol and resuspended in a Ficoll buffer. The Ficoll buffer consisted of 18% Ficoll type 400, 20 mM KH_2PO_4 pH 6.8, 1 mM $MgCl_2$, 0.25 mM EGTA pH 8.0, 0.25 mM EDTA pH 8.0. A volume of 7 ml of the Ficoll buffer was added for every g of cell weight. Lastly, nuclei were divided into aliquots based on the desired wet weight (0.5 or 1 g) and were subjected to centrifugation at 4 ^{o}C, 12000 x g (Beckman Coulter JA 20.1 rotor) for 30 mins. The isolated nuclei were stored at -80 ^{o}C until further processing.

4.2.2.2. Nuclei processing for phospho proteome and whole proteome

Mass spectrometry samples for phospho proteome and whole proteome analysis were processed exactly as previously described [222]. All reagents were prepared with mass spectrometry grade reagents. Briefly, thawed nuclei were first washed with 100 mM Tris-HCl pH 8.5 to remove phosphate buffer residues. Chilled lysis buffer containing 4% Sodium

deoxycholate (D6750, Sigma) and 100 mM Tris-HCl pH 8.5 was added such that total volume is about 600 µl. The lysates were heat inactivated at 95 ^{o}C for 5 mins and then homogenized by bath-sonication using Biorupter Pico at 4 ^{o}C (two times 10 cycles each of 30 sec on and 30 sec off at maximum output power). Lysate was collected in a new eppendorf tube by centrifugation and protein concentration was determined using Bicinchoninic acid (BCA) protein assay kit. All samples were diluted to a final concentration of 300 µg in 270 µl of lysis buffer. Reduction/alkylation buffer containing 100 mM Tris(2-carboxyethyl) phosphine hydrochloride and 400 mM of 2-chloroacetamide (CAM) was added at 1:10 ratio of the total volume (30 µl) and incubated for 5 mins, 45 ^{o}C with shaking at 1500 rpm. At room temperature, using 1:100 enzyme to substrate ratio, 3 µg each of Lys-C and trypsin was added to each 300 µg sample and digested overnight at 37 ^{o}C with shaking at 1500 rpm.

Next day, digested peptides were separated such that 2/3 of the sample was processed for phospho proteome and 1/3 was processed for whole proteome. Stage tips were prepared as described earlier [293]. Phospho peptides were enriched by TiO_2 based enrichment and eluted using C8 material on C8 stage tips. Collected phopsho peptides were desalted and eluted using SDB-RPS (Styroldivinylbenzol Reversed Phase Sulfonat) material on SDB-RPS stage tip. The eluate was evaporated under vacuum to dryness at 45 ^{o}C. Phospho peptides were then reconstituted in 10 µl of MS loading buffer containing 0.3% Trifluoroactetic acid (TFA) and 2% Acetonitrile (ACN).

For whole proteome, 1/3 of the digested peptides were dissolved with 200 µl isopropanol and 1% TFA. Peptides were desalted and eluted using by SDB-RPS material on SDB-RPS stage tip. The eluate was evaporated under vacuum to dryness at 45 ^{o}C and peptides were reconstituted in 15 µl of MS loading buffer.

4.2.2.3. Running samples on Mass spectrometer

For LC-MS purposes, desalted peptides were injected in an Ultimate 3000 RSLCnano system (Thermo Fisher Scientific) and separated in a 25-cm analytical column (75µm ID, 1.6µm C18, IonOpticks) with a 50-min gradient from 2 to 35% or 60-min gradient from 2 to 32% acetonitrile in 0.1% formic acid for proteome and phosphoproteome analysis, respectively.

Phospho proteome: The effluent from the HPLC was directly electrosprayed into an Orbitrap Exploris-480 (Thermo Fisher Scientific) operated in data dependent mode to

automatically switch between full scan MS and MS/MS acquisition. Survey full scan MS spectra (from m/z 350–1400) were acquired with resolution R=60,000 at m/z 400 (AGC target of $3x10^6$). The 15 most intense peptide ions with charge states between 2 and 5 were sequentially isolated to a target value of $2x10^5$, fragmented at 30% normalized collision energy and acquired with resolution R=15,000. Typical mass spectrometric conditions were: spray voltage, 1.5 kV; no sheath and auxiliary gas flow; heated capillary temperature, 275ºC; ion selection threshold, $5x10^3$ counts. For phosphopeptides, MS2 resolution was increased to R=30,000 and ion selection threshold to $3x10^4$ counts.

Whole proteome: Eluting peptides were ionized in a nanoESI source and on-line detected on a QExactive HF mass spectrometer (Thermo Fisher Scientific). The mass spectrometer was operated in a TOP10 method in positive ionization mode, detecting eluting peptide ions in the m/z range from 375 to 1,600 and performing MS/MS analysis of up to 10 precursor ions. Peptide ion masses were acquired at a resolution of 60,000 (at 200 m/z). High-energy collision induced dissociation (HCD) MS/MS spectra were acquired at a resolution of 15,000 (at 200 m/z). All mass spectra were internally calibrated to lock masses from ambient siloxanes. Precursors were selected based on their intensity from all signals with a charge state from 2+ to 5+, isolated in a 2 m/z window and fragmented using a normalized collision energy of 27%. To prevent repeated fragmentation of the same peptide ion, dynamic exclusion was set to 20 s.

4.2.2.4. Phospho proteome and whole proteome data analysis

MaxQuant search parameters: For phospho proteome identification MaxQuant 2.0.3.0 software package was used. Parent ion and fragment mass tolerances were 8 ppm and 0.5 Da, respectively, and allowance for two missed cleavages was made. Yeast canonical protein database from UniProt (*Saccharomyces cerevisiae* (strain ATCC 204508 / S288c)), filtered to retain only the reviewed entries were used for the searches. Regular MaxQuant conditions were the following: site FDR, 0.01; protein FDR, 0.05; minimum peptide length, 6; variable modifications, oxidation (M); phospho (STY); fixed modifications, carbamidomethyl (C); peptides for protein quantitation, razor and unique; minimum peptides, 2; minimum ratio count, 2. Proteins were validated on the basis of at least one unique peptide detected in the proteome of all the three replicates or in at least two of the three replicates.

For whole proteome identification, MaxQuant search parameters were identical except for the variable modifications, which were oxidation (M); acetyl (protein N-term); acetyl (K); dimethyl (KR); methyl (KR).

Data analysis: The phospho-proteomics data was analysed using an R-script developed in-house. Differential and quantitative analysis was performed using phospho-sites with a 75% or higher probability of occurrence (according to MaxQuant output). Phospho-sites and proteins that were present in at least 50% of the replicates were considered for the downstream analysis. Intensity based absolute quantification (iBAQ) values were used to quantify the abundance of phospho-sites and compare it in different conditions. Differential expression analysis at the whole and phospho proteome level was carried out using the DEP package. Briefly, after filtering for all the experimental and analytical contaminants missing values were imputed by the Bayesian principal component analysis (BPCA) method followed by limma statistical analysis [294] using a p-value cut-off of 0.05. The phospho-site abundances were normalised to the total protein abundance of the respective proteins.

4.2.3. XL-MS (Cross-link mass spectrometry)

Protein chemical cross-linking with DSBU cross-linker: Purified wildtype and mutant INO80 were buffer equilibrated in 25 mM HEPES/NaOH (pH 7.2), 5% glycerol, 300 mM NaCl, 1mM DTT, 4mM $MgCl_2$ using an Amicon (3.5 KDa cutoff) for five times.

First a titration of different cross-linker concentration for DSBU (ThermoFisher Scientific) and PhoX (Thermofischer Scientific) were tested to determine the optimal cross-linking concentration for each condition. The INO80 complex (1 µg in total of wildtype or mutant) was cross-linked for 20 min at 30°C on a thermomixer at 1200 rpm.

The optimal cross-linker concentration was determined by SDS-PAGE and silver staining and was applied to 25 µg and 15 µg of complex at 30°C, 1200 rpm for 20 min. In case of DSBU, the optimal cross-linker concentration for wildtype INO80 was at 58 µM and for the mutant at 100 µM. The reaction was quenched by adding ammonium bicarbonate to a final concentration of 100 mM and incubated for 10 min at 30°C subsequently followed by protein denaturation, alkylation, and tryptic digest. Cross-linked samples were denatured by adding two sample volumes of 8 M urea, reduced with 5 mM Tris (2-carboxyethyl) phosphine and alkylated by the addition of 10 mM iodoacetamide for 40 min at RT in the dark. Proteins were digested with Lys-C (1:50 w/w) at 35°C for 2 hr, diluted with 50 mM ammonium bicarbonate, and digested with trypsin (1:50 w/w) overnight. Peptides were acidified with trifluoroacetic acid (TFA) at a final concentration of 1% and purified by reversed phase chromatography using C18 cartridges (stage tips). In case of DSBU cross-linked peptides, peptides were enriched on a Superdex Peptide PC 3.2/30 column using water/acetonitrile/TFA (75/25/0.1, v/v/v) as mobile phase at a flow rate of 50 µl/min. Fractions containing cross-linked peptides

were analysed by liquid chromatography (Dionex 3000, Thermofisher Scientific) coupled to tandem mass spectrometry (LC-MS/MS) using a TimsTOF Pro instrument (Bruker Daltonics).

LC-MS Analysis of enriched cross-linked peptides: Cross-linked peptides were separated on a PepSep column (25 cm, inner diameter 150 µm, Bruker Daltonics) by an online reversed-phase chromatography through a 50 min gradient starting with 3% Buffer B (ACN, 0.1% FA) to a gradient to 43% Buffer B at a flow rate of 300 nl/min. Eluting peptides were directly sprayed via the CSI source into the TimsTOF Pro. Each sample was measured in three independent technical replicates. The mass spectrometric measurement was performed in data-dependent acquisition mode with a top 10 method. The same settings were applied as described [295]. As template the standard DDA-PASEF MS Method provided by Bruker Daltonics was used. Only precursor ions of +3 to +8 charge (in case for DSBU +2 to +8 charge) were selected for fragmentation scan. Raw data files were searched against MaxQuant software package (version 2.0.2.0). Following changes have been applied. Enzyme specificity set to trypsin with a maximum number of missed cleavages 3; DSBU specificity linking (K, S, T, Y); fixed modifications carbamidomethyl (C); variable modifications, oxidation (M). PSM FDR crosslink set to 5%. Inter- and Intra-Crosslinks were filtered by applying an MS1 tolerance window of -3 to 3 ppm and a score ≥ 60 [296]. Cross-links were visualized as network plots using the webserver xiNET [297].

4.2.4. RNA sequencing

For differential gene or transcriptome analysis, Cells were grown overnight until they reached the OD 600nm = 0.8 - 1.0 in 10 ml YPD media. Next day, cells were reinoculated in 100ml fresh YPD media at 0.1 OD. At 0.4 OD cells were collected by centrifugation at 4 ºC, 4500 x g for 10 mins (Beckman Coulter JLA 8.1 rotor). The pellets were washed once with cold distilled water, rapidly frozen in liquid nitrogen and stored at -80 ° C.

For the extraction of total RNA, pellets were resuspended in 1 ml QIAzol Lysis Reagent (Qiagen) and mixed with 250 µl of zirconia beads. Cells were lysed using the Precellys 24 homogenizer (Bertin) for 3 x 30 sec with 5 min rest on ice in between, followed by centrifugation at 12000 x g for 10 min at 4 ° C. The cleared lysate was mixed with 200 µl chloroform by vortexing for 15 sec. After incubation at room temperature for 10 min, samples were centrifuged at 12000 x g for 10 min at 4 ° C. The aqueous phase was extracted with 500 µl chloroform, vortexed briefly and then centrifuged at 12000 x g for 10 min at 4 ° C. The RNA was precipitated from the aqueous phase by adding 500 µl isopropanol and incubating

at 4 ° C for 15 min. The RNA was pelleted by centrifugation at 12000 x g at 4 ° C for 10 min. The Pellets were washed twice with 1 ml of 75% ethanol. RNA was dissolved in 150 µl RNase-free water for a duration of 30 min at 55 º C and photometrically quantified using a DeNovix Spectrophotometer. Of each sample, 10 µg RNA was treated with 10 units recombinant DNase I (Roche) for 1 h at 37 ° C, purified using Agencourt RNAClean XP beads (Beckman Coulter) and photometrically quantified using a DeNovix Spectrophotometer.

Library preparation and sequencing: Of each sample, 1 µg DNaseI-treated RNA was used for rRNA depletion and library preparation. Ribosomal RNA was depleted using the *S. cerevisiae*-specific riboPOOL kit (siTOOLs Biotech) according to the provided protocol. rRNA-depleted RNA was purified using Agencourt RNAClean XP beads (Beckman Coulter) and analyzed on a 4150 TapeStation System using a High Sensitivity RNA Screen Tape (Agilent). Of the rRNA-depleted samples directional libraries were prepared using the NEBNext Ultra II Directional RNA Library Prep Kit for Illumina (New England Biolabs) following the recommended protocol. The quality of the libraries was assessed on a 4150 TapeStation System using a High Sensitivity D1000 Screen Tape (Agilent). Libraries were sequenced on an Illumina NextSeq 2000 instrument in paired-end mode.

Data analysis: Sequencing reads were pseudoaligned to the yeast transcriptome (Ensembl build R64, annotation version 108) using kallisto (version 0.48) using default parameters. Data was further processed in R/bioconductor. Differential expression was tested with DESeq2(version 1.36.0) using the experimental batch as random factor.

4.2.5. Gibson Cloning

To insert a specific gene into a yeast vector, DNA was amplified using Phusion DNA Polymerase from WT yeast genomic DNA. Using restriction enzyme digestion yeast plasmids were linearized. all DNA fragments from agarose gel using the Macherey-Nagel NucleoSpin Gel and PCR Clean-up kit. Using 5x Gibson assembly buffer (450 mM Tris-HCl pH 7.5, 25% PEG 8000, 50 mM $MgCl_2$, 50 mM DTT, 1 mM dNTPs, 5 mM NAD), 1.33X Gibson assembly master mix (5X Gibson Assembly Buffer, 0.005 U/µl T5 exonuclease, 0.033 U/µl Phusion polymerase, 5.33 U/µl Taq Ligase) was prepared in house [298]. Gibson assembly was performed using 1.33X gibson assembly master mix and transformed into NEB 5-alpha competent *Escherichia coli* (C2987, Thermofisher scientific). The correct clones were confirmed by sanger sequencing employing M13 universal primers. Additionally, specific primers targeting regions within the gene were used whenever required.

4.2.6. Primer designing and site directed mutagenesis

The mutagenic oligonucleotide primers used in this protocol must be designed individually according to the desired mutation. Both mutagenic (Forward and reverse) primers contain the desired mutation and anneals to the same DNA sequence on opposite strands of the plasmid. The desired mutation should be in the middle of the primer with ~25 bp of correct sequence on both sides. Mutation generated in this study are point mutations where a serine(s) are mutated to alanine(s).

Site directed mutagenesis reaction was performed using mutagenic primers and 0.04 U/µl Phusion DNA Polymerase. Two 50 µl inverse PCR reactions were setup with 25 ng and 50 ng of template DNA (WT cloned gene in yeast vector) and High-Fidelity buffer as described in table 10. Cycle each reaction in Eppendorf Mastercycler nexus GX2 using the cycling parameters described in table 11. After completion, 1 µl of the Dpn I restriction enzyme (10 U/µl) was added directly to each amplification reaction to digest methylated, parental DNA template. The tube was vortexed briefly, spun down and transferred back to the thermocycler to incubate at 37 ^{o}C for 1 hr. Upon completion, 5 µl of the reaction mixture was used for transformation into NEB 5-alpha competent Escherichia coli. Correct clones were validated by sanger sequencing using M13 universal primers as well as using primers binding within the gene when required.

Table 9: Site directed mutagenesis inverse PCR reaction

Component	Amount
Water	Up to 50 µl
5X High-Fidelity buffer	10 µl
10mM dNTPs	1 µl
10µM Forward Primer	1.5 µl
10µM Reverse Primer	1.5 µl
Template DNA (25 ng or 50 ng)	Variable
Phusion DNA polymerase (0.04 U/µl)	1 µl

Table 10: Site directed mutagenesis parameters

Segment	Temperature	Time	Cycles
Initial denaturation	95 ºC	30 seconds	1 cycle
Denaturation	95 ºC	30 seconds	16 cycles
Annealing	55 ºC	1 minute	
Extension	68 ºC	1 minute/ kb length of the plasmid	

To generate more than one mutation on the same plasmid, the above-mentioned scheme was used to generate one mutation after another.

4.2.7. Cell cycle arrest and release experiments

Cells were grown at 30 ºC in YPD to OD 600nm = 0.2 - 0.5 and arrested in G1 with alpha-factor (MPI core facility alpha factor – 5 mg/ml stock concentration, 5 µg/ml of working concentration) or (GenScript – 10 mg/ml stock concentration and 10 µg/ml working concentration) for 120 mins in total. After 60 mins, a second dose of alpha-factor was added. Cells were then washed once with pre-warmed YPD and then released into fresh pre-warmed YPD to continue progressing the cell cycle. Samples for FACS analyses, immunoblotting and mass spectrometry were collected at specified time points and processed following standard protocols.

4.2.8. Flow cytometry

Cell cycle arrest and release samples were collected as mentioned above. For flow cytometry collected samples were processed as described previously [299]. Briefly, yeast cells were collected by centrifugation (4000 x g. 5 mins, 4 ºC) and then resuspended in 50 mM Tris-HCl pH 8.0 / 70% ethanol. After resuspension the cells were stored at 4 ºC for minimum of one hour for permeabilization and fixation. Cells were then digested with RNAse A and proteinase K. Finally, the cells were stained with 0.5 µM SYTOX green and the DNA content was quantified on a MACSquant analyzer (Miltenyi Biotec).

4.2.9. Protein expression and purification

The INO80, FACT, Nap1, yeast histones, and NuA4 were expressed and purified as previously described [39, 300-304] with modifications.

INO80 expression and purification: Cells were grown in 6 L YPD for 24 hours, collected by centrifugation (6000 x g, 10 mins, 4 ^{o}C) and pellet was resuspended in an equal volume of 2X lysis buffer containing protease inhibitors 0.2 mM PMSF, 1 µM pepstatin A, 1 µg/mL aprotinin, and 2 µM leupeptin. 1X lysis buffer is 25 mM Hepes pH 7.6, 10% glycerol, 0.05% NP-40, 1 mM EDTA, 500 mM KCl, 1 mM DTT, 4 mM $MgCl_2$. Cells were frozen in a dropwise manner in liquid nitrogen and then crushed using a Freezer Mill. The frozen cell powder was thawed, resuspended in an equal volume of lysis buffer with protease inhibitors. The insoluble material was removed by ultracentrifugation (235,000 x g, 1 h, 4 ^{o} C). The supernatant was incubated with 1.5 mL pre-washed anti-FLAG M2 affinity gel resin (Sigma) in a batch for 1 h at 4 ^{o}C. The resin and bound protein were transferred into a disposable column, washed with 4 Column volume (CV) of lysis buffer and 1 CV of wash buffer (25 mM Tris-HCl pH 7.2, 200 mM KCl, 10% glycerol, 0.05% NP-40, 1 mM EDTA, 1 mM DTT, 4 mM $MgCl_2$). INO80 was eluted by 1 CV of the same buffer containing 0.5 mg/ml 3xFLAG peptide (Sigma), followed by 2 CV of buffer containing 0.25 mg/ml 3xFLAG peptide. Eluted fractions were analysed by SDS-PAGE, pooled together, and further purified with a Mono Q 5/50 GL column using a 13 CV gradient from 100 mM to 600 mM KCl (25 mM Tris-HCl pH 7.2, 10% glycerol, 0.05% NP-40, 1 mM EDTA, 1 mM DTT, 4 mM $MgCl_2$). The fractions were again analysed by SDS-PAGE, pooled together, and concentrated using a Vivaspin 20 (100 kDa MWCO Polyethersulfone, Merck). The Concentrated protein was then dialyzed for 1.5 hour in buffer containing 25 mM Tris-HCl pH 7.2, 600 mM NaCl, 40% glycerol, 1 mM EDTA and 1 mM DTT.

Spt6 expression and purification: 6 L of cells were grown in YPD for 24 hours, collected and lysed with a Freezer Mill as described above. The frozen cell powder was thawed and resuspended in an equal volume of lysis buffer (20 mM Tris-HCl pH 7.2, 0.5 M KOAc, 0.1% NP-40, 1 mM EDTA and 10% glycerol) with protease inhibitors. The insoluble material was removed by centrifugation (235,000 x g, 1 h, 4 ^{o}C).The supernatant was incubated with 1.5 mL pre-washed anti-FLAG M2 affinity gel in batch for 1 h at 4 ^{o}C. The resin and bound protein were transferred into a disposable column, washed with 4-5 CV of lysis buffer and 1 CV of wash buffer (10 mM HEPES-KOH pH 7.5, 150 mM NaCl, 0.1% NP-40, 1 mM EDTA, 10% glycerol). Spt6 was then eluted in 1 CV of wash buffer containing 0.5 mg/mL 3xFLAG peptide, followed by 2 CV of wash buffer containing 0.25 mg/mL 3xFLAG peptide. Eluted fractions were then analysed by SDS-PAGE, pooled together, and further purified with a

Mono Q 5/50 GL column using a 15 CV gradient from 100 mM to 1 M NaCl (10 mM HEPES-KOH pH 7.5, 0.1% NP-40, 1 mM EDTA, 1 mM DTT and 10% glycerol).

Nap1 expression and purification: 2 L of BL21 Gold (DE3) cells (Agilent technologies) with a Nap1-GST expression plasmid were grown at 37 °C until they reached the OD 600nm = 0.8. Protein expression was induced with 1 mM IPTG incubated for 2 hours at 37 °C. Cells were harvested by centrifugation (6000 x g, 10 mins, 4 °C) and resuspended in 30 ml of lysis buffer (150 mM KOAc, 0.1% NP-40, 1 mM DTT, 50 mM $KxPO_4$ pH 7.6 and 5 mM $MgCl_2$) with protease inhibitors. Cells were broken by two cycles of sonication (3 mins, 40% amplitude) and centrifuged at described above. 2 ml of glutathione agarose slurry was washed with Nap1 lysis buffer, and incubated with the cleared lysate for 2 hours at 4 °C followed by transfer into a disposable column. Beads were washed extensively with 5 CV of lysis buffer without any protease inhibitors. 3 ml of lysis buffer was incubated with 50 µl of Prescission protease overnight at 4 °C with rotation to cleave Nap1. Next day 3 ml elute was collected and two more 1 ml fractions were eluted with lysis buffer. Eluted fractions were analysed by SDS-PAGE and dialysed in 20 mM Tris-HCl pH 7.2, 100 mM NaCl, 0.5 mM EDTA, 1 mM DTT, 0.1 mM PMSF and 10% glycerol for 2 hours. Nap1 was further purified with a Mono Q 5/50 GL column using a 20 CV gradient from 100 mM to 1 M NaCl (20 mM Tris-HCl pH 7.2, 0.5 mM EDTA, 1 mM DTT and 10% glycerol). Peak fractions were pooled together and concentrated.

HIR expression and purification: 6 L of cells were grown in YPD for 24 hours, collected and lysed with a Freezer Mill as described above. The frozen powder was thawed and resuspended in an equal volume of lysis buffer (40 mM HEPES-KOH pH 7.5, 300 mM NaCl, 0.1% NP-40, 1 mM EDTA, 10% glycerol) with protease inhibitors and centrifuged as described above. The supernatant was incubated with 1.5 mL pre-washed anti-FLAG M2 affinity gel resin in batch for 1.5 h at 4 °C. This was then transferred into a disposable column, washed with 4 CV of lysis buffer and 1 CV of wash buffer (10 mM Tris-HCl pH 7.2, 150 mM NaCl, 0.1% NP-40, 1 mM EDTA, 10% glycerol). HIR was eluted in 1 CV of wash buffer containing 0.5 mg/mL 3xFLAG peptide, followed by 2 CV of wash buffer containing 0.25 mg/mL 3xFLAG peptide. Eluted fractions were analysed by SDS-PAGE and concentrated using a Vivaspin 20.

FACT expression and purification: Plasmids cloned with FACT subunits (Spt16 (-Ura) and Pob3 (-Leu)) were co transformed with appropriate markers at 30 °C. A preculture of cells was grown in YNB (-Ura, -Leu) media + 2% raffinose at 30 °C until saturation and 8 L of YP media + 2% raffinose was inoculated with 0.1 OD cells. Grow the cells until OD 600nM = 0.8 - 1.2 is reached, gene expression was induced with 2% galactose and the cells were

grown for 4 hours. The cells were collected by centrifugation (6000 x g, 10 mins, 4 °C) and resuspend in lysis buffer (20 mM Tris-HCl pH 7.2 and 5 mM Imidazole) with protease inhibitors. Cells were frozen in a dropwise manner in liquid nitrogen and crushed using a Freezer Mill. Cell powder was collected, thawed on ice and lysis buffer (20 mM Tris-HCl pH 7.2, 5 mM Imidazole, 0.5 mM NaCl) with protease inhibitors was added. Because there was no NaCl in the cell resuspension buffer, NaCl was added to obtain a final concentration of 0.5 M NaCl in thawed cell lysate. The insoluble material was removed by ultracentrifugation (235,000 g, 1 h, 4 °C) and the supernatant was incubated with 3 ml of pre wash Talon Metal Affinity resin (Clontech) and gently rotated for 2 hours at 4 °C. The resin and bound protein were transferred into a disposable column, washed with 4 CV of lysis buffer and additional 2 CV of wash buffer (20 mM Tris-HCl pH 7.2, 0.5 mM NaCl and 20 mM Imidazole). FACT was eluted with 8 x 1ml buffer A (20 mM Tris-HCl pH 8, 0.5 M NaCl and 100 mM Imidazole), 2 x 1ml buffer B (20 mM Tris-HCl pH 8, 0.5 M NaCl and 500 mM Imidazole) and 2 x 1 ml buffer C (20 mM Tris-HCl pH 8, 0.5 M NaCl and 1 M Imidazole). Desired fractions were concentrated and loaded onto Superdex S200 column, which was equilibrated with buffer containing 20 mM Tris-HCl pH 7.5, 200 mM NaCl, 10% glycerol and 1 mM β -Mercaptoethanol.

Yeast histones expression and purification: Plasmids cloned with H2A-H2B and H3-H4 were co transformed with appropriate antibiotic resistance at 37 °C. 2 L of BL21 (DE3) cells with histone plasmid expressing were grown at 37 °C until they reached the OD 600nm = 0.6. Protein expression was induced with 1 mM IPTG incubated for 2 hours at 37 °C and cells were harvested by centrifugation (6000 x g, 10 mins, 4 °C). Pellets were thawed on ice before adding 0.5 M NaCl, 20 mM Tris-HCl pH 8, 0.1 mM EDTA, 10 mM β -Mercaptoethanol and protease Inhibitors. Cells were broken by two cycles of sonication (3 minutes, 40% output) and insoluble material was seperated by centrifugation (235,000 x g, 45 minutes, 4 °C). Supernatant was passed over a 5 ml HiTrap Heparin column (GE Healthcare) and eluted with 20 column volumes (CV) of a 0 M to 2 M NaCl gradient (20 mM Tris-HCl pH 8, 0.1 mM EDTA, 10 mM β-Mercaptoethanol without protease inhibitors). Peak fractions were collected, concentrated and passed over a Superdex 200 column (GE Healthcare) using 2 M NaCl buffer (20 mM Tris-HCl pH 8, 0.1 mM EDTA, 10 mM β-Mercaptoethanol, no protease inhibitors). Peak fractions were pooled together and concentrated.

NuA4 / piccolo expression and purification: 2 L of BL21 star (DE3) cells with a piccolo NuA4 complex expression plasmid were grown at 37 °C until they reached the OD 600nm = 0.4. Protein expression was induced with 0.4 mM IPTG incubated for 3 hours at 37 °C and cells were collected by centrifugation (6000 x g, 10 mins, 4 °C). Pellets were thawed on ice before adding lysis buffer with protease inhibitors (50 mM Na_2PO_4 pH 7.0, 300 mM KCl, 10

mM Imidazole, 5 mM β-Mercaptoethanol). Cells were broken by two cycles of sonication (3 minutes, 40% output) and insoluble material was seperated by centrifugation (235,000 x g, 4 ^{o} C, 45 minutes) and the supernatant was incubated with 3 ml of pre wash Talon Metal Affinity resin (Clontech) and gently rotated for 2 hours at 4 ^{o} C. The resin and bound protein were transferred into a disposable column, washed with 4 CV of lysis buffer and additional 2 CV of wash buffer (20 mM Tris-HCl pH 7.2, 150 mM KCl, 5 mM β -Mercaptoethanol and 0.1 mM EDTA). NuA4 was eluted with 7 x 1 ml fraction in wash buffer with 200 mM imidazole. Peak fractions were pooled and concentrated.

4.2.10. *In vitro* kinase assay

15 nM of WT INO80 and mutant versions, were incubated with 5 nM DDK in buffer containing 100 mM potassium-glutamate, 25 mM HEPES-KOH pH 7.6, 10 mM $Mg(OAc)_2$, 0.02% NP-40, 1 mM DTT, 10 mM ATP and 5 mCi ^{32}P-g-ATP for 30 mins at 30 ^{o} C. Proteins were then separated on SDS-PAGE, gels were dried, exposed with Super RX Medical X-Ray Film (FUJI) and autoradiograph was developed using a Typhoon scanner phospho imager (GE Healthcare).

4.2.11. Spot dilution assay

Cells were cultivated overnight until saturation and OD at 600 nm was measured in technical replicates after 1:10 dilutions in water. Cells were diluted to OD = 1.0 in 250 µl water and 10-fold dilutions were generated. 7 µl of the prepared dilutions were spotted onto YPD plates and YPD plates supplemented with desired compound as necessary. These plates were incubated at 30 ° C for a period of 2 days. The assays were repeated three times using the independent colonies of the mutant strains.

4.2.12. Analysis of Rad52 foci and genetic analysis of recombination

Rad52 foci were counted in > 200 S/G2 phase cells transformed with pWJ1213 [305]. Cells were grown in synthetic complete (SC) liquid media with 2% glucose as the carbon

source. Cells were visualised using a Leica DM6 B fluorescent microscope. The mean and SEM of five experiments performed with independent transformants was plotted.

Recombination frequencies were calculated by transforming the indicated yeast strains with the pRS316-L plasmid containing two truncated repeats of the *LEU2* gene sharing 600 bp of homology and placed on a mono-copy *CEN*-based plasmid [249]. Recombinants were obtained by plating appropriate dilutions in SC media lacking leucine and uracil. To calculate total number of cells, they were plated in the same media supplemented with leucine. All plates were grown for 3-7 days at 30 º C. For each transformant, the median value of six independent colonies was obtained. The mean and SEM of at least three independent experiments performed with independent transformants was plotted.

4.2.13. ATP / NADH coupled ATPase assay

30 nM of WT and mutant INO80, were incubated in buffer containing 100 mM potassium-glutamate, 25 mM HEPES-KOH pH 7.6, 10 mM $Mg(OAc)_2$, and 1 mM DTT supplemented with 3 mM ATP and 3 mM $MgCl_2$, 0.6 mM NADH, 3 mM phosphoenolpyruvate (PEP) and 16 U/ml lactic dehydrogenase/pyruvate kinase. 24 µl reactions were prepared in 384 well plate in buffer without ATP and $MgCl_2$. Each reaction was tested with either 100ng/ul DNA (pFMP232) or 90 nM, 25mer chromatin originated from pFMP232.

A DNA fragment containing 25 consecutive copies of a modified 197-bp Widom-601 nucleosome positioning sequence was excised out of the plasmid pFMP232 using appropriate restriction enzymes and chromatin was assembled using salt gradient dialysis (SGD) as previously described [306]. All steps were performed at 4 º C. Briefly, histone octamers and 0.1 µg/µl digested plasmid DNA are mixed in 100 µl buffer containing 10 mM Tris–HCl pH 7.6, 2 M NaCl, 1 mM EDTA pH 8, 0.01% NP-40, 1 mM DTT [15–17]. Samples were placed in Slide-ALyzer devices (MWCO 7K, Thermo-Fisher) in 1 L high salt buffer containing 10 mM Tris–HCl pH 7.6, 2 M NaCl, 1 mM EDTA pH 8, 0.01% NP-40, 1 mM DTT. This was dialyzed in 3 L of low salt buffer containing 10 mM Tris–HCl pH 7.6, 50 mM NaCl, 1 mM EDTA pH 8, 0.01% NP-40, 1 mM DTT into the beaker over a time period of at least 24 h at flow rate of ~ 2 ml / min using peristaltic pump and tubing. Chromatin was then dialyzed for 2 h with 1 L low salt buffer at 30 ˚C and stored at 4 º C.

ATPase reactions were initiated by adding an ATP / $MgCl_2$ mix to a final concentration of 3 mM each. Plates were incubated at 26 º C in a Biotek PowerWave HT plate reader for 60 mins and absorption at 340 nm was determined every 15 s. For analyses, each time course was fitted to a linear function within a time range where all reactions were linear.

From the slope of the reaction and the extinction coefficient of NADH (6220 M^{-1} cm^{-1}), the change in NADH concentration was calculated (for 30 mL reactions in Greiner plates, the path length was 0.27273 cm). As oxidation of 1 NADH equals the hydrolysis of 1 ATP, the ATP hydrolysis rates were calculated from the slopes.

4.2.14. Nucleosome positioning assay

For nucleosome positing assay, chromatin was assembled using salt gradient dialysis (SGD) as previously described [142]. Briefly, a library of yeast origin plasmids, containing ~300 ARS (OriDB) sequence was created from the *S. cerevisiae* genomic library (pGP546, Open Biosytems). The selected plasmids contained an origin of replication at least 1000bp away from the border of plasmid backbone and yeast genomic insert. Using SGD, 10 µg of origin plasmid library DNA was mixed with Drosophila embryo histone in 100 µl SGD buffer containing 10 mM Tris–HCl pH 7.6, 2 M NaCl, 1 mM EDTA pH 8, 20 µg BSA, 0.05% Igepal to a saturated assembly degree. Samples were placed in Slide-ALyzer devices (Thermo-Fisher) in 300 ml high salt buffer containing 10 mM Tris–HCl pH 7.6, 2 M NaCl, 1 mM EDTA pH 8, 0.05% Igepal, 14.3 mM β-mercaptoethanol). This was dialyzed in 3 L of low salt buffer containing 10 mM Tris–HCl pH 7.6, 50 mM NaCl, 1 mM EDTA pH 8, 0.05% NP-40, 1.4 mM β-mercaptoethanol using peristaltic pump at 7.5 rpm, 30 °C for 16 hours. Chromatin was then dialyzed for 1 h with 1 L low salt buffer at 30 °C and stored at 4 °C.

The assay was performed with 30nM ORC and 20nM INO80 or INO80-P in a buffer containing 20 mM HEPES pH 7.5, 50 mM NaCl, 3 mM $MgCl_2$, 2.5 mM ATP, 2.5 mM DTT, 0.5 mM EGTA pH 8, 12% glycerol. The assay was initiated by the addition of SGD chromatin, incubated for 2 hours at 30 °C and stopped by addition of 0.2 U apyrase (NEB), incubated at 30 °C for 20 mins. In order to generate mostly mononucleosomal DNA, the reaction mixture was incubated with 100 U MNase (Sigma-Aldrich) and 1.5 mM $CaCl_2$ for 5 min at 30 °C. The digestion was stopped by the addition of 10 mM EDTA and 0.5% SDS followed by a proteinase K treatment for 1 hour at 37 °C and ethanol precipitation. Samples were run in 1.5% agarose gels for 1.5h at 110 V constant in 1X TAE (40 mM Tris, 20 mM acetic acid, 1 mM EDTA), and mononucleosomal DNA was excised and purified using DNA purification kit.

The sequencing libraries were prepared using 10–50 ng mononucleosomal DNA. The samples were diluted to 10 nM, pooled according to the sequencing reads required (~5 million reads per sample), and quantified via BioAnalyzer (Agilent). The pool was sequenced

either on an Illumina NextSeq 1000 in 50 bp paired-end mode (Laboratory for Functional Genome Analysis, Ludwig-Maximilians-Universität Munich). The MNase-seq data was analysed as previously described [142, 276].

4.3. General methods

4.3.1. Polymerase chain reaction (PCR)

DNA amplification was carried out using Phusion DNA Polymerase in 25 µl reaction volume in the Eppendorf Mastercycler nexus GX2. The primers were designed to have annealing temperatures ranging between 58 - 68 ºC for Phusion Polymerase, and these temperatures were calculated using the online NEB Tm calculator tool. The PCR reaction mixture was prepared as described in table 12.

Table 11: PCR reaction

Component	Amount
Water	Up to 25 µl
5X High-Fidelity buffer	5 µl
10mM dNTPs	0.5 µl
10µM Forward Primer	1.25 µl
10µM Reverse Primer	1.25 µl
Template DNA (20 - 25ng)	Variable
Phusion DNA polymerase	0.3 µl

The PCR was performed using following parameters in table 13.

Table 12: PCR parameters

Segment	Temperature	Time	Cycles
Initial denaturation	98 ºC	30 seconds	1 cycle
Denaturation	98 ºC	10 seconds	35 - 40 cycles
Annealing	58 - 68 ºC	30 seconds	
Extension	72 ºC	30 seconds / kb	
Final extension	72 ºC	10 mins	1 cycle
Hold	10 ºC	∞	

4.3.2. Restriction digestion

Plasmids underwent digestion with the suitable enzymes in a reaction volume ranging from 20 to 50 µl, taking place at 37 ºC for 3 hours. When possible, enzymes with high-fidelity version were employed using the NEB CutSmart buffer. The recommended temperatures, buffers and input DNA amounts were used for each enzyme as described by theNEB. Digested products were later analysed with separation on an agarose gel.

4.3.3. Yeast genomic DNA isolation

To obtain genomic DNA, yeast cultures of 5 - 10 ml were grown overnight until saturation. These cells were then harvested, resuspended in resuspension buffer (0.9 M Sorbitol, 50 mM Sodium phosphate pH 7.5, 140 mM β -Mercaptoethanol). After resuspension cells were lysed through a two-step process: first Zymolyase (20 mg/ml) was employed followed by digestion with Proteinase K (2 mg/ml) for 30 mins each at 37 º C. Genomic DNA was isolated using Phenol: Chloroform: Isoamyl alcohol mix (25:24:1) and Chloroform:Isoamyl alcohol mix (24:1). DNA was precipitated using 100% ethanol and subsequently dissolved in 1X TE buffer. To eliminate RNA content, 15 µl of 10mg/ml RNase A was added and the mixture was incubating for 1 hour at 37 º C. DNA was precipitated using Isopropanol. The DNA pellet was then dissolved in 1X TE buffer and adjusted to a final concentration of 400 ng/µl.

Occasionally Yeast DNA extraction kit (78870, Thermofisher scientific) was used to isolate genomic DNA. Appropriate temperatures and buffers were used for each sample as described by the manufacturer. The DNA pellet was then dissolved in 1X TE buffer and adjusted to a final concentration of 400 ng/µl.

4.3.4. Colony PCR

Colony PCR was used often used to screen for positive transformants after yeast transformation. A small smear of colony was resuspended in 10 µl Zymolyase solution containing 2.5 mg/ml zymolyase, 1.2 M sorbitol and 0.1 M sodium phosphate pH 7.4 and incubated at 37 ºC for 10 mins. The lysed cells were heat inactivated at 95 ºC for 5 mins and

after brief vortex centrifuged at 14,000 x g, 5mins, RT (Room temperature). Solution was collected in a new Eppendorf tube and 2 µl supernatant wasused for PCR. DNA was amplified using Taq polymerase with 10X thermo Taq buffer in 50 µl reaction volume in the Eppendorf Mastercycler nexus GX2. Primers annealing temperatures were calculated using the online NEB Tm calculator tool. The PCR reaction mix was prepared as described in table 14.

Table 13: Colony PCR reaction using Taq polymerase

Component	Amount
Water	Up to 50 µl
10X Thermo Taq buffer	5 µl
10mM dNTPs	1 µl
10µM Forward Primer	2.5 µl
10µM Reverse Primer	2.5 µl
Template DNA	2 µl
Taq DNA polymerase	0.5 µl

4.3.5. Western blot

Cells were grown overnight in 10 ml YPD media. 1 – 1.5ml cells were collected (5000 x g, 2 mins, TX-1000 rotor ThermoFisher Scientific) and resuspended in 500 µl of breaking buffer containing 0.288 M β-mercaptoethanol and 0.2 M sodium hydroxide. Incubate on ice for 10 mins and add 25 µl of trichloro acetic acid to final concentration of 0.321 mM. Incubation on ice for 10 mins and collect cells by centrifugation at 14,000 rpm, 5 mins, 4 ^{o}C FA-45-18-11 Eppendorf rotor [307]. Pellets were resuspended in 80 µl of 1X loading buffer containing 4X NuPAGE™ LDS Sample Buffer and 0.72 M β-mercaptoethanol. 10 µl of cell extract were loaded on a 10% SDS gel and transferred to a nitrocellulose membrane. After transfer membranes were blocked for 60 mins with 5% skimmed milk prepared in PBS with 0.1% Tween-20. After blocking, membrane was incubated for 1 hour at Room temperature (RT) or 24 hours overnight at 4 ^{o}C with primary antibody dissolved in 5% skimmed milk and PBS with 0.1% Tween. The nitrocellulose membrane was washed three times for 30 mins each with 1X PBS and incubated with the secondary antibody dissolved in 5% skimmed milk + PBS with 0.1% Tween-20. The ECL detection system were used for visualization.

4.3.6. Immunoprecipitation

Immunoprecipitation of INO80: Two separate flasks of cells were grown in 2 L YPD until 0.2 OD and treated with DMSO (control) in one flask and with 1-NM-PP1 inhibitor for 20 mins. Cells were collected by centrifugation (6000 x g, 10 mins, 4 ° C) and pellet was resuspended in an equal volume of 2X lysis buffer with protease inhibitors 0.2 mM PMSF, 1 µM pepstatin A, 1 µg/ml aprotinin, and 2 µM leupeptin and phosphate inhibitor. 1X lysis buffer is 25 mM Hepes pH 7.6, 500 mM KCl, 10% glycerol, 1 mM EDTA, 1 mM DTT, 4 mM $MgCl_2$. Cells were frozen in a dropwise manner in liquid nitrogen and crushed using a Freezer Mill. The frozen cell powder was thawed, resuspended in an equal volume of lysis buffer with protease inhibitors and the insoluble material was separated by ultracentrifugation (235,000 g, 1 h, 4 ° C). The supernatant was incubated with 20 µl pre-washed anti-FLAG M2 affinity gel resin (Sigma) in for 1 h at 4 ° C. The resin was washed thrice with NH_4HCO_3 followed by overnight trypsin (Promega) digestion. On the following day, IP samples were processed for mass spectrometry analysis using preomics cartiges using manufactures guidelines.

For RSC Immunoprecipitation, cells were grown and processed in a similar method as mentioned above for INO80 however using a different lysis buffer. 1X lysis buffer for RSC is 25 mM Hepes pH 7.6, 125 mM potassium acetate, 10% glycerol, and 5 mM EDTA.

4.3.7. Plasmid isolation from *E. coli*

To perform the mini-prep and midi-prep of *E. coli* transformed plasmids, 10 ml and 200 ml LB media, respectively, supplemented with the suitable antibiotic were inoculated with a single colony. These cultures were then allowed to grow for a duration of 16 hours. Plasmids were extracted using Plasmid extraction kit or NucleoBond Xtra Midi kit following the protocol for highcopy plasmids from the manufacturer.

4.3.8. *E. coli* transformation

Chemically competent *Escherichia coli* (DH5-alpha) cells were prepared within the department. For transformation, cells were thawed on ice for 10 mins, ~ 100 ng plasmid DNA was added to the competent cells and incubated on ice for another 10 mins. Cells were heat-shocked for 90 secs at 42 ° C, followed by another 10 mins incubation on ice. Cells

were revived by adding 800 µl of LB media and incubating at 37 ^{o}C for 1 hour with shaking. Cells were then plated on LB plates with appropriate antibiotic selection to allow transformed colonies to grow.

4.3.9. *S. cerevisiae* transformation

Yeast cells were transformed using high efficiency transformation protocol. Yeast cells were grown until saturation overnight and next day, the cells were reinoculated at 0.1 OD in 10 ml YPD media. The cells were then grown for 5 hours until OD 600nm = 0.2. Cells were collected by centrifugation, washed with water, resuspended in 1ml of LiOAc buffer containing 0.1 M LiOAc, 1X TE (10 mM Tris-Cl pH 7.2, 1 mM EDTA) and the mixture was incubated at RT for 10 mins. Cells were collected by centrifugation, supernatant was removed and to the pellet 20 µl solution containing 10 µg of PCR product for genomic deletion or integration, 50 µg boiled salmon-sperm DNA, 5 µl 1M LiOAc and 1X TE (upto 20 µl) were added. PEG solution containing 50 µl 1M LiOAc, 50 µl 10X TE (100 mM Tris-Cl pH 7.2, 10 mM EDTA) and 400 µl of 50% PEG was added, cells were mixed and incubated at 30 ^{o}C for 30 mins with shaking. Then, 55 µl of 100% DMSO was added to the cell mixture and heat shocked for 15 mins at 42 ^{o}C. The cells were incubated on ice for 2 min and then washed with sterile water. Finally the cells were resuspended in 100 µl sterile 1X TE and plated on YPD or appropriate selection plates for further growth and analysis.

4.3.10. Electrophoretic separation of DNA using agarose gel

DNA products were separated using 0.8 - 1% agarose gel. The agarose gel was prepared in 1X TBE buffer and 0.1 µg/ml Ethidium bromide. PCR product or restriction digested product was loaded into wells with 6X NEB loading dye, which was further diluted to 1X within the sample. The gel was electrophoresed at 10 - 12 V/cm until desired separation was achieved. DNA bands were visualized using Peqlab Vilber Gel Documentation imaging system.

4.3.11. SDS-PAGE

Sodium dodecyl sulfate polyacrylamide gel electrophoresis (SDS-PAGE) was employed to separate protein samples based on their mass. Protein samples or the whole cell extracts, were denatured and reduced using 4X NuPAGE LDS Sample Buffer containing 0.72 M β-mercaptoethanol, and heated at 95 ^{o} C for 5 min. These treated samples were then loaded onto a 10% or 12% or 4 – 20% gradient gel. To indicate standard molecular weights, a Triple Color Protein Standard II or III was used. The gels were electrophoresed in 1X SDS-PAGE buffer at 200 V until desired separation was achieved.

Appendix I

In the dataset where DDK is inhibited using temperature sensitive *cdc7-4* allele, we found that 17 phospho sites on MCM complex were present in DDK active. The following list contains phospho sites found on MCM complex. In phospho proteome data analysis, intensity values with zero in whole dataset were manually imputed with 100,000 (minimum intensity value in the dataset). Imputed intensity values were averaged and log_2(intensity) was calculated. Using log_2(intensity) values, fold change = Log_2 (Intensity, DDK inactive) - Log_2 (Intensity, DDK active) were calculated. Negative foldchange refers to phospho sites are downregulated in DDK inactive samples and upregulated in DDK active over four replicates. The Values in bracket in phospho peptide and probabilities column refers to the probability of occurrence of this particular phospho site at serine or threonine.

Table 14: MCM phospho sites upon direct DDK inhibition using temperaure sensitive cdc7-4 allele

Protein name	Positions within proteins	Phospho Peptide and Probabilities	Fold change (DDK inactive vs DDK active)
Mcm1	144	QQPQQQQPQQQQQVLNAHANS(1)LGHLNQDQVPAGALK	-4.513430406
Mcm1	2	S(1)DIEEGTPTNNGQQK	-1.624715025
Mcm3	751	FALLGEDIGNDIDEEES(1)EYEEALSK	-1.916417354
Mcm3	779	VRQPAS(0.445)NS(0.816)GS(0.739)PIK	-4.757454887
Mcm2	725	NNGES(1)AIEQGEDEINEQLNAR	-0.974479511
Mcm2	164	RQYEDLENS(1)DDDLLS(1)DMDIDPLREELTLESLSNVK	-2.784308665
Mcm2	170	QYEDLENS(1)DDDLLS(1)DMDIDPLREELTLESLSNVK	-1.015674357
Mcm4	52	NNS(1)QNLS(1)QGEGNIR	-2.47826092
Mcm4	56	NNS(1)QNLS(1)QGEGNIR	-2.035607178
Mcm4	82	QNS(1)DVFQSQGR	-0.41795833
Mcm4	171	S(0.014)GVNT(0.02)LDT(0.153)S(0.171)S(0.191)S(0.214)S(0.24)APPS(0.991)EAS(0.005)EPLR	-4.767628935
Mcm7	816	FVDDGT(0.004)MDT(0.996)DQEDS(1)LVS(0.233)T(0.767)PK	-1.675248667
Mcm6	1016	TVYVIHPNCEVLDQLEPQDS(0.5)S(0.5)	-0.533560765
Mcm2	547	GDINVLLLGDPGT(1)AK	-1.891665361
Mcm5	420	GDINVLLLGDPGT(1)AK	-1.891665361
Mcm7	811	FVDDGTMDT(1)DQEDS(1)LVS(0.081)T(0.92)PK	-2.26481832
Mcm7	820	FVDDGTMDT(0.001)DQEDS(0.993)LVS(0.034)T(0.972)PK	-1.158219392

Appendix II

The following list contains phospho sites found on Rad9, Mrc1 and Dun1. Phosphorylation of these proteins are important in activation of DNA damage response. In the complementary dataset, where DDK is inhibited using checkpoint activation, we found that 14 phospho sites on Rad9, 25 phospho sites on Mrc1 and 12 phospho sites on Dun1 were present in HU sample. In phospho proteome data analysis, intensity values with zero in whole dataset were manually imputed with 120,000 (minimum intensity value in the dataset). Imputed intensity values were averaged and log_2(intensity) was calculated. Using log_2(intensity) values, fold change = Log_2 (Intensity, HU) - Log_2 (Intensity, YPD) were calculated. Positive foldchange refers to phospho sites are upregulated in HU samples and downregulated in YPD samples over four replicates. The Values in bracket in phospho peptide and probabilities column refers to the probability of occurrence of this particular phospho site at serine or threonine.

Table 15: DNA damage associated phospho sites upon indirect DDK inhibition using checkpoint activation.

Protein name	Positions within proteins	Phospho Peptide and Probabilities	Fold change (HU vs YPD)
Rad9	720	DTIEIGEEEENRS(0.755)T(0.243)KT(0.051)S(0.862)PT(0.09)K	3.421962984
Rad9	639	GNS(1)LQLHDDNK	2.965235029
Rad9	493	INFEPILEVPET(0.178)S(0.515)S(0.261)PS(0.046)K	1.420965044
Rad9	1136	LSLDS(0.993)PS(0.007)K	1.291985571
Rad9	506	PS(0.004)NS(0.996)S(1)PIPK	0.702787465
Rad9	507	PS(0.004)NS(0.996)S(1)PIPK	0.702787465
Rad9	575	QIS(0.117)DS(0.858)GS(0.025)DETER	0.683640233
Rad9	729	RNS(1)DLDAAS(1)IK	3.481947554
Rad9	735	RNS(1)DLDAAS(1)IK	3.716264065
Rad9	298	SENYS(0.992)S(0.008)DDLRER	0.918714743
Rad9	299	S(0.001)ENY(0.063)S(0.949)S(0.987)DDLRER	0.263734619
Rad9	56	VNSTNIIEGS(1)PK	3.08916694
Rad9	137	Y(0.003)QS(0.997)S(0.999)DLEDTPLMLR	1.412020475
Rad9	138	Y(0.003)QS(0.997)S(0.999)DLEDTPLMLR	1.412020475
Mrc1	622	ADES(1)LPKR	2.763955868
Mrc1	801	AKNS(1)LELELS(1)DDDEDDVLQQYR	1.536054738
Mrc1	807	NSLELELS(1)DDDEDDVLQQYR	1.461041824
Mrc1	605	HIINES(1)DS(1)DT(1)EVEAKPK	0.095174408
Mrc1	607	HIINES(1)DS(1)DT(1)EVEAKPK	0.435433482
Mrc1	184	IDS(0.998)S(0.002)GATSQTQPIK	6.2156796

Mrc1	189	IDS(0.77)S(0.23)GAT(0.06)S(0.916)QT(0.024)QPIK	2.405849394
Mrc1	1093	LFESGQDS(1)FDN	6.817673748
Mrc1	119	NVS(1)S(0.16)S(0.828)FT(0.012)QTQR	2.227692916
Mrc1	121	NVSS(0.01)S(0.99)FTQTQR	6.847851513
Mrc1	997	RPEDEDEVENGDT(0.094)S(0.906)LVGVFK	3.682571495
Mrc1	1010	S(1)FAS(0.986)RT(0.014)DINDK	5.826118852
Mrc1	1013	S(1)FAS(0.986)RT(0.014)DINDK	6.272902103
Mrc1	961	S(0.954)FT(0.046)NSQTDSTTSK	4.48891627
Mrc1	965	SFTNS(1)QTDSTTSK	3.808779916
Mrc1	969	S(0.002)FT(0.981)NS(0.018)QT(0.008)DS(0.855)T(0.106)T(0.014)S(0.017)K	5.864087223
Mrc1	972	SFTNS(0.996)QT(0.004)DST(0.003)T(0.079)S(0.917)K	4.169835775
Mrc1	918	S(0.697)LS(0.303)FLK	1.13205166
Mrc1	920	SLS(1)FLK	6.677348379
Mrc1	924	S(1)NNYEDFETDK	7.368610927
Mrc1	367	S(1)VELNLTDETR	4.431225086
Mrc1	963	S(0.002)FT(0.981)NS(0.018)QT(0.008)DS(0.855)T(0.106)T(0.014)S(0.017)K	1.230410654
Mrc1	970	SFTNSQT(0.001)DS(0.239)T(0.537)T(0.76)S(0.462)K	1.450968199
Mrc1	971	SFTNSQT(0.001)DS(0.239)T(0.537)T(0.76)S(0.462)K	1.450968199
Mrc1	932	SNNYEDFET(1)DK	6.651098681
Dun1	10	EHS(1)GDVTDSSFKR	6.592335443
Dun1	16	REHS(1)GDVT(0.001)DS(0.641)S(0.359)FK	5.936804398
Dun1	17	REHS(0.99)GDVT(0.009)DS(0.006)S(0.994)FK	6.408553916
Dun1	130	S(1)CS(1)FLFK	4.361957538
Dun1	132	S(1)CS(1)FLFK	6.295502255
Dun1	158	S(1)YKNDDEVFK	2.964265318
Dun1	508	T(0.008)YS(0.992)ELS(1)CL	1.175190841
Dun1	511	T(0.008)YS(0.992)ELS(1)CL	1.175190841
Dun1	139	YAS(1)S(0.001)S(0.206)S(0.78)T(0.014)DIENDDEK	6.606494582
Dun1	140	Y(0.002)AS(0.997)S(0.982)S(0.019)STDIENDDEK	2.154913502
Dun1	141	YAS(0.999)S(0.001)S(0.914)S(0.081)T(0.005)DIENDDEK	2.126519031
Dun1	142	YAS(0.995)S(0.005)SS(0.994)T(0.006)DIENDDEK	5.219975673

Bibliography

1. Kornberg, R.D. and Y. Lorch, *Twenty-five years of the nucleosome, fundamental particle of the eukaryote chromosome.* Cell, 1999. **98**(3): p. 285-94.

2. Luger, K., et al., *Crystal structure of the nucleosome core particle at 2.8 Å resolution.* Nature, 1997. **389**(6648): p. 251-260.

3. Athey, B.D., et al., *The diameters of frozen-hydrated chromatin fibers increase with DNA linker length: evidence in support of variable diameter models for chromatin.* J Cell Biol, 1990. **111**(3): p. 795-806.

4. van Holde, K. and J. Zlatanova, *Chromatin Higher Order Structure: Chasing a Mirage? *.* Journal of Biological Chemistry, 1995. **270**(15): p. 8373-8376.

5. Moraru, M. and T. Schalch, *Chromatin fiber structural motifs as regulatory hubs of genome function?* Essays in Biochemistry, 2019. **63**(1): p. 123-132.

6. Robinson, P.J.J., L. Fairall, V.A.T. Huynh, and D. Rhodes, *EM measurements define the dimensions of the “30-nm” chromatin fiber: Evidence for a compact, interdigitated structure.* Proceedings of the National Academy of Sciences, 2006. **103**(17): p. 6506-6511.

7. Woodcock, C.L. and S. Dimitrov, *Higher-order structure of chromatin and chromosomes.* Current Opinion in Genetics & Development, 2001. **11**(2): p. 130-135.

8. Felsenfeld, G. and M. Groudine, *Controlling the double helix.* Nature, 2003. **421**(6921): p. 448-453.

9. Kireev, I., et al., *In vivo immunogold labeling confirms large-scale chromatin folding motifs.* Nat Methods, 2008. **5**(4): p. 311-3.

10. Davidson, I.F. and J.-M. Peters, *Genome folding through loop extrusion by SMC complexes.* Nature Reviews Molecular Cell Biology, 2021. **22**(7): p. 445-464.

11. Dixon, J.R., et al., *Topological domains in mammalian genomes identified by analysis of chromatin interactions.* Nature, 2012. **485**(7398): p. 376-380.

12. Nora, E.P., et al., *Spatial partitioning of the regulatory landscape of the X-inactivation centre.* Nature, 2012. **485**(7398): p. 381-385.

13. Hansen, A.S., C. Cattoglio, X. Darzacq, and R. Tjian, *Recent evidence that TADs and chromatin loops are dynamic structures.* Nucleus, 2018. **9**(1): p. 20-32.

14. Lieberman-Aiden, E., et al., *Comprehensive mapping of long-range interactions reveals folding principles of the human genome.* Science, 2009. **326**(5950): p. 289-93.

15. Cremer, T. and M. Cremer, *Chromosome territories.* Cold Spring Harb Perspect Biol, 2010. **2**(3): p. a003889.

16. Eaton, M.L., et al., *Conserved nucleosome positioning defines replication origins.* Genes Dev, 2010. **24**(8): p. 748-53.

17. Rando, O.J. and K. Ahmad, *Rules and regulation in the primary structure of chromatin.* Current Opinion in Cell Biology, 2007. **19**(3): p. 250-256.

18. Lai, W.K.M. and B.F. Pugh, *Understanding nucleosome dynamics and their links to gene expression and DNA replication.* Nature Reviews Molecular Cell Biology, 2017. **18**(9): p. 548-562.

19. Davey, C.A., et al., *Solvent mediated interactions in the structure of the nucleosome core particle at 1.9 a resolution.* J Mol Biol, 2002. **319**(5): p. 1097-113.

20. Satchwell, S.C., H.R. Drew, and A.A. Travers, *Sequence periodicities in chicken nucleosome core DNA.* J Mol Biol, 1986. **191**(4): p. 659-75.

21. Drew, H.R. and A.A. Travers, *DNA bending and its relation to nucleosome positioning.* J Mol Biol, 1985. **186**(4): p. 773-90.

22. Voong, L.N., et al., *Insights into Nucleosome Organization in Mouse Embryonic Stem Cells through Chemical Mapping.* Cell, 2016. **167**(6): p. 1555-1570.e15.

23. Brogaard, K., L. Xi, J.-P. Wang, and J. Widom, *A map of nucleosome positions in yeast at base-pair resolution.* Nature, 2012. **486**(7404): p. 496-501.

24. Herzel, H., O. Weiss, and E.N. Trifonov, *Sequence periodicity in complete genomes of archaea suggests positive supercoiling.* J Biomol Struct Dyn, 1998. **16**(2): p. 341-5.

25. Mavrich, T.N., et al., *Nucleosome organization in the Drosophila genome.* Nature, 2008. **453**(7193): p. 358-62.

26. Iyer, V. and K. Struhl, *Poly(dA:dT), a ubiquitous promoter element that stimulates transcription via its intrinsic DNA structure.* Embo j, 1995. **14**(11): p. 2570-9.

27. Simpson, R.T. and P. Künzler, *Cromatin and core particles formed from the inner histones and synthetic polydeoxyribonucleotides of defined sequence.* Nucleic Acids Res, 1979. **6**(4): p. 1387-415.

28. Sekinger, E.A., Z. Moqtaderi, and K. Struhl, *Intrinsic histone-DNA interactions and low nucleosome density are important for preferential accessibility of promoter regions in yeast.* Mol Cell, 2005. **18**(6): p. 735-48.

29. Tsankov, A., et al., *Evolutionary divergence of intrinsic and trans-regulated nucleosome positioning sequences reveals plastic rules for chromatin organization.* Genome Res, 2011. **21**(11): p. 1851-62.

30. Yuan, G.C., et al., *Genome-scale identification of nucleosome positions in S. cerevisiae.* Science, 2005. **309**(5734): p. 626-30.

31. Moyle-Heyrman, G., et al., *Chemical map of Schizosaccharomyces pombe reveals species-specific features in nucleosome positioning.* Proceedings of the National Academy of Sciences, 2013. **110**(50): p. 20158-20163.

32. Eustermann, S., et al., *Energy-driven genome regulation by ATP-dependent chromatin remodellers.* Nature Reviews Molecular Cell Biology, 2024. **25**(4): p. 309-332.

33. Narlikar, G.J., R. Sundaramoorthy, and T. Owen-Hughes, *Mechanisms and functions of ATP-dependent chromatin-remodeling enzymes.* Cell, 2013. **154**(3): p. 490-503.

34. Zhou, C.Y., S.L. Johnson, N.I. Gamarra, and G.J. Narlikar, *Mechanisms of ATP-Dependent Chromatin Remodeling Motors.* Annual Review of Biophysics, 2016. **45**(1): p. 153-181.

35. Rhee, H.S., A.R. Bataille, L. Zhang, and B.F. Pugh, *Subnucleosomal structures and nucleosome asymmetry across a genome.* Cell, 2014. **159**(6): p. 1377-88.

36. Pokholok, D.K., et al., *Genome-wide map of nucleosome acetylation and methylation in yeast.* Cell, 2005. **122**(4): p. 517-27.

37. Strahl, B.D. and C.D. Allis, *The language of covalent histone modifications.* Nature, 2000. **403**(6765): p. 41-5.

38. Weber, C.M. and S. Henikoff, *Histone variants: dynamic punctuation in transcription.* Genes Dev, 2014. **28**(7): p. 672-82.

39. Kurat, C.F., et al., *Chromatin Controls DNA Replication Origin Selection, Lagging-Strand Synthesis, and Replication Fork Rates.* Mol Cell, 2017. **65**(1): p. 117-130.

40. Shen, X., G. Mizuguchi, A. Hamiche, and C. Wu, *A chromatin remodelling complex involved in transcription and DNA processing.* Nature, 2000. **406**(6795): p. 541-4.

41. Lans, H., J.A. Marteijn, and W. Vermeulen, *ATP-dependent chromatin remodeling in the DNA-damage response.* Epigenetics & Chromatin, 2012. **5**(1): p. 4.

42. Clapier, C.R. and B.R. Cairns, *The Biology of Chromatin Remodeling Complexes.* Annual Review of Biochemistry, 2009. **78**(1): p. 273-304.

43. Lorch, Y., M. Zhang, and R.D. Kornberg, *Histone octamer transfer by a chromatin-remodeling complex.* Cell, 1999. **96**(3): p. 389-92.

44. Brahma, S., et al., *INO80 exchanges H2A.Z for H2A by translocating on DNA proximal to histone dimers.* Nat Commun, 2017. **8**: p. 15616.

45. Mizuguchi, G., et al., *ATP-driven exchange of histone H2AZ variant catalyzed by SWR1 chromatin remodeling complex.* Science, 2004. **303**(5656): p. 343-8.

46. Markert, J. and K. Luger, *Nucleosomes Meet Their Remodeler Match.* Trends in Biochemical Sciences, 2021. **46**(1): p. 41-50.

47. Flaus, A., D.M. Martin, G.J. Barton, and T. Owen-Hughes, *Identification of multiple distinct Snf2 subfamilies with conserved structural motifs.* Nucleic Acids Res, 2006. **34**(10): p. 2887-905.

48. Clapier, C.R., J. Iwasa, B.R. Cairns, and C.L. Peterson, *Mechanisms of action and regulation of ATP-dependent chromatin-remodelling complexes.* Nat Rev Mol Cell Biol, 2017. **18**(7): p. 407-422.

49. Mueller-Planitz, F., H. Klinker, and P.B. Becker, *Nucleosome sliding mechanisms: new twists in a looped history.* Nature Structural & Molecular Biology, 2013. **20**(9): p. 1026-1032.

50. Tyagi, M., N. Imam, K. Verma, and A.K. Patel, *Chromatin remodelers: We are the drivers!!* Nucleus, 2016. **7**(4): p. 388-404.

51. Clapier, C.R., J. Iwasa, B.R. Cairns, and C.L. Peterson, *Mechanisms of action and regulation of ATP-dependent chromatin-remodelling complexes.* Nature Reviews Molecular Cell Biology, 2017. **18**(7): p. 407-422.

52. Singh, A.K. and F. Mueller-Planitz, *Nucleosome Positioning and Spacing: From Mechanism to Function.* Journal of Molecular Biology, 2021. **433**(6): p. 166847.

53. Vary, J.C., Jr., et al., *Yeast Isw1p forms two separable complexes in vivo.* Mol Cell Biol, 2003. **23**(1): p. 80-91.

54. Tran, H.G., D.J. Steger, V.R. Iyer, and A.D. Johnson, *The chromo domain protein chd1p from budding yeast is an ATP-dependent chromatin-modifying factor.* Embo j, 2000. **19**(10): p. 2323-31.

55. Ito, T., et al., *ACF, an ISWI-Containing and ATP-Utilizing Chromatin Assembly and Remodeling Factor.* Cell, 1997. **90**(1): p. 145-155.

56. Tsukiyama, T., et al., *Characterization of the imitation switch subfamily of ATP-dependent chromatin-remodeling factors in Saccharomyces cerevisiae.* Genes Dev, 1999. **13**(6): p. 686-97.

57. Stockdale, C., A. Flaus, H. Ferreira, and T. Owen-Hughes, *Analysis of nucleosome repositioning by yeast ISWI and Chd1 chromatin remodeling complexes.* J Biol Chem, 2006. **281**(24): p. 16279-88.

58. Deindl, S., et al., *ISWI Remodelers Slide Nucleosomes with Coordinated Multi-Base-Pair Entry Steps and Single-Base-Pair Exit Steps.* Cell, 2013. **152**(3): p. 442-452.

59. Krietenstein, N., et al., *Genomic Nucleosome Organization Reconstituted with Pure Proteins.* Cell, 2016. **167**(3): p. 709-721.e12.

60. Lusser, A., D.L. Urwin, and J.T. Kadonaga, *Distinct activities of CHD1 and ACF in ATP-dependent chromatin assembly.* Nature Structural & Molecular Biology, 2005. **12**(2): p. 160-166.

61. Gkikopoulos, T., et al., *A role for Snf2-related nucleosome-spacing enzymes in genome-wide nucleosome organization.* Science, 2011. **333**(6050): p. 1758-60.

62. Ocampo, J., R.V. Chereji, P.R. Eriksson, and D.J. Clark, *The ISW1 and CHD1 ATP-dependent chromatin remodelers compete to set nucleosome spacing in vivo.* Nucleic Acids Res, 2016. **44**(10): p. 4625-35.

63. Vasseur, P., et al., *Dynamics of Nucleosome Positioning Maturation following Genomic Replication.* Cell Reports, 2016. **16**(10): p. 2651-2665.

64. Yadav, T. and I. Whitehouse, *Replication-Coupled Nucleosome Assembly and Positioning by ATP-Dependent Chromatin-Remodeling Enzymes.* Cell Reports, 2016. **15**(4): p. 715-723.

65. Guillemette, B. and L. Gaudreau, *Reuniting the contrasting functions of H2A.Z.* Biochemistry and Cell Biology, 2006. **84**(4): p. 528-535.

66. Colino-Sanguino, Y., S.J. Clark, and F. Valdes-Mora, *The H2A.Z-nucleosome code in mammals: emerging functions.* Trends in Genetics, 2022. **38**(3): p. 273-289.

67. Papamichos-Chronakis, M., S. Watanabe, O.J. Rando, and C.L. Peterson, *Global regulation of H2A.Z localization by the INO80 chromatin-remodeling enzyme is essential for genome integrity.* Cell, 2011. **144**(2): p. 200-13.

68. Udugama, M., A. Sabri, and B. Bartholomew, *The INO80 ATP-dependent chromatin remodeling complex is a nucleosome spacing factor.* Mol Cell Biol, 2011. **31**(4): p. 662-73.

69. Singh, A.K., et al., *The biogenesis and function of nucleosome arrays.* Nature Communications, 2021. **12**(1): p. 7011.

70. Bantele, S.C.S. and B. Pfander, *Nucleosome Remodeling by Fun30(SMARCAD1) in the DNA Damage Response.* Front Mol Biosci, 2019. **6**: p. 78.

71. Adkins, N.L., et al., *Nucleosome-like, Single-stranded DNA (ssDNA)-Histone Octamer Complexes and the Implication for DNA Double Strand Break Repair.* J Biol Chem, 2017. **292**(13): p. 5271-5281.

72. Awad, S., et al., *The Snf2 homolog Fun30 acts as a homodimeric ATP-dependent chromatin-remodeling enzyme.* J Biol Chem, 2010. **285**(13): p. 9477-9484.

73. Byeon, B., et al., *The ATP-dependent chromatin remodeling enzyme Fun30 represses transcription by sliding promoter-proximal nucleosomes.* J Biol Chem, 2013. **288**(32): p. 23182-93.

74. Ghaemmaghami, S., et al., *Global analysis of protein expression in yeast.* Nature, 2003. **425**(6959): p. 737-741.

75. Cairns, B.R., et al., *RSC, an essential, abundant chromatin-remodeling complex.* Cell, 1996. **87**(7): p. 1249-60.

76. Kubik, S., et al., *Opposing chromatin remodelers control transcription initiation frequency and start site selection.* Nature Structural & Molecular Biology, 2019. **26**(8): p. 744-754.

77. Ganguli, D., et al., *RSC-dependent constructive and destructive interference between opposing arrays of phased nucleosomes in yeast.* Genome Res, 2014. **24**(10): p. 1637-49.

78. Kubik, S., et al., *Nucleosome Stability Distinguishes Two Different Promoter Types at All Protein-Coding Genes in Yeast.* Molecular cell, 2015. **60**(3): p. 422-434.

79. Rawal, Y., et al., *SWI/SNF and RSC cooperate to reposition and evict promoter nucleosomes at highly expressed genes in yeast.* Genes Dev, 2018. **32**(9-10): p. 695-710.

80. De Koning, L., A. Corpet, J.E. Haber, and G. Almouzni, *Histone chaperones: an escort network regulating histone traffic.* Nat Struct Mol Biol, 2007. **14**(11): p. 997-1007.

81. Ransom, M., B.K. Dennehey, and J.K. Tyler, *Chaperoning Histones during DNA Replication and Repair.* Cell, 2010. **140**(2): p. 183-195.

82. Elsässer, S.J. and S. D'Arcy, *Towards a mechanism for histone chaperones.* Biochim Biophys Acta, 2013. **1819**(3-4): p. 211-221.

83. Pardal, A.J., F. Fernandes-Duarte, and A.J. Bowman, *The histone chaperoning pathway: from ribosome to nucleosome.* Essays Biochem, 2019. **63**(1): p. 29-43.

84. Ray-Gallet, D. and G. Almouzni, *H3-H4 histone chaperones and cancer.* Curr Opin Genet Dev, 2022. **73**: p. 101900.

85. Das, C., J.K. Tyler, and M.E. Churchill, *The histone shuffle: histone chaperones in an energetic dance.* Trends Biochem Sci, 2010. **35**(9): p. 476-89.

86. Groth, A., W. Rocha, A. Verreault, and G. Almouzni, *Chromatin challenges during DNA replication and repair.* Cell, 2007. **128**(4): p. 721-33.

87. Alabert, C. and A. Groth, *Chromatin replication and epigenome maintenance.* Nat Rev Mol Cell Biol, 2012. **13**(3): p. 153-67.

88. Burgess, R.J. and Z. Zhang, *Histone chaperones in nucleosome assembly and human disease.* Nat Struct Mol Biol, 2013. **20**(1): p. 14-22.

89. English, C.M., et al., *Structural basis for the histone chaperone activity of Asf1.* Cell, 2006. **127**(3): p. 495-508.

90. Natsume, R., et al., *Structure and function of the histone chaperone CIA/ASF1 complexed with histones H3 and H4.* Nature, 2007. **446**(7133): p. 338-341.

91. Franco, A.A., W.M. Lam, P.M. Burgers, and P.D. Kaufman, *Histone deposition protein Asf1 maintains DNA replisome integrity and interacts with replication factor C.* Genes Dev, 2005. **19**(11): p. 1365-75.

92. Ito, T., M. Bulger, R. Kobayashi, and J.T. Kadonaga, *Drosophila NAP-1 is a core histone chaperone that functions in ATP-facilitated assembly of regularly spaced nucleosomal arrays.* Mol Cell Biol, 1996. **16**(6): p. 3112-24.

93. Orphanides, G., et al., *FACT, a factor that facilitates transcript elongation through nucleosomes.* Cell, 1998. **92**(1): p. 105-16.

94. Formosa, T. and F. Winston, *The role of FACT in managing chromatin: disruption, assembly, or repair?* Nucleic Acids Research, 2020. **48**(21): p. 11929-11941.

95. Foltman, M., et al., *Eukaryotic replisome components cooperate to process histones during chromosome replication.* Cell Rep, 2013. **3**(3): p. 892-904.

96. Formosa, T., *The role of FACT in making and breaking nucleosomes.* Biochim Biophys Acta, 2013. **1819**(3-4): p. 247-55.

97. Wittmeyer, J. and T. Formosa, *The Saccharomyces cerevisiae DNA polymerase alpha catalytic subunit interacts with Cdc68/Spt16 and with Pob3, a protein similar to an HMG1-like protein.* Molecular and Cellular Biology, 1997. **17**(7): p. 4178-4190.

98. Gambus, A., et al., *GINS maintains association of Cdc45 with MCM in replisome progression complexes at eukaryotic DNA replication forks.* Nature Cell Biology, 2006. **8**(4): p. 358-366.

99. VanDemark, A.P., et al., *The Structure of the yFACT Pob3-M Domain, Its Interaction with the DNA Replication Factor RPA, and a Potential Role in Nucleosome Deposition.* Molecular Cell, 2006. **22**(3): p. 363-374.

100. Liu, Y., et al., *FACT caught in the act of manipulating the nucleosome.* Nature, 2020. **577**(7790): p. 426-431.

101. Tan, B.C.-M., C.-T. Chien, S. Hirose, and S.-C. Lee, *Functional cooperation between FACT and MCM helicase facilitates initiation of chromatin DNA replication.* The EMBO Journal, 2006. **25**(17): p. 3975-3985.

102. Liu, W.H., S.C. Roemer, A.M. Port, and M.E. Churchill, *CAF-1-induced oligomerization of histones H3/H4 and mutually exclusive interactions with Asf1 guide H3/H4 transitions among histone chaperones and DNA.* Nucleic Acids Res, 2012. **40**(22): p. 11229-39.

103. Liu, W.H., et al., *The Cac1 subunit of histone chaperone CAF-1 organizes CAF-1-H3/H4 architecture and tetramerizes histones.* Elife, 2016. **5**.

104. Ransom, M., B.K. Dennehey, and J.K. Tyler, *Chaperoning histones during DNA replication and repair.* Cell, 2010. **140**(2): p. 183-95.

105. Yang, J., et al., *The Histone Chaperone FACT Contributes to DNA Replication-Coupled Nucleosome Assembly.* Cell Rep, 2016. **14**(5): p. 1128-1141.

106. Morgan, D.O., *The cell cycle: principles of control*. 2007: New science press.

107. Barik, D., et al., *A model of yeast cell-cycle regulation based on multisite phosphorylation.* Mol Syst Biol, 2010. **6**: p. 405.

108. Grant, G.D., et al., *Identification of cell cycle-regulated genes periodically expressed in U2OS cells and their regulation by FOXM1 and E2F transcription factors.* Mol Biol Cell, 2013. **24**(23): p. 3634-50.

109. Li, F., et al., *The yeast cell-cycle network is robustly designed.* Proceedings of the National Academy of Sciences, 2004. **101**(14): p. 4781-4786.

110. Hartwell, L.H., *Saccharomyces cerevisiae cell cycle.* Bacteriol Rev, 1974. **38**(2): p. 164-98.

111. Bloom, J. and F.R. Cross, *Multiple levels of cyclin specificity in cell-cycle control.* Nature Reviews Molecular Cell Biology, 2007. **8**(2): p. 149-160.

112. Smets, B., et al., *Life in the midst of scarcity: adaptations to nutrient availability in Saccharomyces cerevisiae.* Curr Genet, 2010. **56**(1): p. 1-32.

113. Tyers, M., G. Tokiwa, and B. Futcher, *Comparison of the Saccharomyces cerevisiae G1 cyclins: Cln3 may be an upstream activator of Cln1, Cln2 and other cyclins.* Embo j, 1993. **12**(5): p. 1955-68.

114. Wijnen, H., A. Landman, and B. Futcher, *The G(1) cyclin Cln3 promotes cell cycle entry via the transcription factor Swi6.* Mol Cell Biol, 2002. **22**(12): p. 4402-18.

115. Koch, C., et al., *A role for the transcription factors Mbp1 and Swi4 in progression from G1 to S phase.* Science, 1993. **261**(5128): p. 1551-7.

116. de Bruin, R.A., et al., *Cln3 activates G1-specific transcription via phosphorylation of the SBF bound repressor Whi5.* Cell, 2004. **117**(7): p. 887-98.

117. Wagner, M.V., et al., *Whi5 regulation by site specific CDK-phosphorylation in Saccharomyces cerevisiae.* PLoS One, 2009. **4**(1): p. e4300.

118. Costanzo, M., et al., *CDK activity antagonizes Whi5, an inhibitor of G1/S transcription in yeast.* Cell, 2004. **117**(7): p. 899-913.

119. Schneider, B.L., Q.H. Yang, and A.B. Futcher, *Linkage of replication to start by the Cdk inhibitor Sic1.* Science, 1996. **272**(5261): p. 560-2.

120. Schwob, E., T. Böhm, M.D. Mendenhall, and K. Nasmyth, *The B-type cyclin kinase inhibitor p40SIC1 controls the G1 to S transition in S. cerevisiae.* Cell, 1994. **79**(2): p. 233-44.

121. Verma, R., et al., *Phosphorylation of Sic1p by G1 Cdk required for its degradation and entry into S phase.* Science, 1997. **278**(5337): p. 455-60.

122. Mendenhall, M.D. and A.E. Hodge, *Regulation of Cdc28 cyclin-dependent protein kinase activity during the cell cycle of the yeast Saccharomyces cerevisiae.* Microbiol Mol Biol Rev, 1998. **62**(4): p. 1191-243.

123. Surana, U., et al., *The role of CDC28 and cyclins during mitosis in the budding yeast S. cerevisiae.* Cell, 1991. **65**(1): p. 145-61.

124. Amon, A., M. Tyers, B. Futcher, and K. Nasmyth, *Mechanisms that help the yeast cell cycle clock tick: G2 cyclins transcriptionally activate G2 cyclins and repress G1 cyclins.* Cell, 1993. **74**(6): p. 993-1007.

125. Rudner, A.D. and A.W. Murray, *Phosphorylation by Cdc28 activates the Cdc20-dependent activity of the anaphase-promoting complex.* J Cell Biol, 2000. **149**(7): p. 1377-90.

126. Reed, S.I., *Ratchets and clocks: the cell cycle, ubiquitylation and protein turnover.* Nat Rev Mol Cell Biol, 2003. **4**(11): p. 855-64.

127. Pfleger, C.M., E. Lee, and M.W. Kirschner, *Substrate recognition by the Cdc20 and Cdh1 components of the anaphase-promoting complex.* Genes Dev, 2001. **15**(18): p. 2396-407.

128. Pfleger, C.M. and M.W. Kirschner, *The KEN box: an APC recognition signal distinct from the D box targeted by Cdh1.* Genes Dev, 2000. **14**(6): p. 655-65.

129. Yu, H., *Regulation of APC-Cdc20 by the spindle checkpoint.* Curr Opin Cell Biol, 2002. **14**(6): p. 706-14.

130. Ciosk, R., et al., *An ESP1/PDS1 complex regulates loss of sister chromatid cohesion at the metaphase to anaphase transition in yeast.* Cell, 1998. **93**(6): p. 1067-76.

131. Wäsch, R. and F.R. Cross, *APC-dependent proteolysis of the mitotic cyclin Clb2 is essential for mitotic exit.* Nature, 2002. **418**(6897): p. 556-62.

132. Pereira, G. and E. Schiebel, *The role of the yeast spindle pole body and the mammalian centrosome in regulating late mitotic events.* Curr Opin Cell Biol, 2001. **13**(6): p. 762-9.

133. Holt, L.J., A.N. Krutchinsky, and D.O. Morgan, *Positive feedback sharpens the anaphase switch.* Nature, 2008. **454**(7202): p. 353-7.

134. Bell, S.P. and K. Labib, *Chromosome Duplication in Saccharomyces cerevisiae.* Genetics, 2016. **203**(3): p. 1027-67.

135. Rivera-Mulia, Juan C. and David M. Gilbert, *Replicating Large Genomes: Divide and Conquer.* Molecular Cell, 2016. **62**(5): p. 756-765.

136. Broach, J.R., et al., *Localization and sequence analysis of yeast origins of DNA replication.* Cold Spring Harb Symp Quant Biol, 1983. **47 Pt 2**: p. 1165-73.

137. Nieduszynski, C.A., Y. Knox, and A.D. Donaldson, *Genome-wide identification of replication origins in yeast by comparative genomics.* Genes Dev, 2006. **20**(14): p. 1874-9.

138. Xu, W., J.G. Aparicio, O.M. Aparicio, and S. Tavaré, *Genome-wide mapping of ORC and Mcm2p binding sites on tiling arrays and identification of essential ARS consensus sequences in S. cerevisiae.* BMC Genomics, 2006. **7**: p. 276.

139. Liachko, I., R.A. Youngblood, U. Keich, and M.J. Dunham, *High-resolution mapping, characterization, and optimization of autonomously replicating sequences in yeast.* Genome Res, 2013. **23**(4): p. 698-704.

140. Lai, W.K.M. and B.F. Pugh, *Understanding nucleosome dynamics and their links to gene expression and DNA replication.* Nat Rev Mol Cell Biol, 2017. **18**(9): p. 548-562.

141. Berbenetz, N.M., C. Nislow, and G.W. Brown, *Diversity of eukaryotic DNA replication origins revealed by genome-wide analysis of chromatin structure.* PLoS Genet, 2010. **6**(9): p. e1001092.

142. Chacin, E., et al., *Establishment and function of chromatin organization at replication origins.* Nature, 2023. **616**(7958): p. 836-842.

143. Remus, D. and J.F. Diffley, *Eukaryotic DNA replication control: lock and load, then fire.* Curr Opin Cell Biol, 2009. **21**(6): p. 771-7.

144. Remus, D., et al., *Concerted loading of Mcm2-7 double hexamers around DNA during DNA replication origin licensing.* Cell, 2009. **139**(4): p. 719-30.

145. Diffley, J.F., J.H. Cocker, S.J. Dowell, and A. Rowley, *Two steps in the assembly of complexes at yeast replication origins in vivo.* Cell, 1994. **78**(2): p. 303-16.

146. Coster, G., et al., *Origin Licensing Requires ATP Binding and Hydrolysis by the MCM Replicative Helicase.* Molecular Cell, 2014. **55**(5): p. 666-677.

147. Douglas, M.E., F.A. Ali, A. Costa, and J.F.X. Diffley, *The mechanism of eukaryotic CMG helicase activation.* Nature, 2018. **555**(7695): p. 265-268.

148. Dahmann, C., J.F. Diffley, and K.A. Nasmyth, *S-phase-promoting cyclin-dependent kinases prevent re-replication by inhibiting the transition of replication origins to a pre-replicative state.* Curr Biol, 1995. **5**(11): p. 1257-69.

149. Detweiler, C.S. and J.J. Li, *Ectopic induction of Clb2 in early G1 phase is sufficient to block prereplicative complex formation in Saccharomyces cerevisiae.* Proc Natl Acad Sci U S A, 1998. **95**(5): p. 2384-9.

150. Drury, L.S. and J.F.X. Diffley, *Factors Affecting the Diversity of DNA Replication Licensing Control in Eukaryotes.* Current Biology, 2009. **19**(6): p. 530-535.

151. Diffley, J.F.X., *Regulation of Early Events in Chromosome Replication.* Current Biology, 2004. **14**(18): p. R778-R786.

152. Drury, L.S., G. Perkins, and J.F. Diffley, *The cyclin-dependent kinase Cdc28p regulates distinct modes of Cdc6p proteolysis during the budding yeast cell cycle.* Curr Biol, 2000. **10**(5): p. 231-40.

153. Elsasser, S., Y. Chi, P. Yang, and J.L. Campbell, *Phosphorylation controls timing of Cdc6p destruction: A biochemical analysis.* Mol Biol Cell, 1999. **10**(10): p. 3263-77.

154. Mimura, S., T. Seki, S. Tanaka, and J.F. Diffley, *Phosphorylation-dependent binding of mitotic cyclins to Cdc6 contributes to DNA replication control.* Nature, 2004. **431**(7012): p. 1118-23.

155. Elsasser, S., et al., *Interaction between yeast Cdc6 protein and B-type cyclin/Cdc28 kinases.* Mol Biol Cell, 1996. **7**(11): p. 1723-35.

156. Labib, K., J.F.X. Diffley, and S.E. Kearsey, *G1-phase and B-type cyclins exclude the DNA-replication factor Mcm4 from the nucleus.* Nature Cell Biology, 1999. **1**(7): p. 415-422.

157. Nguyen, V.Q., C. Co, K. Irie, and J.J. Li, *Clb/Cdc28 kinases promote nuclear export of the replication initiator proteins Mcm2–7.* Current Biology, 2000. **10**(4): p. 195-205.

158. Tanaka, S. and J.F.X. Diffley, *Interdependent nuclear accumulation of budding yeast Cdt1 and Mcm2–7 during G1 phase.* Nature Cell Biology, 2002. **4**(3): p. 198-207.

159. Nguyen, V.Q., C. Co, and J.J. Li, *Cyclin-dependent kinases prevent DNA re-replication through multiple mechanisms.* Nature, 2001. **411**(6841): p. 1068-1073.

160. Sheu, Y.J. and B. Stillman, *The Dbf4-Cdc7 kinase promotes S phase by alleviating an inhibitory activity in Mcm4.* Nature, 2010. **463**(7277): p. 113-7.

161. Hardy, C.F., et al., *mcm5/cdc46-bob1 bypasses the requirement for the S phase activator Cdc7p.* Proc Natl Acad Sci U S A, 1997. **94**(7): p. 3151-5.

162. Tanaka, S., et al., *CDK-dependent phosphorylation of Sld2 and Sld3 initiates DNA replication in budding yeast.* Nature, 2007. **445**(7125): p. 328-32.

163. Zegerman, P. and J.F. Diffley, *Phosphorylation of Sld2 and Sld3 by cyclin-dependent kinases promotes DNA replication in budding yeast.* Nature, 2007. **445**(7125): p. 281-5.

164. Ilves, I., T. Petojevic, J.J. Pesavento, and M.R. Botchan, *Activation of the MCM2-7 helicase by association with Cdc45 and GINS proteins.* Mol Cell, 2010. **37**(2): p. 247-58.

165. Kanemaki, M. and K. Labib, *Distinct roles for Sld3 and GINS during establishment and progression of eukaryotic DNA replication forks.* Embo j, 2006. **25**(8): p. 1753-63.

166. Aggarwal, P., et al., *Nuclear accumulation of cyclin D1 during S phase inhibits Cul4-dependent Cdt1 proteolysis and triggers p53-dependent DNA rereplication.* Genes Dev, 2007. **21**(22): p. 2908-22.

167. Gaillard, H., T. García-Muse, and A. Aguilera, *Replication stress and cancer.* Nature Reviews Cancer, 2015. **15**(5): p. 276-289.

168. Green, B.M., K.J. Finn, and J.J. Li, *Loss of DNA Replication Control Is a Potent Inducer of Gene Amplification.* Science, 2010. **329**(5994): p. 943-946.

169. Bellush, J.M. and I. Whitehouse, *DNA replication through a chromatin environment.* Philos Trans R Soc Lond B Biol Sci, 2017. **372**(1731).

170. Devbhandari, S., et al., *Chromatin Constrains the Initiation and Elongation of DNA Replication.* Mol Cell, 2017. **65**(1): p. 131-141.

171. Azmi, I.F., et al., *Nucleosomes influence multiple steps during replication initiation.* eLife, 2017. **6**: p. e22512.

172. Lipford, J.R. and S.P. Bell, *Nucleosomes Positioned by ORC Facilitate the Initiation of DNA Replication.* Molecular Cell, 2001. **7**(1): p. 21-30.

173. Simpson, R.T., *Nucleosome positioning can affect the function of a cis-acting DNA element in vivo.* Nature, 1990. **343**(6256): p. 387-9.

174. Belsky, J.A., et al., *Genome-wide chromatin footprinting reveals changes in replication origin architecture induced by pre-RC assembly.* Genes Dev, 2015. **29**(2): p. 212-24.

175. Stewart-Morgan, K.R., N. Petryk, and A. Groth, *Chromatin replication and epigenetic cell memory.* Nature Cell Biology, 2020. **22**(4): p. 361-371.

176. Grunstein, M., *Histone acetylation in chromatin structure and transcription.* Nature, 1997. **389**(6649): p. 349-352.

177. Hebbes, T.R., A.W. Thorne, and C. Crane-Robinson, *A direct link between core histone acetylation and transcriptionally active chromatin.* The EMBO Journal, 1988. **7**(5): p. 1395-1402.

178. Unnikrishnan, A., P.R. Gafken, and T. Tsukiyama, *Dynamic changes in histone acetylation regulate origins of DNA replication.* Nat Struct Mol Biol, 2010. **17**(4): p. 430-7.

179. Chacin, E., et al., *A CDK-regulated chromatin segregase promoting chromosome replication.* Nature Communications, 2021. **12**(1): p. 5224.

180. Ubersax, J.A., et al., *Targets of the cyclin-dependent kinase Cdk1.* Nature, 2003. **425**(6960): p. 859-864.

181. Cho, W.H., et al., *CDC7 kinase phosphorylates serine residues adjacent to acidic amino acids in the minichromosome maintenance 2 protein.* Proc Natl Acad Sci U S A, 2006. **103**(31): p. 11521-6.

182. Sasanuma, H., et al., *Cdc7-dependent phosphorylation of Mer2 facilitates initiation of yeast meiotic recombination.* Genes Dev, 2008. **22**(3): p. 398-410.

183. Gillespie, P.J. and J.J. Blow, *DDK: The Outsourced Kinase of Chromosome Maintenance.* Biology (Basel), 2022. **11**(6).

184. Alver, R.C., G.S. Chadha, P.J. Gillespie, and J.J. Blow, *Reversal of DDK-Mediated MCM Phosphorylation by Rif1-PP1 Regulates Replication Initiation and Replisome Stability Independently of ATR/Chk1.* Cell Rep, 2017. **18**(10): p. 2508-2520.

185. Sheu, Y.-J., et al., *Domain within the helicase subunit Mcm4 integrates multiple kinase signals to control DNA replication initiation and fork progression.* Proceedings of the National Academy of Sciences, 2014. **111**(18): p. E1899-E1908.

186. Yeeles, J.T.P., A. Janska, A. Early, and J.F.X. Diffley, *How the Eukaryotic Replisome Achieves Rapid and Efficient DNA Replication.* Molecular Cell, 2017. **65**(1): p. 105-116.

187. Lewis, J.S., et al., *Single-molecule visualization of Saccharomyces cerevisiae leading-strand synthesis reveals dynamic interaction between MTC and the replisome.* Proc Natl Acad Sci U S A, 2017. **114**(40): p. 10630-10635.

188. Hodgson, B., A. Calzada, and K. Labib, *Mrc1 and Tof1 Regulate DNA Replication Forks in Different Ways during Normal S Phase.* Molecular Biology of the Cell, 2007. **18**(10): p. 3894-3902.

189. Szyjka, S.J., C.J. Viggiani, and O.M. Aparicio, *Mrc1 Is Required for Normal Progression of Replication Forks throughout Chromatin in S. cerevisiae.* Molecular Cell, 2005. **19**(5): p. 691-697.

190. Osborn, A.J. and S.J. Elledge, *Mrc1 is a replication fork component whose phosphorylation in response to DNA replication stress activates Rad53.* Genes Dev, 2003. **17**(14): p. 1755-67.

191. Abd Wahab, S. and D. Remus, *Antagonistic control of DDK binding to licensed replication origins by Mcm2 and Rad53.* eLife, 2020. **9**: p. e58571.

192. Almawi, A.W., et al., *'AND' logic gates at work: Crystal structure of Rad53 bound to Dbf4 and Cdc7.* Scientific Reports, 2016. **6**(1): p. 34237.

193. Chen, Y.C., et al., *DNA replication checkpoint signaling depends on a Rad53-Dbf4 N-terminal interaction in Saccharomyces cerevisiae.* Genetics, 2013. **194**(2): p. 389-401.

194. Dohrmann, P.R., G. Oshiro, M. Tecklenburg, and R.A. Sclafani, *RAD53 Regulates DBF4 Independently of Checkpoint Function in Saccharomyces cerevisiae.* Genetics, 1999. **151**(3): p. 965-977.

195. Furuya, K., et al., *DDK phosphorylates checkpoint clamp component Rad9 and promotes its release from damaged chromatin.* Mol Cell, 2010. **40**(4): p. 606-18.

196. González-Garrido, C. and F. Prado, *Novel insights into the roles of Cdc7 in response to replication stress.* The FEBS Journal. **n/a**(n/a).

197. Bonte, D., et al., *Cdc7-Dbf4 kinase overexpression in multiple cancers and tumor cell lines is correlated with p53 inactivation.* Neoplasia, 2008. **10**(9): p. 920-31.

198. Cheng, A.N., et al., *Increased Cdc7 expression is a marker of oral squamous cell carcinoma and overexpression of Cdc7 contributes to the resistance to DNA-damaging agents.* Cancer Lett, 2013. **337**(2): p. 218-25.

199. Hou, Y., H.Q. Wang, and Y. Ba, *High expression of cell division cycle 7 protein correlates with poor prognosis in patients with diffuse large B-cell lymphoma.* Med Oncol, 2012. **29**(5): p. 3498-503.

200. Hou, Y., H.Q. Wang, and Y. Ba, *Effects of CDC7 gene silencing and Rituximab on apoptosis in diffuse large B cell lymphoma cells.* J Cancer Res Clin Oncol, 2012. **138**(12): p. 2027-34.

201. Malumbres, M., *Physiological relevance of cell cycle kinases.* Physiol Rev, 2011. **91**(3): p. 973-1007.

202. Montagnoli, A., J. Moll, and F. Colotta, *Targeting cell division cycle 7 kinase: a new approach for cancer therapy.* Clin Cancer Res, 2010. **16**(18): p. 4503-8.

203. Chen, H.J., et al., *Expression of huCdc7 in colorectal cancer.* World J Gastroenterol, 2013. **19**(20): p. 3130-3.

204. Fluge, Ø., et al., *Gene expression in poorly differentiated papillary thyroid carcinomas.* Thyroid, 2006. **16**(2): p. 161-75.

205. Kulkarni, A.A., et al., *Cdc7 kinase is a predictor of survival and a novel therapeutic target in epithelial ovarian carcinoma.* Clin Cancer Res, 2009. **15**(7): p. 2417-25.

206. Choschzick, M., et al., *Overexpression of cell division cycle 7 homolog is associated with gene amplification frequency in breast cancer.* Hum Pathol, 2010. **41**(3): p. 358-65.

207. Sasi, N.K., et al., *The potent Cdc7-Dbf4 (DDK) kinase inhibitor XL413 has limited activity in many cancer cell lines and discovery of potential new DDK inhibitor scaffolds.* PLoS One, 2014. **9**(11): p. e113300.

208. Gérard, A., et al., *The replication kinase Cdc7-Dbf4 promotes the interaction of the p150 subunit of chromatin assembly factor 1 with proliferating cell nuclear antigen.* EMBO reports, 2006. **7**(8): p. 817-823.

209. Young, T.J., Y. Cui, J. Irudayaraj, and A.L. Kirchmaier, *Modulation of Gene Silencing by Cdc7p via H4 K16 Acetylation and Phosphorylation of Chromatin Assembly Factor CAF-1 in Saccharomyces cerevisiae.* Genetics, 2019. **211**(4): p. 1219-1237.

210. Shibahara, K.-i. and B. Stillman, *Replication-Dependent Marking of DNA by PCNA Facilitates CAF-1-Coupled Inheritance of Chromatin.* Cell, 1999. **96**(4): p. 575-585.

211. Zhang, Z., K.-i. Shibahara, and B. Stillman, *PCNA connects DNA replication to epigenetic inheritance in yeast.* Nature, 2000. **408**(6809): p. 221-225.

212. Gan, H., et al., *The Mcm2-Ctf4-Polα Axis Facilitates Parental Histone H3-H4 Transfer to Lagging Strands.* Molecular Cell, 2018. **72**(1): p. 140-151.e3.

213. Petryk, N., et al., *MCM2 promotes symmetric inheritance of modified histones during DNA replication.* Science, 2018. **361**(6409): p. 1389-1392.

214. Katou, Y., K. Kaneshiro, H. Aburatani, and K. Shirahige, *Genomic approach for the understanding of dynamic aspect of chromosome behavior.* Methods Enzymol, 2006. **409**: p. 389-410.

215. Tanaka, S., et al., *Origin association of Sld3, Sld7, and Cdc45 proteins is a key step for determination of origin-firing timing.* Curr Biol, 2011. **21**(24): p. 2055-63.

216. Fang, D., et al., *Dbf4 recruitment by forkhead transcription factors defines an upstream rate-limiting step in determining origin firing timing.* Genes Dev, 2017. **31**(23-24): p. 2405-2415.

217. Pasero, P., B.P. Duncker, E. Schwob, and S.M. Gasser, *A role for the Cdc7 kinase regulatory subunit Dbf4p in the formation of initiation-competent origins of replication.* Genes Dev, 1999. **13**(16): p. 2159-76.

218. Duncker, B.P., et al., *An N-terminal domain of Dbf4p mediates interaction with both origin recognition complex (ORC) and Rad53p and can deregulate late origin firing.* Proceedings of the National Academy of Sciences, 2002. **99**(25): p. 16087-16092.

219. Wierer, M. and M. Mann, *Proteomics to study DNA-bound and chromatin-associated gene regulatory complexes.* Human Molecular Genetics, 2016. **25**(R2): p. R106-R114.

220. Narula, K., A. Datta, N. Chakraborty, and S. Chakraborty, *Comparative analyses of nuclear proteome: extending its function.* Front Plant Sci, 2013. **4**: p. 100.

221. On, K.F., et al., *Prereplicative complexes assembled in vitro support origin-dependent and independent DNA replication.* Embo j, 2014. **33**(6): p. 605-20.

222. Humphrey, S.J., O. Karayel, D.E. James, and M. Mann, *High-throughput and high-sensitivity phosphoproteomics with the EasyPhos platform.* Nature Protocols, 2018. **13**(9): p. 1897-1916.

223. Shteinfer-Kuzmine, A., et al., *Mitochondria and nucleus cross-talk: Signaling in metabolism, apoptosis, and differentiation, and function in cancer.* IUBMB Life, 2021. **73**(3): p. 492-510.

224. Saleh, A., et al., *The structural basis of Cdc7-Dbf4 kinase dependent targeting and phosphorylation of the MCM2-7 double hexamer.* Nature Communications, 2022. **13**(1): p. 2915.

225. Zegerman, P. and J.F. Diffley, *Checkpoint-dependent inhibition of DNA replication initiation by Sld3 and Dbf4 phosphorylation.* Nature, 2010. **467**(7314): p. 474-8.

226. Lopes, M., et al., *The DNA replication checkpoint response stabilizes stalled replication forks.* Nature, 2001. **412**(6846): p. 557-61.

227. Santocanale, C. and J.F. Diffley, *A Mec1- and Rad53-dependent checkpoint controls late-firing origins of DNA replication.* Nature, 1998. **395**(6702): p. 615-8.

228. Koç, A., L.J. Wheeler, C.K. Mathews, and G.F. Merrill, *Hydroxyurea arrests DNA replication by a mechanism that preserves basal dNTP pools.* J Biol Chem, 2004. **279**(1): p. 223-30.

229. Xu, Y.J., A. Singh, and G.M. Alter, *Hydroxyurea Induces Cytokinesis Arrest in Cells Expressing a Mutated Sterol-14α-Demethylase in the Ergosterol Biosynthesis Pathway.* Genetics, 2016. **204**(3): p. 959-973.

230. Pardo, B., L. Crabbé, and P. Pasero, *Signaling pathways of replication stress in yeast.* FEMS Yeast Research, 2016. **17**(2).

231. Tosi, A., et al., *Structure and subunit topology of the INO80 chromatin remodeler and its nucleosome complex.* Cell, 2013. **154**(6): p. 1207-19.

232. Poli, J., S.M. Gasser, and M. Papamichos-Chronakis, *The INO80 remodeller in transcription, replication and repair.* Philosophical Transactions of the Royal Society B: Biological Sciences, 2017. **372**(1731): p. 20160290.

233. Lee, H.S., et al., *Stabilization and targeting of INO80 to replication forks by BAP1 during normal DNA synthesis.* Nat Commun, 2014. **5**: p. 5128.

234. Papamichos-Chronakis, M. and C.L. Peterson, *The Ino80 chromatin-remodeling enzyme regulates replisome function and stability.* Nature Structural & Molecular Biology, 2008. **15**(4): p. 338-345.

235. Falbo, K.B., et al., *Involvement of a chromatin remodeling complex in damage tolerance during DNA replication.* Nat Struct Mol Biol, 2009. **16**(11): p. 1167-72.

236. Vincent, J.A., T.J. Kwong, and T. Tsukiyama, *ATP-dependent chromatin remodeling shapes the DNA replication landscape.* Nat Struct Mol Biol, 2008. **15**(5): p. 477-84.

237. Shimada, K., et al., *Ino80 chromatin remodeling complex promotes recovery of stalled replication forks.* Curr Biol, 2008. **18**(8): p. 566-75.

238. Vassileva, I., et al., *The mammalian INO80 chromatin remodeling complex is required for replication stress recovery.* Nucleic Acids Res, 2014. **42**(14): p. 9074-86.

239. Yeeles, J.T.P., A. Janska, A. Early, and J.F.X. Diffley, *How the Eukaryotic Replisome Achieves Rapid and Efficient DNA Replication.* Mol Cell, 2017. **65**(1): p. 105-116.

240. Zhou, C.Y., et al., *The Yeast INO80 Complex Operates as a Tunable DNA Length-Sensitive Switch to Regulate Nucleosome Sliding.* Mol Cell, 2018. **69**(4): p. 677-688.e9.

241. Szerlong, H., et al., *The HSA domain binds nuclear actin-related proteins to regulate chromatin-remodeling ATPases.* Nat Struct Mol Biol, 2008. **15**(5): p. 469-76.

242. Eustermann, S., et al., *Structural basis for ATP-dependent chromatin remodelling by the INO80 complex.* Nature, 2018. **556**(7701): p. 386-390.

243. Shen, X., R. Ranallo, E. Choi, and C. Wu, *Involvement of actin-related proteins in ATP-dependent chromatin remodeling.* Mol Cell, 2003. **12**(1): p. 147-55.

244. Kapoor, P., et al., *Evidence for monomeric actin function in INO80 chromatin remodeling.* Nat Struct Mol Biol, 2013. **20**(4): p. 426-32.

245. Brahma, S., et al., *The Arp8 and Arp4 module acts as a DNA sensor controlling INO80 chromatin remodeling.* Nature Communications, 2018. **9**(1): p. 3309.

246. Knoll, K., et al., *The nuclear actin-containing Arp8 module is a linker DNA sensor driving INO80 chromatin remodeling.* Nature Structural & Molecular Biology, 2018. **25**.

247. Greiwe, J.F., et al., *Structural mechanism for the selective phosphorylation of DNA-loaded MCM double hexamers by the Dbf4-dependent kinase.* Nature Structural & Molecular Biology, 2022. **29**(1): p. 10-20.

248. Lisby, M., R. Rothstein, and U.H. Mortensen, *Rad52 forms DNA repair and recombination centers during S phase.* Proc Natl Acad Sci U S A, 2001. **98**(15): p. 8276-82.

249. Gómez-González, B., J.F. Ruiz, and A. Aguilera, *Genetic and molecular analysis of mitotic recombination in Saccharomyces cerevisiae.* Methods Mol Biol, 2011. **745**: p. 151-72.

250. Yen, K., V. Vinayachandran, and B.F. Pugh, *SWR-C and INO80 chromatin remodelers recognize nucleosome-free regions near +1 nucleosomes.* Cell, 2013. **154**(6): p. 1246-56.

251. Yao, W., et al., *The INO80 Complex Requires the Arp5-Ies6 Subcomplex for Chromatin Remodeling and Metabolic Regulation.* Mol Cell Biol, 2016. **36**(6): p. 979-91.

252. O'Reilly, F.J. and J. Rappsilber, *Cross-linking mass spectrometry: methods and applications in structural, molecular and systems biology.* Nature Structural & Molecular Biology, 2018. **25**(11): p. 1000-1008.

253. Pan, D., et al., *Simplified Protocol for Cross-linking Mass Spectrometry Using the MS-Cleavable Cross-linker DSBU with Efficient Cross-link Identification.* Analytical Chemistry, 2018. **90**(18): p. 10990-10999.

254. Leitner, A., M. Faini, F. Stengel, and R. Aebersold, *Crosslinking and Mass Spectrometry: An Integrated Technology to Understand the Structure and Function of Molecular Machines.* Trends Biochem Sci, 2016. **41**(1): p. 20-32.

255. Walzthoeni, T., A. Leitner, F. Stengel, and R. Aebersold, *Mass spectrometry supported determination of protein complex structure.* Curr Opin Struct Biol, 2013. **23**(2): p. 252-60.

256. Rappsilber, J., *The beginning of a beautiful friendship: cross-linking/mass spectrometry and modelling of proteins and multi-protein complexes.* J Struct Biol, 2011. **173**(3): p. 530-40.

257. Tran, B.Q., D.R. Goodlett, and Y.A. Goo, *Advances in protein complex analysis by chemical cross-linking coupled with mass spectrometry (CXMS) and bioinformatics.* Biochim Biophys Acta, 2016. **1864**(1): p. 123-9.

258. Wu, H., et al., *Reorientation of INO80 on hexasomes reveals basis for mechanistic versatility.* Science, 2023. **381**(6655): p. 319-324.

259. Zhang, M., et al., *Hexasome-INO80 complex reveals structural basis of noncanonical nucleosome remodeling.* Science, 2023. **381**(6655): p. 313-319.

260. Chen, Y. and J. Nielsen, *Flux control through protein phosphorylation in yeast.* FEMS Yeast Research, 2016. **16**(8).

261. Olsen, J.V. and M. Mann, *Status of Large-scale Analysis of Post-translational Modifications by Mass Spectrometry *.* Molecular & Cellular Proteomics, 2013. **12**(12): p. 3444-3452.

262. Humphrey, S.J., D.E. James, and M. Mann, *Protein Phosphorylation: A Major Switch Mechanism for Metabolic Regulation.* Trends Endocrinol Metab, 2015. **26**(12): p. 676-687.

263. Sharma, K., et al., *Ultradeep human phosphoproteome reveals a distinct regulatory nature of Tyr and Ser/Thr-based signaling.* Cell Rep, 2014. **8**(5): p. 1583-94.

264. Smolka, M.B., C.P. Albuquerque, S.H. Chen, and H. Zhou, *Proteome-wide identification of in vivo targets of DNA damage checkpoint kinases.* Proc Natl Acad Sci U S A, 2007. **104**(25): p. 10364-9.

265. Bodenmiller, B., et al., *Phosphoproteomic analysis reveals interconnected system-wide responses to perturbations of kinases and phosphatases in yeast.* Sci Signal, 2010. **3**(153): p. rs4.

266. Holt, L.J., et al., *Global analysis of Cdk1 substrate phosphorylation sites provides insights into evolution.* Science, 2009. **325**(5948): p. 1682-6.

267. Kanshin, E., et al., *Phosphoproteome dynamics of Saccharomyces cerevisiae under heat shock and cold stress.* Mol Syst Biol, 2015. **11**(6): p. 813.

268. Needham, E.J., et al., *Illuminating the dark phosphoproteome.* Sci Signal, 2019. **12**(565).

269. Lanz, M.C., et al., *In-depth and 3-dimensional exploration of the budding yeast phosphoproteome.* EMBO reports, 2021. **22**(2): p. e51121.

270. Li, J., et al., *Investigation of Proteomic and Phosphoproteomic Responses to Signaling Network Perturbations Reveals Functional Pathway Organizations in Yeast.* Cell Reports, 2019. **29**(7): p. 2092-2104.e4.

271. Sheu, Y.J. and B. Stillman, *Cdc7-Dbf4 phosphorylates MCM proteins via a docking site-mediated mechanism to promote S phase progression.* Mol Cell, 2006. **24**(1): p. 101-13.

272. Bousset, K. and J.F. Diffley, *The Cdc7 protein kinase is required for origin firing during S phase.* Genes Dev, 1998. **12**(4): p. 480-90.

273. Donaldson, A.D., W.L. Fangman, and B.J. Brewer, *Cdc7 is required throughout the yeast S phase to activate replication origins.* Genes Dev, 1998. **12**(4): p. 491-501.

274. Rossbach, D., D.S. Bryan, J.R. Hesselberth, and R. Sclafani, *Localization of Cdc7 Protein Kinase During DNA Replication in Saccharomyces cerevisiae.* G3 (Bethesda), 2017. **7**(11): p. 3757-3774.

275. Weinreich, M. and B. Stillman, *Cdc7p-Dbf4p kinase binds to chromatin during S phase and is regulated by both the APC and the RAD53 checkpoint pathway.* Embo j, 1999. **18**(19): p. 5334-46.

276. Oberbeckmann, E., et al., *Ruler elements in chromatin remodelers set nucleosome array spacing and phasing.* Nature Communications, 2021. **12**(1): p. 3232.

277. Miller, C.L.W. and F. Winston, *The conserved histone chaperone Spt6 is strongly required for DNA replication and genome stability.* Cell Rep, 2023. **42**(3): p. 112264.

278. Ardehali, M.B., et al., *Spt6 enhances the elongation rate of RNA polymerase II in vivo.* Embo j, 2009. **28**(8): p. 1067-77.

279. DeGennaro, C.M., et al., *Spt6 regulates intragenic and antisense transcription, nucleosome positioning, and histone modifications genome-wide in fission yeast.* Mol Cell Biol, 2013. **33**(24): p. 4779-92.

280. Ivanovska, I., et al., *Control of chromatin structure by spt6: different consequences in coding and regulatory regions.* Mol Cell Biol, 2011. **31**(3): p. 531-41.

281. Bortvin, A. and F. Winston, *Evidence that Spt6p controls chromatin structure by a direct interaction with histones.* Science, 1996. **272**(5267): p. 1473-6.

282. Neigeborn, L., J.L. Celenza, and M. Carlson, *SSN20 is an essential gene with mutant alleles that suppress defects in SUC2 transcription in Saccharomyces cerevisiae.* Mol Cell Biol, 1987. **7**(2): p. 672-8.

283. Neigeborn, L., K. Rubin, and M. Carlson, *Suppressors of SNF2 mutations restore invertase derepression and cause temperature-sensitive lethality in yeast.* Genetics, 1986. **112**(4): p. 741-53.

284. McCullough, L., Z. Connell, C. Petersen, and T. Formosa, *The Abundant Histone Chaperones Spt6 and FACT Collaborate to Assemble, Inspect, and Maintain Chromatin Structure in Saccharomyces cerevisiae.* Genetics, 2015. **201**(3): p. 1031-45.

285. Formosa, T., et al., *Spt16–Pob3 and the HMG protein Nhp6 combine to form the nucleosome-binding factor SPN.* The EMBO Journal, 2001. **20**(13): p. 3506-3517.

286. McDonald, S.M., et al., *Structure and biological importance of the Spn1-Spt6 interaction, and its regulatory role in nucleosome binding.* Molecular cell, 2010. **40**(5): p. 725-735.

287. Belotserkovskaya, R., et al., *FACT facilitates transcription-dependent nucleosome alteration.* Science, 2003. **301**(5636): p. 1090-1093.

288. Ralser, M., et al., *The Saccharomyces cerevisiae W303-K6001 cross-platform genome sequence: insights into ancestry and physiology of a laboratory mutt.* Open Biol, 2012. **2**(8): p. 120093.

289. Winston, F., C. Dollard, and S.L. Ricupero-Hovasse, *Construction of a set of convenient Saccharomyces cerevisiae strains that are isogenic to S288C.* Yeast, 1995. **11**(1): p. 53-5.

290. Brachmann, C.B., et al., *Designer deletion strains derived from Saccharomyces cerevisiae S288C: a useful set of strains and plasmids for PCR-mediated gene disruption and other applications.* Yeast, 1998. **14**(2): p. 115-32.

291. Bishop, A.C., et al., *A chemical switch for inhibitor-sensitive alleles of any protein kinase.* Nature, 2000. **407**(6802): p. 395-401.

292. Almer, A. and W. Hörz, *Nuclease hypersensitive regions with adjacent positioned nucleosomes mark the gene boundaries of the PHO5/PHO3 locus in yeast.* The EMBO journal, 1986. **5**(10): p. 2681-2687.

293. Rappsilber, J., M. Mann, and Y. Ishihama, *Protocol for micro-purification, enrichment, pre-fractionation and storage of peptides for proteomics using StageTips.* Nat Protoc, 2007. **2**(8): p. 1896-906.

294. Zhang, X., et al., *Proteome-wide identification of ubiquitin interactions using UbIA-MS.* Nature Protocols, 2018. **13**(3): p. 530-550.

295. Ihling, C.H., L. Piersimoni, M. Kipping, and A. Sinz, *Cross-Linking/Mass Spectrometry Combined with Ion Mobility on a timsTOF Pro Instrument for Structural Proteomics.* Anal Chem, 2021. **93**(33): p. 11442-11450.

296. Yılmaz, Ş., F. Busch, N. Nagaraj, and J. Cox, *Accurate and Automated High-Coverage Identification of Chemically Cross-Linked Peptides with MaxLynx.* Anal Chem, 2022. **94**(3): p. 1608-1617.

297. Combe, C.W., L. Fischer, and J. Rappsilber, *xiNET: cross-link network maps with residue resolution.* Mol Cell Proteomics, 2015. **14**(4): p. 1137-47.

298. Gibson, D.G., *Enzymatic assembly of overlapping DNA fragments.* Methods Enzymol, 2011. **498**: p. 349-61.

299. Reusswig, K.-U., et al., *Unscheduled DNA replication in G1 causes genome instability through head-to-tail replication fork collisions.* bioRxiv, 2021: p. 2021.09.06.459115.

300. Barrios, A., et al., *Expression and purification of recombinant yeast Ada2/Ada3/Gcn5 and Piccolo NuA4 histone acetyltransferase complexes.* Methods, 2007. **41**(3): p. 271-7.

301. Biswas, D., et al., *The yeast FACT complex has a role in transcriptional initiation.* Mol Cell Biol, 2005. **25**(14): p. 5812-22.

302. Dyer, P.N., et al., *Reconstitution of nucleosome core particles from recombinant histones and DNA.* Methods Enzymol, 2004. **375**: p. 23-44.

303. Kingston, I.J., J.S. Yung, and M.R. Singleton, *Biophysical characterization of the centromere-specific nucleosome from budding yeast.* J Biol Chem, 2011. **286**(5): p. 4021-6.

304. Shen, X., *Preparation and analysis of the INO80 complex.* Methods Enzymol, 2004. **377**: p. 401-12.

305. Lisby, M., R. Rothstein, and U.H. Mortensen, *Rad52 forms DNA repair and recombination centers during S phase.* Proceedings of the National Academy of Sciences, 2001. **98**(15): p. 8276-8282.

306. Ludwigsen, J., et al., *Remodeling and Repositioning of Nucleosomes in Nucleosomal Arrays.* Methods Mol Biol, 2018. **1805**: p. 349-370.

307. Knop, M., et al., *Epitope tagging of yeast genes using a PCR-based strategy: more tags and improved practical routines.* Yeast, 1999. **15**(10b): p. 963-72.

Acknowledgements

Dr. Daisaku Ikeda says “Young people are in the process of building their lives and for this very reason they are incomplete. They are unknown quantities with limitless possibilities. Young people bring with them the winds of change and reform and they are possessors of an enormous irrepressible vitality”. My doctorate journey has been an amazing opportunity to build my life in many different ways and these lines from my mentor has been the road map towards my human revolution and value creation. I would like to dedicate this scientific work to my mentor Dr. Daisaku Ikeda, my parents and my brother for their faith in me, for believing in me when I could not believe in myself. I am eternally grateful for their unconditional love, support and motivation during happy as well as challenging times.

First and foremost, I want to express my deepest gratitude to my direct supervisor Dr. Christoph F. Kurat for giving this wonderful opportunity to pursue PhD in his lab. My time in the lab has been an amazing experience and has helped me develop both as a person and as a scientist. I am deeply grateful for your patience, constant support, encouragement, and freedom in the lab. Your valuable guidance and kind advice has always strengthened my resolve to challenge scientific and non-scientific problems. Thank you so much for the wonderful training during PhD and I am sure that this training will greatly influence my future.

I would also like to thank my Doktorvater Prof. Dr. Axel Imhof for agreeing to supervise my thesis and for his valuable feedback during my PhD. Additionally, I am thankful to Prof. Dr. Peter Becker for establishing an amazing collaborative and supportive environment in the department. This study would not be possible without the constructive feedback received during the departmental presentations.

Next, I would like to thank my thesis advisory committee (TAC), Prof. Dr. Axel Imhof, Prof. Dr. Boris Pfander and Dr. Catherine Regnard for their valuable discussions and feedbacks. Every TAC meeting discussion helped in developing the project from different perspectives and therefore helped polish the story in many ways. I would further like to extend my thanks to all my collaborators for their support with experiments and help in pushing the study forward.

I would like to express my sincere thanks to integrated research training (IRTG) 1064 particularly to Dr. Elizabeth Schroeder-Reiter, who organized insightful seminars, amazing workshops and networking events, and retreats, which made the time during the PhD special. It helped me to acquire skills which were very helpful during my project and will be essential for future as well.

Further, I would like to thank all previous and current lab members (Silvia, Jessica and Nandini) of the Kurat lab. I would like to particularly thank Silvia Härtel for preparing countless number of plates, media, and powder for protein purification. I had a great time working and learning while supervising the master's thesis of Nandini Saxena. Additionally, I would like to thank my dear friend and previous colleague Dr. Sunil Nahata for correcting the material and methods part of the thesis.

Last but not the least, I would like to thank my friends in Germany, and India, Nicole, Tais, Albert, Lukas, Salinee, Bhawna, Federico, Francesca, Debjani, Archana, Morgane, Richa, Palak, Geetika, Chandrika and many others across the borders. I would also like to express my gratitude to Abhishek, Florian, Michael, and Gaby for always keeping an open ear and caring with unlimited support. I would also like to express my appreciation for Soka family across the globe. Thank you very much for always being there when I needed the most. This would not have been possible without your support!